NASA Technical Paper 1515

Wind-Tunnel/Flight Correlation Study of Aerodynamic Characteristics of a Large Flexible Supersonic Cruise Airplane (XB-70-1)

II - Extrapolation of Wind-Tunnel Data to Full-Scale Conditions

John B. Peterson, Jr., Michael J. Mann,
Russell B. Sorrells III, Wallace C. Sawyer,
and Dennis E. Fuller

FEBRUARY 1980

NASA

NASA Technical Paper 1515

Wind-Tunnel/Flight Correlation Study of Aerodynamic Characteristics of a Large Flexible Supersonic Cruise Airplane (XB-70-1)

II - Extrapolation of Wind-Tunnel Data to Full-Scale Conditions

John B. Peterson, Jr., Michael J. Mann,
Russell B. Sorrells III, Wallace C. Sawyer,
and Dennis E. Fuller
Langley Research Center
Hampton, Virginia

SUMMARY

This report contains the results of calculations made to extrapolate wind-tunnel data on an XB-70-1 wind-tunnel model to full-scale airplane conditions at Mach numbers from 0.76 to 2.53. The extrapolation was part of a joint program between the NASA Ames, Langley, and Dryden Flight Research Centers to evaluate present-day performance-prediction techniques for large flexible supersonic airplanes similar to a supersonic transport. The extrapolation procedure included interpolation of the wind-tunnel data at specific conditions of the flight test points; determination of the drag increments to be applied to the wind-tunnel data, such as spillage drag, boundary-layer trip drag, and skin-friction increments; and estimates of the drag items not represented on the wind-tunnel model such as bypass doors, roughness, protuberances, and leakage drag. In addition, estimates of the effects of the flexibility of the airplane were determined.

INTRODUCTION

Accurate prediction of full-scale performance from data obtained in the wind tunnel is an important problem for aircraft design engineers. If faulty performance estimates are made, there may be a severe economic penalty in the design or operation of the aircraft (refs. 1, 2, and 3). The problem is of such importance that, in order to increase the accuracy of performance prediction at transonic speeds, a new national high Reynolds number transonic wind-tunnel facility, based on the cryogenic-tunnel concept, is under construction at the NASA Langley Research Center (refs. 4, 5, and 6). This tunnel would eliminate one of the major sources of uncertainty in transonic tests by insuring that the shock-wave—boundary-layer interactions on the model would be the same as on the full-scale aircraft. A test at full-scale Reynolds number would also eliminate the problem of extrapolation of skin friction to full scale, which is usually the largest adjustment in drag coefficient when extrapolating wind-tunnel model data to full scale. But many other steps in the extrapolation procedure would still have to be calculated, such as the protuberance and roughness drags; the change in drag due to aeroelasticity; the drag of bleed, diverters, and bypass air; and the drag associated with interference effects of the model support sting. Since no practical way has yet been found to make supersonic wind-tunnel tests at full-scale Reynolds numbers, supersonic tests will still require extrapolation to full-scale Reynolds numbers.

Several reports have been written on the extrapolation of wind-tunnel data and the comparison of predicted performance with measured full-scale performance, but most have been for subsonic or transonic speeds (refs. 7 to 17). Some of these reports used wind-tunnel data that were obtained on models whose geometry did not correspond accurately to the flight test airplane, and, in some cases, did not include all of the extrapolation items. Fewer reports have been published on the comparison of wind-tunnel data with full-scale performance at supersonic speeds (refs. 18 to 25), especially for large flexible

supersonic-cruise-type airplanes such as supersonic transports or bombers (refs. 21 and 22).

The NASA Dryden Flight Research Center conducted extensive flight tests on the XB-70-1 airplane at both supersonic and subsonic speeds to obtain high-quality performance data. These data provide a unique opportunity to evaluate present-day wind-tunnel data-extrapolation and performance-prediction techniques for large, flexible supersonic airplanes similar to a supersonic transport.

Fourteen flight test points obtained under equilibrium conditions were selected to be compared with extrapolated wind-tunnel results. These points cover a range of Mach numbers from 0.76 to 2.56. To obtain wind-tunnel data to be used as a basis for the extrapolation to full scale, a new 0.03-scale wind-tunnel model which accurately represented the final version of the XB-70-1 was built specifically for this correlation study and was tested at NASA Ames Research Center in the Ames 11-Foot Transonic Wind Tunnel and the Ames 9- by 7-Foot Supersonic Wind Tunnel (ref. 26).

This report includes the procedures used and the calculated incremental coefficients necessary to extrapolate the XB-70-1 wind-tunnel model data to full scale and also presents the predicted performance of the XB-70-1 at the 14 selected flight test points. The calculation procedure includes interpolation of the wind-tunnel data at the specific conditions of the flight test points; determination of the drag increments (e.g., spillage drag, boundary-layer trip drag, and skin-friction increments) to be applied to the wind-tunnel data; and estimates of the drag items not represented on the wind-tunnel model such as bypass doors, roughness, protuberances, and leakage drag. In addition, estimates were made of the effects of the flexibility of the airplane. A comparison of the extrapolated results with flight test results is included in Part III of this series of reports (ref. 27).

SYMBOLS

The units used for the physical quantities in this paper are given both in the International System of Units (SI) and the U.S. Customary Units. The measurements and calculations were made in the U.S. Customary Units. The data presented in this report are referenced to the stability axis system. The moment reference point was taken to be the quarter-chord point of the mean aerodynamic chord. (See table I.)

A_{inlet} total frontal area of inlet, 7.2258 m^2 (11 200 in^2)

C_D drag coefficient, Drag/$q_\infty S$

$C_{D,min}$ minimum drag coefficient (see eq. (1))

C_L lift coefficient, Lift/$q_\infty S$

$C_{L\alpha}$ lift-curve slope, $\partial C_L/\partial \alpha$, per degree

2

$C_{L,md}$ lift coefficient at which $C_{D,min}$ occurs (see eq. (1))

C_m pitching-moment coefficient relative to $0.25\text{-}\bar{c}$ station, Pitching moment$/q_\infty S \bar{c}$

$C_{m_{C_L}}$ slope of pitching-moment coefficient, $\partial C_m/\partial C_L$, per degree

C_{m_α} longitudinal stability parameter, $\partial C_m/\partial \alpha$, per degree

$C_{m_{\delta_c}}$ canard control effectiveness, $\partial C_m/\partial \delta_c$, per degree

$C_{m_{\delta_e}}$ elevon control effectiveness, $\partial C_m/\partial \delta_e$, per degree

C_N normal-force coefficient, Normal force$/q_\infty S$

C_{N_α} slope of normal-force coefficient, $\partial C_N/\partial \alpha$, per degree

$C_{N_{\delta_c}}$ normal-force effectiveness of canard, $\partial C_N/\partial \delta_c$, per degree

$C_{N_{\delta_e}}$ normal-force effectiveness of elevon, $\partial C_N/\partial \delta_e$, per degree

$\bar{c}$ mean aerodynamic chord, 23.94 m (942.38 in.)

c.g.   center-of-gravity position, percent of $\bar{c}$

K drag-due-to-lift parameter (eq. (1))

k height of transition trip

M Mach number

$\dot{m}$ inlet mass flow, kg/sec (slugs/sec)

$\dot{m}_\infty$ free-stream mass flow, $\rho_\infty V_\infty A_{inlet}$, kg/sec (slugs/sec)

$\dot{m}/\dot{m}_\infty$ inlet mass-flow ratio

P1 to P10   identification number of flight test point

P_∞ free-stream static pressure, N/m^2 (psf)

q_∞ free-stream dynamic pressure, N/m^2 (psf)

$R_{\bar{c}}$ Reynolds number based on $\bar{c}$

R_k transition-trip Reynolds number based on condition at tip of trip, $R_k = ku_k/\nu_k$

R_x Reynolds number based on streamwise distance from leading edge

S reference wing area including fuselage intersection, $585.08\ m^2$ ($6297.8\ ft^2$)

T_{aw}	adiabatic wall temperature, K (^{O}R)
T_w	wall surface temperature, K (^{O}R)
T_∞	free-stream air temperature, K (^{O}R)
V_∞	free-stream velocity, m/sec (ft/sec)
u_k	velocity in undisturbed laminar boundary layer at height of transition trip k, m/sec (ft/sec)
α	angle of attack, measured from fuselage reference line, deg
Δ	increment to be added to obtain prediction of full-scale aerodynamic characteristics
δ_{bp}	average deflection of forward set of bypass doors, deg
δ_c	deflection of canard, positive with trailing edge down, deg
δ_e	average deflection of elevons, positive with trailing edge down, deg
δ_r	deflection of rudder, positive with trailing edge left, deg
δ_y	deflection of wing tip, positive down, deg
ν_k	kinematic viscosity in undisturbed laminar boundary layer at height of transition trip k, m^2/sec (ft^2/sec)
ρ_∞	free-stream density, kg/m^3 (slugs/ft^3)

Subscripts:

bli	due to bleed-air interference
bpi	due to bypass-air interference
$C_L = C$	at a constant C_L
div	due to diverter-air interference
flex	due to flexibility or flexible value
flt	value in flight tests
L	left
leak	due to leakage of air
lift	due to lift
pred	predicted value

4

prot   due to protuberances

R   right

rigid   rigid value

rough   due to roughness

sf   due to skin friction

wt   value from wind-tunnel tests

DESCRIPTION OF FLIGHT TEST VEHICLE

The XB-70-1 airplane was designed as a weapon system with intercontinental supersonic-cruise capabilities. It had a take-off weight of over 226 796 kg (500 000 lb) and was designed to cruise at Mach 3 at altitudes of 21 336 to 24 384 m (70 000 to 80 000 ft). A three-view drawing of the XB-70-1 airplane is shown in figure 1, and the basic geometric characteristics are given in table I. The airplane had a thin, low-aspect-ratio, 65.6° leading-edge-sweep delta wing. The wing tips could be folded down about a slightly skewed longitudinal axis to increase the directional stability at supersonic speeds and to capture the shock off the side of the engine nacelle pack under the wing in order to reduce drag. In normal operation, the wing tips were undeflected up to high subsonic speeds; deflected down to 25° between Mach numbers of approximately 0.8 and 1.4; and deflected down to 65° at Mach numbers above 1.4. Twin movable vertical stabilizers were used for directional control, and a canard and elevons electromechanically coupled to move together were used for longitudinal control. The airplane was equipped with a stability augmentation control system which was in operation during the flight test points selected for this report, and whereas the elevons and canard moved together under the pilot's command, the stability augmentation system caused additional deflections only to the elevons and did not affect the canard. A more detailed description of the stability augmentation system is given in references 28 and 29. The elevons were differentially deflected by the pilot to provide lateral control. The elevons were split into six segments on each wing semispan to prevent binding when the wing deflected under aerodynamic loads. When the wing tips were deflected, the two outboard segments on each tip remained at a zero setting and were folded with the tip.

Propulsion was provided by six YJ93-GE-3 engines mounted side by side in a single integrated nacelle under the wing. The nacelle was divided into twin, two-dimensional, vertical-ramp, mixed-compression inlets. The air inlet ducts were equipped with six bypass doors (fig. 1) on each side which were located just forward and inboard of the leading edge of the vertical fins. The inlets incorporated boundary-layer bleed-air extraction through perforated panels in the region near the throat of the inlet. Part of the bleed air was dumped overboard just behind and below the inlet opening, and the rest was ducted to the base region of the airplane. Additional information on the XB-70-1 inlet system is given in references 28, 30, and 31.

FLIGHT TEST CONFIGURATION AND CONDITIONS

The results of the flight tests and the accuracy of the flight test measurements are discussed in reference 32. A summary of the flight test conditions and the XB-70-1 configuration during the flight tests is given in reference 28 and in tables II and III of this report.

Table II shows the airplane configuration at the time the 14 flight test data points were taken. The nose-ramp position, given in column 11 of table II, refers to the variable-position canopy ramp on the XB-70-1 which could be raised to reduce the wave drag at supersonic speeds and lowered to increase the visibility from the cockpit during low speeds. (See fig. 2.) The shaker vane shown in column 13 of table II was a small horizontal vane added to each side of the fuselage ahead of the canard. (See fig. 2.) These vanes were on the XB-70-1 for all test flights except tests P7 and P10. The vanes were used to excite structural vibrations for aeroelastic studies of the XB-70-1.

As mentioned previously, the stability augmentation system was in operation during the chosen flight test points, and this system affected the elevon deflections but not the canard deflection. Therefore, the elevon deflections were changing with time, but the canard deflection was relatively constant during the time the performance data were taken. Figure 3, which was taken from reference 28, shows the time histories of the elevon deflections near the data time for the flight test points. These time histories show that the elevons moved as much as $\pm 0.5^{\circ}$ over a period of approximately 5 sec before the data were taken. The elevon deflections given in column 8 of table II are the average of all the segments at the time the performance data were taken and are the same as the deflections given in table I of reference 28, except for P3 which was changed from 10.9° to 10.4°. The time history for P3 indicated that 10.4° was more representative of the elevon deflection than 10.9°.

The flight conditions for the 14 test cases are shown in table III. The Reynolds number $R_{\overline{c}}$ is based on the measured Mach number, pressure, temperature, and the XB-70-1 mean aerodynamic chord of 23.94 m (78.53 ft). As shown in column 15, the first 10 cases were in approximately 1g equilibrium flight, and the last 4 cases were obtained in low g (P3L and P8L) or high g (P3H and P8H) "roller-coaster" maneuvers. The roller-coaster points at $M = 1.2$ and $M = 2.5$ were obtained a short time after the corresponding approximately 1g equilibrium points, as can be seen from the flight numbers and data times in columns 2 and 3.

Flight test P10 at $M = 1.06$ was chosen to represent a case in which the drag coefficient was very high due to transonic drag rise, and the excess thrust available from the engine to accelerate the airplane to supersonic speeds was very low.

WIND-TUNNEL MODEL AND TESTS

A 0.03-scale model with geometry that accurately represented the final version of the XB-70-1 was built expressly for the XB-70-1 wind-tunnel/flight correlation project. The model was built in the 1g shape calculated for the

6

XB-70-1 at the conditions given in table III for P8. The model contours were measured at Langley Research Center on a digital, surface-measuring apparatus to verify that the model was built to the correct shape. The shape of the model was altered slightly from the airplane shape in the region of the fuselage afterbody to accommodate the wind-tunnel model support sting. A discussion of the effects of the model support sting is included in reference 26. The model had flow-through engine nacelles, but the inlet bleed and bypass passages were not simulated on the model. Various sizes of nozzle plugs were used at the exit of the engine nacelles to vary the inlet mass flow and to determine the effect of these variations on the measured forces in the wind tunnel. The model was tested at the Ames Research Center in the Ames 11-Foot Transonic Wind Tunnel and the Ames 9- by 7-Foot Supersonic Wind Tunnel. These tests were conducted using very precise test techniques to insure that the wind-tunnel results were as accurate as possible. A boundary-layer trip consisting of 0.023-cm (0.0090-in.) diameter sieved glass beads placed at 1.27 cm (0.5 in.) streamwise on the wings, nacelles, and tails, and at 2.54 cm (1.0 in.) streamwise on the fuselage was used on the model for tests at transonic speeds $(0.75 \leqq M \leqq 1.4)$. A different trip consisting of 0.039-cm (0.0152-in.) diameter sieved glass beads placed at 0.64 cm (0.25 in.) streamwise on the wings, nacelles, and tails, and at 2.54 cm (1.0 in.) streamwise on the fuselage was used at supersonic speeds $(1.6 \leqq M \leqq 2.53)$. A report on the procedures used and the results obtained in these tests is given in reference 26.

DEFINITION OF DRAG

In any extrapolation of wind-tunnel data to full scale for comparison with full-scale tests, the items which are included in the definition of drag, as compared to items which reduce the net thrust, must be carefully defined. For the purpose of this report, drag is defined as all aerodynamic forces acting on the external surfaces of the airplane in the streamwise direction. The underside of the wing apex ahead of the inlet is not considered part of the external surface of the airplane since the inlet air scrubbed this area and then entered the inlet. Therefore, the drag of this surface was part of the internal drag of the model and was subtracted from the wind-tunnel drag. However, the additive drag of the inlet airflow was included in the definition of drag. The inlet airflow includes all the air which entered the inlet, including engine primary air, and all the secondary air supplies such as, the engine cooling air, the inlet bleed air, the inlet diverter air, the inlet bypass air, the engine bleed air, and the environmental control-system air. The change in momentum and pressure from the free stream to the exits was considered part of the thrust of the XB-70-1. For the secondary air supplies, this change in momentum and pressure acted in the drag direction and, therefore, resulted in a decrease in net thrust.

No attempt was made to predict the base drag in this report since no powered-jet wind-tunnel model tests of the XB-70-1 were conducted, and predictions based on unpowered models of the XB-70-1 and powered-jet models of other similar configurations were known to be a source of error in the prediction of the XB-70-1 full-scale base drag (ref. 33). The wind-tunnel model base drag was removed from the wind-tunnel data, and the flight-measured base drag was added to the extrapolated drag for comparison with flight data (ref. 27).

7

EXTRAPOLATION PROCEDURES

As previously stated, 14 points obtained during the flight tests at Dryden Flight Research Center at Mach numbers from 0.76 to 2.56 were selected to be compared with extrapolated wind-tunnel results. Since the flight test conditions were already known, the wind-tunnel data (which were taken at nominal Mach numbers, control deflections, and angles of attack) were interpolated to obtain data at the specific Mach numbers, control deflections, and angles of attack of the selected test points.

Interpolation of Wind-Tunnel Data

Canard and elevon deflection.- The wind-tunnel tests were made with the canard and the elevon deflected separately. The results from these tests had to be combined to obtain the data for combined deflections of the canard and elevon. This procedure was carried out at a constant angle of attack and is illustrated in figure 4 for flight test P8. First, the wind-tunnel data taken at $\delta_e = 0.0°$ and at $\delta_c = 0°$, $1.5°$, $3.0°$, and $4.5°$ were interpolated to obtain data at the flight-measured canard deflection of $2.8°$. Then the wind-tunnel data taken at $\delta_c = 0.0°$ and at $\delta_e = -5°$, $0°$, $5°$, $10°$, and $15°$ were interpolated to obtain data at the flight-measured elevon deflection of $3.2°$. The difference between each of these curves and the basic wind-tunnel data taken at $\delta_e = 0°$ and $\delta_c = 0°$ provided the increments to be added to the base curve to obtain a curve for the combined canard and elevon deflection.

As a check on this procedure, one run was made in the wind tunnel at $M = 2.53$ with the canard and elevon deflected simultaneously. The results obtained with the controls deflected simultaneously agree well with the results obtained from separate control increments added to the basic data, as shown in figure 4 and in the following table:

Source of data	Mach	α, deg	δ_c, deg	δ_e, deg	C_L	C_D	C_m
Basic wind-tunnel data	2.53	4.54	0.0	0.0	0.106	0.01663	-0.0019
Interpolation of canard data	2.53	4.54	2.8	.0	.108	.01715	.0026
Interpolation of elevon data	2.53	4.54	.0	3.2	.108	.01714	-.0038
Separate control increments added to basic data	2.53	4.54	2.8	3.2	.110	.01766	.0007
Controls deflected simultaneously	2.53	4.54	2.8	3.2	.111	.01761	.0001

As shown in figure 4, the results agree well, especially the lift and pitching-moment coefficients. However, figure 4 also shows that the C_D determined from separate increments added to the basic data is about 0.0003 higher at a constant lift coefficient than the C_D determined from the controls deflected simultaneously.

The increments in lift, drag, and pitching moment due to canard and elevon deflections for each of the 14 selected flight conditions are shown in table IV.

8

Except for conditions P5, P7, and P10, the wind-tunnel tests were made at a Mach number very close to the flight condition, and only very small corrections were necessary to the data due to Mach number. These corrections were made to the C_D, C_m, and α at constant lift coefficient from plots like those shown in figures 5, 6, and 7. The corrected values are given at the bottom of table IV. For conditions P5 and P7 (M = 1.67 and 2.15), the increments were calculated from the wind-tunnel data at M = 1.60, 2.10, and 2.53 and linearly interpolated to get the results at the flight Mach number.

Interpolation of wind-tunnel data at M = 1.06.- Accurate wind-tunnel data could not be obtained at M = 1.06 (the conditions of P10) because shock reflections from the tunnel walls would impinge on the model; therefore, the wind-tunnel data at M = 0.75, 0.8, 0.95, 1.2, and 1.4 were interpolated to obtain data at M = 1.06. Interpolation of data at M = 1.06 is very difficult because of the rapid variation of the data near M = 1.0; therefore, the interpolated values are probably not very accurate. When accurate data near M = 1.0 are important, small models which avoid the wall interference problem should be used.

The data were interpolated at a constant angle of attack for values of C_L and C_m at various canard and elevon settings. (See figs. 8 and 9.) These data were then used to obtain the C_L and C_m for the combined canard and elevon deflections measured in flight. (The lift-curve slope $C_{L\alpha}$ and the

stability parameter $C_{m_{C_L}}$ are shown plotted against Mach number in fig.10.

These parameters are used later to plot curves which can be compared with flight data.) To estimate the drag coefficient at M = 1.06, the drag polars (C_D versus C_L) at Mach numbers of 0.75, 0.8, 0.95, 1.2, and 1.4 were fitted by a least-squares curve of the form

$$C_D = C_{D,min} + K(C_L - C_{L,md})^2 \tag{1}$$

The three constants of this equation ($C_{D,min}$, K, and $C_{L,md}$) were plotted against Mach number (see figs. 11 to 16) to obtain interpolated constants at M = 1.06. The interpolated values of $C_{D,min}$, K, and $C_{L,md}$ were then used to estimate the drag at the C_L determined from figure 8. The drag increments between the drag calculated for the measured canard and elevon deflections and the drag calculated for zero control deflection were added to the drag estimates for zero control deflection at M = 1.06 to get the total drag. The increments used to determine C_L, C_D, and C_m for P10 are shown in table IV.

Angle of attack.- It should be noted that the airplane angle-of-attack values used in table IV are different from those that were measured in flight and given in table III. It was thought that the flight lift coefficient was probably known more accurately than the flight angle of attack; therefore, the wind-tunnel angles of attack used in table IV were chosen to give predicted lift coefficients that were closer to the measured flight lift coefficient. In the section of this report entitled "Prediction of Full-Scale Aerodynamic Characteristics," the effect of small changes in angle of attack on the lift, drag,

and pitching moment is shown so that a comparison between the flight results and the extrapolated wind-tunnel data can be made at angles of attack other than those given in table IV. Possible sources of error that are responsible for the discrepancy in angle of attack in flight will also be discussed in this same section.

The corrections to the canard deflection $\Delta\delta_{c,flex}$ in table IV are due to fuselage bending on the XB-70-1 airplane in flight. Aeroelastic-bending angle of the fuselage at the canard station was determined by North American Rockwell Corporation (now Rockwell International Corporation) and is given in reference 28. The deflection of the canard was increased for the wind-tunnel results by this angle so that the angle of attack of the canard would be the same as it was in flight.

Adjustments to Wind-Tunnel Data

Small adjustments to wind-tunnel data were obtained from wind-tunnel test results where the effects of small changes to the wind-tunnel model configuration were determined. These changes were necessary to make the model conform more closely to the XB-70-1 flight configuration. The effects of these changes to the wind-tunnel model configuration are discussed in the following sections.

Wing-tip deflection.- The actual deflections of the wing tips were measured during each of the flight test points and were slightly different than the nominal deflections of 0°, 25°, and 65°. (See table II.) Wind-tunnel tests were made with the wing tips deflected at angles slightly different from the nominal deflection at each of the test Mach numbers, and plots of the lift and drag at various tip deflections showed no changes in lift or drag except for P2 where the drag was decreased by 0.0006. The moment coefficients were changed, however, and these were significant for P2, P4, P6, and P7. (See fig. 17.) The increments for these points are shown in table V.

Rudder deflection.- Rudder deflections were measured during the flight tests and are given in table II. The effects of small rudder deflection $(\delta_r = -1^{\circ}$ and $-3^{\circ})$ on the wind-tunnel test results for lift, drag, and pitching moment were so small that they were essentially within the repeatability of the data. The increments for the smaller rudder deflections of the flight tests were, therefore, considered to be negligible.

In cases where increments must be used, such as increments for rudder deflections and wing-tip deflections different from the nominal positions, it would improve the accuracy of determining the increments if more data were obtained for larger deflections even though the deflections in flight may be small. The increments for larger deflections can be determined more accurately, and these increments can then be interpolated to give the increments for smaller deflections. Care should be taken, however, to insure that the interpolation is performed correctly and that only linearly varying data are interpolated linearly.

Shaker vane.- Small shaker vanes were located on each side of the XB-70-1 fuselage ahead of the canard for aeroelastic studies during all flights except

10

P7 and P10. The increment in lift measured in the wind-tunnel tests with the shaker vane on the model as compared with the lift without the shaker vane was negligible. The increments in drag and pitching moment are shown in figures 18 and 19 and in table V. The drag increment for the shaker vane was quite high at transonic speeds (0.0002 to 0.0005), but as the Mach number increased above 1.4, the drag increment became progressively less until above about Mach 2.3, the increment actually became slightly negative, possibly due to a more favorable wave-drag area distribution with the shaker vane added to the fuselage.

Afterbody.- During the supersonic tests ($1.6 \leq M \leq 2.53$), the afterbody closure around the support sting of the wind-tunnel model was very near to the lines of XB-70-1, but for transonic tests, the afterbody was changed to give greater clearance to avoid fouling of the model on the sting. Wind-tunnel tests were also made with the supersonic afterbody at transonic speeds and low angles of attack to determine the difference in results between the two afterbodies. The wind-tunnel data showed that there was no difference in lift, but that there were changes in drag and pitching moment as shown in figures 18 and 19. The increase in drag shown in figure 18 for the transonic afterbody, which had lower boattail angles, indicates that the sting may have induced positive pressures on the aft portion of the model at transonic speeds. The increments for the transonic test points are given in table V.

Canopy ramp.- The XB-70-1 incorporated a two-position ramp ahead of the canopy. When this canopy ramp was in the high-speed, up position (the position shown in fig. 1 and as a solid line in fig. 2), it faired the body lines so that the wave drag was reduced at supersonic speeds. When the canopy ramp was in the low-speed, down position (dashed outline shown in fig. 2), the ramp folded down to allow the crew greater visibility. The effect of lowering the canopy ramp was determined by plotting the results of wind-tunnel tests with the canopy ramp in both positions. The increments in lift were found to be negligible, and the increments in drag and pitching moment are shown in figures 18 and 19 and table V. For P8, P8L, and P8H, the canopy ramp was up in flight; and the increments are therefore zero for these cases.

Spillage drag.- The spillage drag of the XB-70-1 was dependent on the inlet mass-flow ratio m/m_∞. In order to determine the change in drag as the mass-flow ratio changed, wind-tunnel tests were made at several mass-flow ratios by varying the nozzle exit area at each of the test Mach numbers. The results of these tests are presented in reference 26, and some results are shown in figure 20. The mass-flow ratio m/m_∞ of the basic wind-tunnel model configuration was maintained very close to the mass-flow ratio in flight by using the appropriate nozzle exit areas. The values of the mass-flow ratios and the increments in lift, drag, and pitching moment are given in table V. Above a Mach number of 2.0, the inlets were started on both the XB-70-1 airplane and the wind-tunnel model. Since the inlets were geometrically similar, the mass-flow ratio should be the same for the wind-tunnel model as for the full-scale airplane except for small changes due to a variation in the boundary-layer growth on the inlet ramps. The differences in mass-flow ratio between the wind-tunnel model and full scale were within the accuracy of the wind-tunnel and flight measurements, and therefore no corrections for differences in mass-flow ratio were made at Mach numbers above 2.0.

Boundary-layer trip drag.- The basic boundary-layer trip used for the XB-70-1 wind-tunnel tests was described previously in the description of the wind-tunnel model. In addition to tests with the basic trips, tests were also made with trips of several smaller sizes and also without trips in order to determine the trip drag. Plots of the drag against trip height for several test Mach numbers are shown in figure 21. Also shown by arrows in figure 21 is the trip height for $R_k = 600$, the "critical" roughness Reynolds number. (See refs. 34 and 35.) Generally, the trips were above the critical height, and the drag increase above the smooth-model drag level indicates that the trips moved transition forward from the natural transition position on the model. The drag was generally constant as the trip size was increased above the critical size, except for the largest size which was the basic trip size. This indicates that transition was moved up to the trip as the trip size was increased and that the trip did not cause any additional drag until the largest size was used. The drag increment between the plateau value and the drag of the largest trip (used on the basic configuration) was caused by the trip itself, and this trip drag is subtracted from the basic data as indicated on table V.

All the corrections were applied to the wind-tunnel model data, and the results are shown at the bottom of table V. These results are the wind-tunnel data that most closely represent the XB-70-1 flight test configurations.

Extrapolation of Wind-Tunnel Results to Flight Conditions

In order to extrapolate the data obtained from wind-tunnel tests to full-scale conditions, additional corrections to the data had to be made from theoretical analyses of the differences between the wind-tunnel model and the full-scale XB-70-1. The calculated increments due to these differences are given in table VI.

Skin friction.- Since the wind-tunnel tests could not be conducted at full-scale Reynolds numbers, the skin friction on the wind-tunnel model was corrected for the effect of Reynolds number. To correct the skin friction, the skin friction was first calculated on the wind-tunnel model and then calculated for the XB-70-1 airplane, and the difference $\Delta C_{D,sf}$ was added to the wind-tunnel results as shown in table VI. The skin friction was calculated by using the Chapman and Rubesin method (ref. 36) for the laminar skin friction, and both the Karman-Schoenherr skin-friction law (ref. 37) and the Sommer and Short compressibility correction (ref. 38) for the turbulent skin friction. The boundary layer was assumed laminar back to the trip and turbulent after the trip. The wall temperature was assumed to be adiabatic. The component wetted areas, average lengths, and shape factors which were used to calculate the skin friction on both the wind-tunnel model and the airplane are shown in table VII. The shape factors are due to two effects. The first is due to taper and is a result of the difference in skin friction at various spanwise stations due to the variation of Reynolds number on a tapered wing or tail. The second is due to dynamic pressure and is a result of the difference between the dynamic pressure at the edge of the boundary layer and the dynamic pressure in the free stream. At subsonic speeds, this difference is due to the supervelocity over the wing, tail, or body. At supersonic speeds, the dynamic pressure is increased behind shock waves, such as the shock waves from the duct sides.

12

The shape factors due to taper, given in table VII, were determined by using the shape factors given in figure 20 of reference 37. The shape factors due to dynamic pressure were determined from the formulas given in reference 39 at subsonic and transonic speeds and by consideration of the increase in dynamic pressure due to shock waves over some of the surfaces at supersonic speeds.

The XB-70-1 airplane surfaces were generally rough enough to fix transition very near the leading edge, and therefore, the boundary layer was assumed to be fully turbulent from the leading edge on the airplane. To determine the effect of any laminar flow on the airplane, the skin friction was also calculated for transition at $R_x = 3.5 \times 10^6$ (approximately the Reynolds number at which transition would be expected to occur if the airplane surfaces were smooth), and the skin-friction drag was decreased by from 0.00007 (for P4) to 0.00012 (for P2).

The airplane wall temperature was assumed to be adiabatic since very few wall temperatures were measured on the XB-70-1. The actual wall temperatures would be dependent not only on a heat balance between convection from the boundary layer, convection from interior heat sinks such as the fuel tanks, radiation from the surface to the surroundings, and radiation from the Sun, but also on the previous history of heat transfer to the surface during the flight. To get an indication of the possible magnitude of the effect of wall temperature, skin friction was calculated for a wall temperature ratio $T_w/T_{aw} = 0.935$ which was measured at $M = 2.53$ on the wing during flight 70 (ref. 40). The calculated skin-friction drag at this wall temperature and at $M = 2.53$ was 0.00006 higher than the skin-friction drag at adiabatic wall temperature and $M = 2.53$. The effect of nonadiabatic wall temperatures was probably less than this at lower Mach numbers because the heat transfer rate would be lower.

Boundary-layer bleed dump.- The boundary-layer bleed dump is the sugar-scoop-like fairing under the front of the intake duct. (See fig. 1.) On the airplane, inlet boundary-layer bleed air was discharged overboard at the base of the bleed dump. The increments in lift, drag, and moment due to bleed dump at subsonic speeds were determined from the difference in the wind-tunnel data with and without the bleed dump on the model, but the drag increments at supersonic speeds were calculated because at supersonic speeds, the stream of air which is exhausted at the base of the bleed dump interacts with the area distribution of the airplane downstream of the bleed dump and has an important effect on the wave drag of the airplane. On the wind-tunnel model, there was no airflow through the bleed dump to duplicate the airflow that was present on the airplane. Therefore, the XB-70-1 wave drag was calculated with the NASA wave-drag computer program (ref. 41) which assumes that there was a flow of air to fill the area behind the bleed-dump base. The difference in the calculated wave drag at supersonic speeds with and without the bleed dump was used as the drag increment of the bleed dump. A comparison between the calculated drag increment and the drag increment determined from the wind-tunnel tests at supersonic speeds is shown in figure 22.

Closure.- Even though the wind-tunnel model conformed very closely to the XB-70-1 airplane, there was a slight difference in the closure at the aft end of the fuselage to allow clearance for the model sting mount. The difference

in wave drag between the model closure and the airplane closure was calculated
with the NASA wave-drag program and then added to the wind-tunnel results. The
calculated increment in drag is shown in table VI.

Bypass doors.- The drag of the bypass doors was calculated from the theo-
retical pressure on the doors. These doors were opened only at supersonic
speeds. A picture of the bypass doors on the XB-70-1 is shown in figure 23.
The opening angle of each of the bypass doors was measured during the XB-70-1
flights, and the average angle of the front set of doors is shown in table VI.
In calculating the drag of the bypass doors, the back set of doors was consid-
ered to be shielded by the front set and therefore did not contribute to the
drag. The effect of air exiting from the front set of doors on the pressure
drag of the aft set of doors is included in the section entitled "Air Interfer-
ence Drag." The change in momentum from free stream to the momentum of the air
exiting the doors is charged to the propulsion system as a decrease in the net
thrust. The drag of the front set of doors was calculated from the pressure
rise on a two-dimensional wedge at the angle of the doors and at the free-
stream Mach number or from the pressure necessary to separate the turbulent
boundary layer, whichever was lower. This pressure value, multiplied by the
frontal area, was used for the drag increment shown in table VI. The moment
increments shown at transonic speeds were obtained from the wind-tunnel tests
by using bypass doors without airflow. These tests showed no change in moment
except at $M = 1.2$.

Flexibility.- The wind-tunnel model was built to the shape calculated for
the XB-70-1 in 1g flight at $M = 2.53$ at an altitude of 19 187 m (62 950 ft),
which are the conditions of P8 on table III. (Further wind-tunnel data, taken
after these calculations were made, changed the calculated airplane shape
slightly at P8.) Using the latest wind-tunnel data, the airplane camber shape
was calculated for all the flight test points chosen for comparison (ref. 28,
appendixes F and H). The lift, drag, and pitching moment of both the wind-
tunnel model shape and the airplane shape were calculated with the NASA vortex-
lattice program (ref. 42) at subsonic speeds and with the numerical method of
reference 43 at supersonic speeds. The increments in lift, drag, and pitching
moment due to flexibility were calculated by subtracting the values calculated
for the wind-tunnel model shape from the values calculated for the airplane
shape at the same angle of attack. The differences are shown in table VI. The
major effect of flexibility was the change in moment coefficient at a constant
angle of attack. The lift also changed, and the change in lift caused a major
part of the change in drag. A smaller part of the change in drag was caused
by a redistribution of the lift over the wing due to the aeroelasticity of the
wing. The following table shows these drag increments separately:

Point	$\Delta c_{D,C_L=C}$	$\Delta c_{D,lift}$	$\Delta c_{D,flex}$	Point	$\Delta c_{D,C_L=C}$	$\Delta c_{D,lift}$	$\Delta c_{D,flex}$
P1	0.00004	-0.00088	-0.00084	P8	0.00000	-0.00004	-0.00004
P2	.00011	-.00137	-.00126	P9	.00000	-.00004	-.00004
P3	.00019	-.00076	-.00057	P3L	.00011	-.00028	-.00017
P4	.00003	-.00041	-.00038	P3H	.00021	-.00076	-.00055
P5	-.00015	.00013	-.00002	P8L	-.00001	-.00003	-.00004
P6	.00005	.00039	-.00034	P8H	.00000	-.00003	-.00003
P7	-.00001	.00002	-.00034				

The $\Delta C_{D,C_L=C}$ is the change in drag as the lift was redistributed over the wing at a constant lift coefficient, and $C_{D,lift}$ is the change in drag as the lift is changed at a constant angle of attack. As can be seen, the values of $\Delta C_{D,C_L=C}$ are very small, which indicates that the effect of flexibility on the drag polar (C_D versus C_L) is almost negligible. Reference 2 showed that this was also true for the C-141A airplane, for which the effects of flexibility on the C-141A drag polar were generally negligible except at the extremes of the flight envelope. However, flexibility does have a significant effect on the lift at a given angle of attack. It also affects the moment coefficient significantly, and, therefore, also affects the control deflections required to trim the airplane. It should be noted that, if the pitching moment were held constant rather than the control deflections as in this report, the flexibility effects on the drag polar could be significant because the control deflection, and therefore the trim drag, would change due to flexibility.

Roughness, protuberance, and leakage drag.- Roughness is defined as any deviation from the desired smooth outside surface of the airplane, such as holes, bumps, screw heads, rivet heads, steps, and slots, whereas protuberances are additions to the airplane which improve the operational convenience and performance, such as antennas, lights, test instrumentation, air data probes, fuel vents, air exits, and bomb-bay door rails. Leakage is any unintentional flow of air through gaps and holes in the airplane. All three items (i.e., roughness, protuberances, and leakage drag) produce drag which is not represented on the wind-tunnel model; therefore, these drags must be added to the wind-tunnel results in the extrapolation procedure.

For this report, the XB-70-1 used in the flight tests was closely examined at the Air Force Museum in Dayton, Ohio, where it is currently on display. The first author, with the help of Albert J. Murn of the Air Force Flight Dynamics Laboratory, measured and recorded the sizes, positions, and types of all roughnesses on the airplane. A total of 852 roughnesses were measured, many of which consisted of large groups of roughnesses such as groups of rivets or screw heads. As originally constructed, the airplane was quite smooth with very few projecting rivet heads or access panels, but many patches and doublers were attached to the skin after the airplane was put into service. Figure 24 shows examples of the types of roughnesses found on the XB-70-1 airplane.

The roughness types, sizes, and locations were coded on IBM cards, and the drag of each was calculated on an electronic computer. The formulas used to calculate the drag of the roughnesses were obtained from references 44, 45, and 46. Almost all of the roughnesses on the XB-70-1 fell within the range of parameters (Reynolds number and Mach number) tested in these references and, therefore, the calculated drags should be quite accurate. The drag of distributed surface roughness such as paint roughness was estimated to be negligible for all of the test points. For example, the surface roughness would have to be over 0.0025 cm (0.0010 in.) in height to cause an increase in turbulent skin friction at the worst flight conditions (P10). Generally, the roughness height of paint is about 0.0005 cm (0.0002 in.) to 0.0025 cm (0.0010 in.). (See ref. 39.)

The total roughness drags calculated for the measured roughnesses are shown in table VI as $\Delta C_{D,rough}$. These values are somewhat lower than might be expected from roughness drags calculated for other airplanes, especially since there were so many patches on the XB-70-1. For instance, the roughness drag calculated for the airplanes of references 7, 9, 10, 11, 13, 14, and 25 ranges from 0.00006 to 0.00031, based on the total wetted area, whereas the roughness drag on the XB-70-1 at subsonic Mach numbers is 0.00006, based on wetted area. One reason for this is that the XB-70-1 is a larger airplane and, therefore, the boundary layers are larger. This larger boundary layer cushions the roughnesses and the roughness drag is, therefore, lower. Also, the roughness drag calculated from the data of references 44, 45, and 46, which incorporate more recent data, is somewhat lower than that calculated from the traditional reference 39 for the same size rivet or step roughness, especially for roughness near the leading edge.

The protuberances which were present on the XB-70-1 during the flight tests are listed in reference 28 on page 178 and are shown in figures 62 to 80 of the same reference. They include the nose boom, radio antennas, several air data instrumentation probes, lights, bomb-bay doors and rails, fuel vents, environmental control system (ECS) outlets, and three boundary-layer survey rakes. In addition to the protuberances listed in reference 28, six nozzle-position transducers which were located beneath the nozzle exits were included in the protuberance drag on the XB-70-1. The drags of the protuberances were calculated from the data presented in reference 39 and are included in table VI.

Leakage drag is caused by the ram drag of air that leaks through the holes and cracks in the airplane. No thrust is credited to the leakage air since it usually exits perpendicular to the surface of the airplane. The sources of leakage air on the XB-70-1 are listed in table 41 of reference 28 and consist of ECS air, equipment cooling air, weapons-bay and landing-gear-compartment leakage, and engine ground cooling-door leakage. The airflow rates listed in reference 28 which come from the engine bleed air do not contribute to leakage drag since this air entered the inlet and its drag is used to reduce the engine thrust. The leakage drags of the various sources listed in reference 28 were negligible except for the leakage through the engine ground cooling doors. There were 18 of these doors located on the bottom of the engine nacelle. Each door was 23 cm (9 in.) wide and 64 cm (25 in.) long. The doors opened to supply cooling air to the engine compartment during ground operation and low-speed flight, but they were closed during the 14 test flights shown on table III. No special precautions were used to seal these doors on the XB-70-1, and the metal doors closed onto a metal frame. Pressures and temperatures in the engine compartment behind these doors were measured during each of the test flights. The leakage flow rate and drag were calculated by using the total perimeter of the doors (31 m (102 ft)) and an assumed clearance of 0.013 cm (0.005 in.), together with the measured pressures and temperatures. The calculated leakage drags are shown in table VI as $\Delta C_{D,leak}$.

Air interference drag.- As the air exits from the inlet bleed, diverter, and bypass exits, it interacts with the surrounding surfaces of the airplane to cause changes in pressures on these surfaces. For instance, the air flowing through the forward set of bypass doors will cause increases in pressure on the

16

face of the aft set of bypass doors and, therefore, will cause an increase in drag. (See fig. 23.) The amount of this drag increase was calculated by North American Rockwell as part of their drag substantiation report (ref. 28) by using data obtained for flush and protruding exhaust nozzles like those in references 47 and 48. The drag increments are given in tables 32 and 33 of reference 28 and are shown as the drag increments for air interference drag in table VI of this report.

Base drag.- No attempt was made to estimate the base pressure drag on the airplane since wind-tunnel tests of a powered-jet model were not available. The base pressure drag on the XB-70-1 is a known source of error (see ref. 33); therefore, in order to eliminate this source of error from the comparison, the flight-measured values from reference 33 of base pressure drag were used in table VI.

The increments in lift, drag, and pitching moment derived in this paper were added to the wind-tunnel data, and the predicted aerodynamic characteristics of the XB-70-1 at the 14 selected flight test points are summarized at the end of table VI.

Prediction of Full-Scale Aerodynamic Characteristics

In addition to the selected points given at the end of table VI, curves giving the predicted aerodynamic characteristics of the XB-70-1 in the vicinity of these points are shown in figure 25. The circles represent the predicted points of table VI and the lines show the effects of changes in angle of attack and control deflection on the predicted lift, drag, and moment coefficients. The solid curves represent the results with the control deflections (δ_c and δ_e) measured in flight. The short-dash curves represent the results with the canard deflected 0.5° more, and the long-dash short-dash curves represent the results with the canard deflection 0.5° less, than the measured flight deflection. As stated before, the elevons on the XB-70-1 were electromechanically coupled to move together with the canard to increase the control power of the pilot's control. When the canard deflection was increased, the elevon deflection was decreased. The ratio of the elevon movement to the canard movement was 6.67. Therefore, when the canard deflection was increased by 0.5°, the elevon deflection decreased by 3.33°. This ratio of elevon movement is included in figure 25 for the ±0.5° canard-deflection curves.

The curves of C_L plotted against α are determined from the wind-tunnel test results for C_{L_α} corrected by the flexible-rigid ratio $\dfrac{\left(C_{N_\alpha}\right)_{flex}}{\left(C_{N_\alpha}\right)_{rigid}}$ given in tables 8 to 18 of reference 28. (The flexible-rigid ratios for C_L were assumed to be equal to the flexible-rigid ratios for C_N.) The change in C_L with control deflection was determined by the change measured in the wind-tunnel tests and corrected by the values of flexible-rigid ratios $\dfrac{\left(C_{N_{\delta_e}}\right)_{flex}}{\left(C_{N_{\delta_e}}\right)_{rigid}}$

17

and $\dfrac{\left(C_{N_{\delta_c}}\right)_{\text{flex}}}{\left(C_{N_{\delta_c}}\right)_{\text{rigid}}}$ given in reference 28. The increments in lift were added to

the predicted point (circles) to produce the curves in figure 25.

Similarly, the curves of C_m plotted against C_L are determined from the $C_{m_{C_L}}$ measured in the wind-tunnel tests and corrected by the flexible-rigid

ratios $\dfrac{\left(C_{m_\alpha}\right)_{\text{flex}}}{\left(C_{m_\alpha}\right)_{\text{rigid}}}$ given in reference 28. The change in C_m with control

deflection was determined by the change in C_m measured in the wind-tunnel

tests and corrected by the values of flexible-rigid ratios $\dfrac{\left(C_{m_{\delta_e}}\right)_{\text{flex}}}{\left(C_{m_{\delta_e}}\right)_{\text{rigid}}}$ and

$\dfrac{\left(C_{m_{\delta_c}}\right)_{\text{flex}}}{\left(C_{m_{\delta_c}}\right)_{\text{rigid}}}$ given in reference 28. The curves of C_D plotted against C_L

were developed by determining the change in drag due to a change in C_L in the wind-tunnel tests and by adding the drag increment to the predicted point. Similarly, the curves for the other two control deflections were developed by determining the change in drag due to the control deflections from the wind-tunnel data and by adding the increment to the predicted point.

These drag polars are not trim polars and they are not valid for large changes in lift or control deflection from the selected point. However, these curves can be used to determine the effect of small changes in the flight-measured values of α or control deflection. In fact, of the five variables presented on these plots (i.e., α, control deflection (δ_c and δ_e), C_L, C_D, and C_m), any two can be used to find the other three. Of course, some combination of the two variables selected would not lead to accurate results for the other three variables (i.e., if control deflection and C_m were selected). However, if it were felt that the flight values of C_L and C_m (i.e., center of gravity) were known more accurately than the measured α and control deflections, then the C_L and C_m could be used as the independent variables and the predicted α, control deflection, and C_D could be determined. Also, if the flight-measured data are taken at a lift coefficient different from the predicted lift coefficient, the effect of this change in lift coefficient on the predicted α, C_D, and C_m can be found from the curves in figure 25.

It is apparent that in some cases in this study there is a discrepancy between the angle of attack measured in the flight tests and the angle of attack predicted from the wind-tunnel tests at the same lift coefficient. These discrepancies are tabulated in table VIII. The flight-measured C_L for each point is shown in table VIII as $C_{L,\text{flt}}$, and the angle of attack from figure 25 necessary to obtain the $C_{L,\text{flt}}$ is shown as α_{pred}. Also shown in table VIII is the angle of attack measured during the flight tests α_{flt} and

18

the difference in the two angle of attacks $\Delta\alpha$. Several of the differences in angle of attack shown in table VIII are higher than would be expected from errors in the wind tunnel or the flight instrumentation, especially those for P8, P8H, and P9. The errors shown for P2 and P10 are probably due to the difficulty of obtaining accurate data at Mach numbers near 1.0. The estimated errors in the angle-of-attack measurements are less than $\pm 0.1^\circ$ in the wind-tunnel tests and $\pm 0.3^\circ$ in the flight tests. The only adjustments to angle of attack or C_L that were applied to the wind-tunnel data during the extrapolation process were small corrections for the compressibility on table IV and flexibility on table VI.

The reasons for the discrepancies in α and C_L are not known, but possible sources of error in the flight data are bending of the fuselage and nose boom and upwash around the nose boom, none of which were known for the flight data. The amount of bending of the fuselage at the canard station is shown in table IV as $\Delta\delta_{c,flex}$. These values are generally small compared with the differences in angle of attack shown in table VIII. The bending of the fuselage and the nose boom where the angle-of-attack vane was mounted was not calculated but is estimated to be small. An indication of the magnitude of the errors in measuring angle of attack due to boom bending and upwash around the boom can be obtained from the calibration reported in reference 49. This reference shows that the upwash at any point around the boom is dependent on the distance of that point from the boom relative to the diameter of the boom. For the particular installation calibrated in reference 49, the upwash around the boom increased the indicated angle of attack by 5.8 percent of the angle of boom relative to the free stream. This same calibration would indicate that the upwash around the boom on the XB-70-1 would increase the indicated angle of attack by only 2.5 percent of the angle of attack of the boom. It should be noted that since the boom on the XB-70-1 was mounted at an angle of -4.17° (see fig. 2), the upwash would be zero at an airplane angle of attack of 4.17°. Other possible sources of error indicated in reference 49 are the aerodynamic-vane floating angle and the position error (upwash due to the fuselage and wing). Of course, position error is zero at a Mach number greater than 1.0.

The total effect of all the previously discussed error sources (i.e., fuselage and nose-boom bending, upwash around the nose boom, and aerodynamic-vane floating angle) is not believed to be large enough to cause the errors in angle of attack given on table VIII for points P8, P8H, and P9.

CONCLUDING REMARKS

Based on Reynolds number corrections and detailed drag estimates associated with measured airplane roughness, protuberance, and leakage drag, wind-tunnel data on an XB-70-1 model have been extrapolated to predict full-scale XB-70-1 performance at 14 selected flight test points. These predicted points are compared with the flight test data in Part III of this series of reports. The extrapolation process has indicated several areas of difficulty which should be noted.

The interpolation of the transonic wind-tunnel data to obtain data at Mach 1.06 can obviously lead to large errors. Only by obtaining good experi-

mental data free from wall interference effects at Mach 1.06, or at Mach numbers closer to 1.06 than the Mach 1.2 of this test, can the accuracy of the prediction be improved.

Part of the XB-70-1 extrapolation process required that increments in drag coefficient and pitching-moment coefficient for the low-speed canopy and shaker vane be added to the basic wind-tunnel-configuration data. These increments were obtained from wind-tunnel tests made both with and without the low-speed canopy and the shaker vane added to the model. It is apparent that these increments (less than 0.0007 in drag coefficient and 0.002 in pitching-moment coefficient) are subject to error since they are determined from the small differences in drag coefficient and pitching-moment coefficient measured on two different configurations. In fact, every increment of this type used to correct the basic wind-tunnel data also increases the possible errors in the predicted characteristics by an amount equal to the repeatability of the wind-tunnel data. During wind-tunnel tests, the model should correspond as closely as possible to the airplane flight configuration to increase the accuracy of the predicted aerodynamic characteristics.

In certain cases where increments must be used, such as increments for rudder deflection and wing-tip deflection different from the nominal deflections, it would improve the accuracy of determining the increments if more data were obtained for larger deflections even though the deflections in flight may be small. The increments for larger deflections can be determined more accurately, and these increments can then be interpolated to give the increments for smaller deflections. Care should be taken, however, to insure that the interpolation is performed correctly and that only linearly varying data are interpolated linearly.

During the flight tests, the stability augmentation system was left on and the elevons were constantly changing position in response to the signals from this system. Time histories of the elevon deflections were available for the times ahead of the flight test points, but there was still some uncertainty as to what the effective elevon deflection should be for the test point. Therefore, it would probably improve the validity of the wind-tunnel/flight correlation if the flight data were obtained with the stability system off.

Finally, it is apparent that in some cases in this study there is a discrepancy between the angle of attack measured in the flight tests and the angle of attack predicted from the wind-tunnel tests at the same lift coefficient. This discrepancy is larger than the expected accuracy of the measurements. An examination of possible sources of error in the angle-of-attack measurements, such as fuselage and nose-boom bending, upwash around the nose boom, and aerodynamic-vane floating error, did not indicate any sources that are believed large enough to account for these discrepancies.

Langley Research Center
National Aeronautics and Space Administration
Hampton, VA 23665
August 14, 1979

20

REFERENCES

1. Brown, Clinton E.; and Chen, Chuan Fang: An Analysis of Performance Estimation Methods for Aircraft. NASA CR-921, 1967.

2. Paterson, J. H.; Blackerby, W. T.; Schwanebeck, J. C.; and Braddock, W. F.: An Analysis of Flight Test Data on the C-141A Aircraft. NASA CR-1558, 1970.

3. Norton, D. A.: Airplane Drag Prediction. Ann. N.Y. Acad. Sci., vol. 154, art. 2, Nov. 22, 1968, pp. 306-328.

4. Goodyer, Michael J.; and Kilgore, Robert A.: High-Reynolds-Number Cryogenic Wind Tunnel. AIAA J., vol. 11, no. 5, May 1973, pp. 613-619.

5. Polhamus, E. C.; Kilgore, R. A.; Adcock, J. B.; and Ray, E. J.: The Langley Cryogenic High Reynolds Number Wind-Tunnel Program. Astronaut. & Aeronaut., vol. 12, no. 10, Oct. 1974, pp. 30-40.

6. Nicks, Oran W.; and McKinney, Linwood W.: Status and Operational Characteristics of the National Transonic Facility. AIAA Paper 78-770, Apr. 1978.

7. Hopps, R. H.; and Danforth, E. C. B.: Correlation of Wind-Tunnel and Flight-Test Data for the Lockheed L-1011 Tri-Star Airplane. Performance Prediction Methods, AGARD-CP-242, May 1978, pp. 21-1 - 21-12.

8. Maestrati, J.: Comparison of Wind Tunnel Tests and Flight Tests on an Executive Aircraft. NASA TT F-17068, 1976.

9. Capone, Francis J.: Wind Tunnel/Flight Data Correlation for the Boeing 737-100 Transport Airplane. NASA TM X-72715, 1975.

10. Pyle, Jon S.; and Steers, Louis L.: Flight-Determined Lift and Drag Characteristics of an F-8 Airplane Modified With a Supercritical Wing With Comparisons to Wind-Tunnel Results. NASA TM X-3250, 1975.

11. MacWilkinson, D. G.; Blackerby, W. T.; and Paterson, J. H.: Correlation of Full-Scale Drag Predictions With Flight Measurements on the C-141A Aircraft - Phase II, Wind Tunnel Test, Analysis and Prediction Techniques. Volume 1 - Drag Predictions, Wind Tunnel Data Analysis and Correlation. NASA CR-2333, 1974.

12. Van Doorn, J. T. M.; Han, S. O. T. H.; and Obert, E.: Comparison of Fokker F28 "Fellowship" Wind Tunnel and Flight Data - A Summary. Jaarboek 1973, Netherlandse Ver. voor Luchtvaarttech., [1974], pp. 5-1 - 5-28.

13. Paterson, J. H.; MacWilkinson, D. G.; and Blackerby, W. T.: A Survey of Drag Prediction Techniques Applicable to Subsonic and Transonic Aircraft Design. Aerodynamic Drag, AGARD-CP-124, Oct. 1973, pp. 1-1 - 1-38.

14. Horton, Elmer A.; and Tetervin, Neal: Measured Surface Defects on Typical Transonic Airplanes and Analysis of Their Drag Contribution. NASA TN D-1024, 1962.

15. Rolls, L. Stewart; and Wingrove, Rodney C.: An Investigation of the Drag Characteristics of a Tailless Delta-Wing Airplane in Flight, Including Comparison With Wind-Tunnel Data. NASA MEMO 10-8-58A, 1958.

16. Bird, K. D.; and Kelsey, H. F.: Transonic Wind Tunnel Research Tests Using a 1/18 Scale Bell X-1 Model in the CAL 4-ft. Transonic Tunnel. WADC Tech. Rep. 55-273, U.S. Air Force, Mar. 1956.

17. Gieseman, Earl Ralph, Jr.: Drag Correlation of Wind-Tunnel and Flight-Test Data in the Transonic Range. Graduate Thesis (1-GAE-55), U.S. Air Force Inst. Technol., Aug. 1955. (Available from DDC as AD 81 421.)

18. Abercrombie, J. M.: Flight Test Verification of F-15 Performance Predictions. Performance Prediction Methods, AGARD-CP-242, May 1978, pp. 17-1 - 17-13.

19. Grellmann, H. W.: YF-17 Full Scale Minimum Drag Prediction. Performance Prediction Methods, AGARD-CP-242, May 1978, pp. 18-1 - 18-12.

20. Webb, T. S.; Kent, D. R.; and Webb, J. B.: Correlations of F-16 Aerodynamics and Performance Predictions With Early Flight Test Results. Performance Prediction Methods, AGARD-CP-242, May 1978, pp. 19-1 - 19-17.

21. Berger, J.: Comparaison Entre Les Previsions Deduites Des Essais En Soufflerie Et Les Resultats De Vol En Croisiere. Performance Prediction Methods, AGARD-CP-242, May 1978, pp. 20-1 - 20-50. (Also available as NASA TM-75238.)

22. Poisson-Quinton, Philippe: First Generation Supersonic Transports. The Future of Aeronautical Transportation, Dep. Aerosp. & Mech. Sci., Princeton Univ., 1975, pp. 1-1 - 1-57.

23. Rooney, E. C.: Development of Techniques To Measure In-Flight Drag of a U.S. Navy Fighter Airplane and Correlation of Flight Measured Drag With Wind-Tunnel Data. Aerodynamic Drag, AGARD-CP-124, Oct. 1973, pp. 24-1 - 24-18.

24. Hopkins, Edward J.; Fetterman, David E., Jr.; and Saltzman, Edwin J.: Comparison of Full-Scale Lift and Drag Characteristics of the X-15 Airplane With Wind-Tunnel Results and Theory. NASA TM X-713, 1962.

25. Cook, T. A.; and Hayward, R. W.: Force Measurements on a 1/9 Scale Model of the FD2 Research Aircraft at Mach Numbers Between 0.6 and 1.8. Tech. Rep. 68294, British R.A.E., Dec. 1968.

26. Daugherty, James C.: Wind-Tunnel/Flight Correlation Study of Aerodynamic Characteristics of a Large Flexible Supersonic Cruise Airplane (XB-70-1). I – Wind-Tunnel Tests of a 0.03-Scale Model at Mach Numbers From 0.6 to 2.53. NASA TP-1514, 1980.

27. Arnaiz, Henry H.; Peterson, John B., Jr.; and Daugherty, James C.: Wind-Tunnel/Flight Correlation Study of Aerodynamic Characteristics of a Large Flexible Supersonic Cruise Airplane (XB-70-1). III – A Comparison Between Characteristics Predicted From Wind-Tunnel Measurements and Those Measured in Flight. NASA TP-1516, 1980.

28. Wykes, John H.; and Lawrence, Robert E.: Estimated Performance and Stability and Control Data for Correlation With XB-70-1 Flight Test Data. NASA CR-114335, 1971.

29. Wolowicz, Chester H.; and Yancey, Roxanah B.: Comparison of Predictions of the XB-70-1 Longitudinal Stability and Control Derivatives With Flight Results for Six Flight Conditions. NASA TM X-2881, 1973.

30. Arnaiz, Henry H.; and Schweikhard, William G.: Validation of the Gas Generator Method of Calculating Jet-Engine Thrust and Evaluation of XB-70-1 Airplane Engine Performance at Ground Static Conditions. NASA TN D-7028, 1970.

31. Randall, L. M.: The XB-70A Air Induction System. AIAA Paper No. 66-634, June 1966.

32. Arnaiz, Henry H.: Flight-Measured Lift and Drag Characteristics of a Large, Flexible, High Supersonic Cruise Airplane. NASA TM X-3532, 1977.

33. Saltzman, Edwin J.; Goecke, Sheryll A.; and Pembo, Chris: Base Pressure Measurements on the XB-70 Airplane at Mach Numbers From 0.4 to 3.0. NASA TM X-1612, 1968.

34. Braslow, Albert L.; Hicks, Raymond M.; and Harris, Roy V., Jr.: Use of Grit-Type Boundary-Layer-Transition Trips on Wind-Tunnel Models. NASA TN D-3579, 1966.

35. Braslow, Albert L.; and Knox, Eugene C.: Simplified Method for Determination of Critical Height of Distributed Roughness Particles for Boundary-Layer Transition at Mach Numbers From 0 to 5. NACA TN 4363, 1958.

36. Chapman, Dean R.; and Rubesin, Morris W.: Temperature and Velocity Profiles in the Compressible Laminar Boundary Layer With Arbitrary Distribution of Surface Temperature. J. Aeronaut. Sci., vol. 16, no. 9, Sept. 1949, pp. 547-565.

37. Bertram, Mitchel H.: Calculations of Compressible Average Turbulent Skin Friction. NASA TR R-123, 1962.

38. Sommer, Simon C.; and Short, Barbara J.: Free-Flight Measurements of Turbulent-Boundary-Layer Skin Friction in the Presence of Severe Aerodynamic Heating at Mach Numbers From 2.8 to 7.0. NACA TN-3391, 1955.

39. Hoerner, Sighard F.: Fluid-Dynamic Drag. Publ. by the author (148 Busteed Drive, Midland Park, New Jersey 07432), 1965.

40. Fisher, David F.; and Saltzman, Edwin J.: Local Skin Friction Coefficients and Boundary-Layer Profiles Obtained in Flight From the XB-70-1 Airplane at Mach Numbers up to 2.5. NASA TN D-7220, 1973.

41. Harris, Roy V., Jr.: An Analysis and Correlation of Aircraft Wave Drag. NASA TM X-947, 1964.

42. Lamar, John E.; and Gloss, Blair B.: Subsonic Aerodynamic Characteristics of Interacting Lifting Surfaces With Separated Flow Around Sharp Edges Predicted by a Vortex-Lattice Method. NASA TN D-7921, 1975.

43. Shrout, Barrett L.: Extension of a Numerical Solution for the Aerodynamic Characteristics of a Wing To Include a Canard or Horizontal Tail. Aerodynamic Interference, AGARD-CP-71-71, Jan. 1971, pp. 8-1 - 8-9.

44. Gaudet, L.; and Johnson, P.: Measurements of the Drag of Various Two Dimensional Excrescences Immersed in Turbulent Boundary Layers at Mach Numbers Between 0.2 and 2.8. Tech. Rep. 70190, British R.A.E., Oct. 1970.

45. Gaudet, L.; and Johnson, P.: Measurements of the Drag of Excrescences Immersed in Turbulent Boundary Layers at Mach Numbers Between 0.2 and 2.8: Circular Holes. Tech. Rep. 71181, British R.A.E., Sept. 1971.

46. Westkaemper, John Conrad: The Drag of Cylinders All or Partially Immersed in a Turbulent, Supersonic Boundary Layer. DRL-549, Univ. of Texas, Mar. 1, 1967. (Available from DDC as AD 813 886.)

47. Cnossen, J. W.: Efficiency of Flush Oblique Nozzles Exhausting Into Supersonic Streams Having Mach Numbers up to 4. R-1285-10 (Contract NOa(S)55-133-C), Res. Dept., United Aircraft Corp., Sept. 1959.

48. Abdalla, Kaleel L.: Performance Characteristics of Flush and Shielded Auxiliary Exits at Mach Numbers of 1.5 to 2.0. NASA MEMO 5-18-59E, 1959.

49. McFadden, Norman M.; Holden, George R.; and Ratcliff, Jack W.: Instrumentation and Calibration Technique for Flight Calibration of Angle-of-Attack Systems on Aircraft. NACA RM A52I23, 1952.

TABLE I.- GEOMETRIC CHARACTERISTICS OF THE XB-70-1 AIRPLANE

Wing:
Total area, includes 230.62 m^2 (2482.34 ft^2) covered by
fuselage but not 3.12 m^2 (33.53 ft^2) of wing ramp area,
m^2 (ft^2) 585.08 (6297.8)
Span, m (ft) 32 (105)
Aspect ratio 1.751
Taper ratio 0.019
Dihedral angle, deg 0
Root chord (wing station 0), m (ft) 35.89 (117.76)
Tip chord (wing station 16 m (630 in.)), m (ft) 0.67 (2.19)
Mean aerodynamic chord, m (in.) 23.94 (942.38)
Wing station of mean aerodynamic chord, m (in.) 5.43 (213.85)
Fuselage station of 25-percent wing mean aerodynamic chord,
m (in.) 41.18 (1621.22)
Sweepback angle at -
Leading edge, deg 65.57
25-percent element, deg 58.79
Trailing edge, deg 0
Airfoil section . . . . 0.30 to 0.70 hexagonal (modified)
Thickness at wing station -
Root to 4.72 m (186 in.), percent chord 2.0
11.68 m to 16 m (460 in. to 630 in.), percent chord 2.5

Folding wing tip (data for one tip only):
Area, m^2 (ft^2) 48.39 (520.90)
Span, m (ft) 6.33 (20.78)
Aspect ratio 0.829
Taper ratio 0.046
Root chord (wing station 9.67 m (380.62 in.)), m (ft) 14.61 (47.94)
Tip chord (wing station 16 m (630 in.)), m (ft) 0.67 (2.19)
Mean aerodynamic chord (wing station 11.87 m (467.37 in.)),
m (in.) 9.76 (384.25)
Down deflection from inboard wing, deg 0, 25.65
Angle of tip fold hinge line -
Leading edge in, deg 1.5
Leading edge down, deg 3

TABLE I.- Continued

Elevons (data for one side):
  Total effective area aft of hinge line, includes 0.31 m^2
    (3.33 ft^2) air gap at wing-tip fold line, m^2 (ft^2) 18.37 (197.7)
  Span for -
    Wing tips up, m (ft) 6.23 (20.44)
    Wing tips down, m (ft) 4.26 (13.98)
  Chord, m (in.) 2.95 (116)
  Sweepback of hinge line, deg 0
  Deflection -
    As elevator, deg . . . . -25 to 15
    As aileron with elevators at $\pm15^o$ or less, deg . . . . -15 to 15
    As aileron with elevators at -25°, deg . . . . -5 to 5
    Total, deg . . . . -30 to 30

Canard:
  Area, includes 13.96 m^2 (150.31 ft^2) covered by fuselage,
    m^2 (ft^2) 38.61 (415.59)
  Span, m (ft) 8.78 (28.81)
  Aspect ratio 1.997
  Taper ratio 0.388
  Dihedral angle, deg 0
  Root chord (canard station 0), m (ft) 6.34 (20.79)
  Tip chord (canard station 4.39 m (172.86 in.)), m (ft) 2.46 (8.06)
  Mean aerodynamic chord, m (in.) 4.68 (184.3)
  Canard station of mean aerodynamic chord, m (in.) 1.87 (73.71)
  Fuselage station of 25-percent chord, m (in.) 14.06 (553.73)
  Sweepback angle at -
    Leading edge, deg 31.70
    25-percent element, deg 21.64
    Trailing edge, deg . . . . -14.91
  Incidence angle (nose up), deg . . . . 0 to 6
  Airfoil section at -
    Root (thickness-chord ratio
      2.5 percent) . . . . 0.34 to 0.66 hexagonal (modified)
    Tip (thickness-chord ratio
      2.52 percent) . . . . 0.34 to 0.66 hexagonal (modified)
  Ratio of canard area to wing area 0.066

TABLE I.- Continued

Canard flap (one of two) -
   Area (aft of hinge line), m^2 (ft^2) 5.08 (54.69)
   Ratio of flap area to canard semiarea 0.263

Vertical tail (one of two):
  Area (includes 0.83 m^2 (8.96 ft^2) blanketed area),
    m^2 (ft^2) 21.74 (233.96)
  Span, m (ft) 4.57 (15)
  Aspect ratio 1
  Taper ratio 0.30
  Root chord (vertical-tail station 0), m (ft) 7.03 (23.08)
  Tip chord (vertical-tail station 4.57 m (180 in.), m (ft) . . . 2.11 (6.92)
  Mean aerodynamic chord (vertical-tail station 1.88 m
    (73.85 in.)), m (in.) 5.01 (197.40)
  Fuselage station of 25-percent vertical-tail mean
    aerodynamic chord, m (in.) 55.59 (2188.50)
  Sweepback angle at -
    Leading edge, deg 51.77
    25-percent element, deg 45
    Trailing edge, deg 10.89
  Airfoil section at -
    Root (thickness-chord ratio
      3.75 percent) . . . . 0.30 to 0.70 hexagonal (modified)
    Tip (thickness-chord ratio
      2.5 percent) . . . . 0.30 to 0.70 hexagonal (modified)
  Cant angle, deg 0
  Ratio of vertical tail to wing area 0.037
  Rudder travel with -
    Gear extended, deg . . . . ±12
    Gear retracted, deg . . . . ±3

Shaker vane (one of two):
  Area (exposed), m^2 (ft^2) 0.20 (2.11)
  Span (exposed), m (ft) 0.63 (2.08)
  Aspect ratio 2.05
  Taper ratio 0.50
  Root chord, m (ft) 0.41 (1.36)
  Tip chord, m (ft) 0.20 (0.67)

TABLE I.- Concluded

Mean aerodynamic chord, m (ft) 0.32 (1.06)
Fuselage station of shaker vane, 25-percent mean aerodynamic
   chord, m (in.) 8.22 (323.5)
Sweepback angle at -
   Leading edge, deg 6.5
   Trailing edge, deg . . . . -12.4
Airfoil section at -
   Root (thickness-chord ratio 7.8 percent) . . . . . . 0.20 to 0.40 hexagonal
   Tip (thickness-chord ratio 10.4 percent) . . . . . . 0.27 to 0.54 hexagonal

Fuselage (includes canopy):
   Length, m (ft) 56.62 (185.75)
   Maximum depth (fuselage station 22.30 m (878 in.)),
     m (in.) 2.72 (106.92)
   Maximum breadth (fuselage station 21.72 m (855 in.)),
     m (in.) 2.54 (100)
   Side area, m^2 (ft^2) 87.3 (939.72)
   Planform area, m^2 (ft^2) 110.07 (1184.78)
   Center of gravity of -
     Forward limit, percent mean aerodynamic chord 19.0
     Aft limit, percent mean aerodynamic chord 25.0

Duct:
   Length, m (ft) 31.96 (104.84)
   Maximum depth (fuselage station 34.93 m (1375 in.)),
     m (in.) 2.31 (90.75)
   Maximum breadth (fuselage station 53.34 m (2100 in.)),
     m (in.) 9.16 (360.70)
   Side area, m^2 (ft^2) 66.58 (716.66)
   Planform area, m^2 (ft^2) 217.61 (2342.33)
   Inlet captive area (each), m^2 (in^2) 3.61 (5600)

Surface areas (net wetted), m^2 (ft^2):
   Fuselage, canopy, boundary-layer gutter, and tailpipes . . . 264.77 (2850.0)
   Duct 318.71 (3430.6)
   Wing, wing tips, and wing ramp 864.71 (9307.7)
   Vertical tails (two) 87.12 (937.7)
   Canard 49.47 (532.5)
   Total 1584.79 (17 058.5)

Engines 6 YJ93-GE-3

TABLE II.- AIRPLANE CONFIGURATION FOR XB-70-1 FLIGHT TESTS

Point	Mass		c.g., percent $\bar{c}$	$\delta_{y,L}$, deg	$\delta_{y,R}$, deg	δ_c, deg	δ_e, deg	$\delta_{r,L}$, deg	$\delta_{r,R}$, deg	Nose-ramp position	δ_{bp}, deg	Shaker vane
	kg	lb										
P1	144 421	318 394	24.1	-1.0	-0.5	2.26	2.7	0.1	-0.2	Down	0.0	On
P2	217 865	480 310	21.9	23.0	24.7	2.15	2.4	.6	-.1	Down	.0	On
P3	156 240	344 450	22.3	23.8	25.3	.90	10.4	.1	.3	Down	3.2	On
P4	181 484	400 104	21.7	60.0	63.7	1.14	9.7	-.4	.1	Down	3.3	On
P5	170 687	376 300	22.0	64.9	67.2	1.38	9.3	-.4	-.1	Down	2.8	On
P6	177 994	392 409	21.1	60.8	63.8	1.98	6.2	-.5	.0	Down	7.4	On
P7	160 361	353 535	21.1	63.4	61.7	2.59	3.7	-.8	-.1	Down	6.8	Off
P8	170 785	376 516	21.8	63.9	62.9	2.82	3.2	-.7	.2	Up	1.8	On
P9	173 087	381 591	21.6	61.1	63.2	2.76	3.0	-.3	.4	Down	3.8	On
P10	198 209	436 975	22.3	24.0	24.0	.51	12.4	(a)	(a)	Down	1.5	Off
P3L	155 751	342 050	21.5	23.2	24.7	.41	12.8	(a)	(a)	Down	3.4	On
P3H	154 788	341 250	21.0	23.2	24.8	1.61	6.8	(a)	(a)	Down	3.2	On
P8L	163 981	361 516	20.5	64.2	62.5	2.70	4.6	-.8	.3	Up	2.1	On
P8H	163 663	360 816	20.5	64.0	62.2	4.07	-5.2	-.6	.1	Up	2.1	On

aRudder deflections were not measured during P10, P3L, and P3H.

TABLE III.- FLIGHT CONDITIONS FOR XB-70-1 FLIGHT TESTS

Point	Flight	Data time	Mach	Pressure altitude		p_∞		q_∞		T_∞		$R_{\bar{c}}$	α, deg	Normal acceleration, g units	Pitch rate, deg/sec
				m	ft	N/m²	lb/ft²	N/m²	lb/ft²	K	°R				
P1	81	2:47:35	0.76	7 842	25 730	36 414	760.5	14 684	306.7	240.2	432.3	191.3 × 10⁶	4.4	1.015	0.0
P2	76	1:23:18	.93	9 988	32 770	26 477	553.0	16 030	334.8	235.9	424.6	174.3	5.7	1.020	.0
P3	76	2:14:16	1.18	10 278	33 720	25 328	529.0	24 478	511.3	232.5	418.5	216.5	3.2	1.017	.0
P4	81	1:55:50	1.60	11 756	38 570	20 086	419.5	36 355	759.3	207.7	373.8	269.1	3.1	1.000	.0
P5	79	1:53:47	1.67	12 807	42 020	17 017	355.4	33 260	694.7	212.5	382.5	231.2	2.9	1.000	.0
P6	79	1:42:41	2.10	14 813	48 600	12 406	259.1	38 297	799.8	210.5	378.9	216.5	2.9	1.000	.0
P7	67	2:11:59	2.15	17 563	57 620	8 039	167.9	26 037	543.8	207.9	374.2	147.3	4.3	1.049	.0
P8	70	1:58:06	2.53	19 187	62 950	6 226	130.0	27 801	580.6	210.9	379.6	133.0	4.7	.983	.0
P9	82	1:50:48	2.50	18 784	61 630	6 631	138.5	28 966	605.0	213.8	384.8	137.8	4.6	1.000	.0
P10	66	1:35:02	1.06	8 272	27 140	34 220	714.7	26 813	560.0	247.4	445.3	242.0	3.9	1.000	.0
P3L	76	2:15:49	1.15	10 400	34 121	24 855	519.1	23 130	483.1	232.2	417.9	208.7	2.2	.656	-.55
P3H	76	2:16:08	1.17	10 046	32 960	26 243	548.1	25 233	527.0	234.4	422.0	221.3	4.4	1.508	.83
P8L	70	2:05:25	2.51	19 205	63 010	6 205	129.6	27 257	569.3	211.1	380.0	130.0	3.7	.811	-.18
P8H	70	2:05:45	2.56	19 224	63 070	6 186	129.2	28 468	594.6	208.3	374.8	134.5	6.7	1.497	.57

TABLE IV.- INTERPOLATED WIND-TUNNEL DATA

Wind-tunnel tests	P1	P2	P3	P4	P5	P6	P7		P8	P9	P10	P3L	P3H	P8L	P8H
Point / Flight Mach number	0.76	0.93	1.18	1.60	1.67	2.10	2.15		2.53	2.50	1.06	1.15	1.17	2.51	2.56
Test conditions:															
Mach number	0.75	0.95	1.20	1.60	2.10	2.10	2.10	2.15	2.53	2.53	(a)	1.20	1.20	2.53	2.53
$R_c \times 10^{-6}$	9.42	9.42	9.42	9.42	9.42	9.42	9.42	9.42	9.42	9.42	9.42	9.42	9.42	9.42	9.42
δ_y, deg	0	25	25	65	65	65	65	65	65	65	25	25	25	65	65
α_{wt}, deg	4.53	5.91	3.22	2.93	3.07	2.88	3.95	3.95	4.20	4.08	2.83	2.32	4.24	3.25	5.80
Data for $\delta_c = \delta_e = 0°$:															
C_L	0.152	0.226	0.094	0.074	0.078	0.068	0.098	0.093	0.098	0.095	0.077	0.055	0.140	0.074	0.139
C_D	.01638	.02696	.01547	.01362	.01386	.01308	.01548	.01511	.01567	.01533	.01506	.01372	.01886	.01333	.02157
C_m	-.0005	-.0028	.0078	.0066	.0063	.0017	.0000	-.0012	-.0015	-.0013	.0118	.0119	.0024	.0000	-.0042
Data for canard:															
$\delta_{c,flt}$, deg	2.26	2.15	0.90	1.14	1.38	1.98	2.59	2.59	2.82	2.76	0.51	0.41	1.61	2.70	4.07
$\delta_{c,flex}$, deg	.07	.17	.08	.01	.00	-.21	-.09	-.09	.01	-.03	.08	.08	.09	-.03	.10
$\delta_{c,wt}$, deg	2.33	2.32	.98	1.15	1.38	1.77	2.50	2.50	2.83	2.73	.59	.49	1.70	2.67	4.17
ΔC_L	0	0	0	0	0	0	0	0	.002	.002	0	0	0	-.002	.003
ΔC_D	.00073	.00126	.00013	.00032	.00038	.00030	.00041	.00045	.00050	.00048	.00002	.00004	.00048	.00038	.00102
ΔC_m	.0070	.0079	.0023	.0024	.0028	.0036	.0048	.0040	.0045	.0044	.0024	.0011	.0040	.0044	.0070
Data for elevon:															
δ_e, deg	2.7	2.4	10.4	9.7	9.3	6.2	3.7	3.7	3.2	3.0	12.4	12.8	6.8	4.6	-5.2
ΔC_L	.022	.013	.024	.016	.015	-.007	.004	.002	.002	.002	.053	.029	.017	.003	-.004
ΔC_D	.00167	.00154	.00502	.00352	.00342	.00148	.00087	.00058	.00048	.00043	.00772	.00634	.00297	.00070	-.00030
ΔC_m	-.0118	-.0087	-.0176	-.0106	-.0101	-.0044	-.0025	-.0022	-.0019	-.0018	-.0403	-.0220	-.0116	-.0028	-.0026
At test Mach number:															
C_L	0.174	0.239	0.118	0.090	0.093	0.075	0.102	0.097	0.102	0.099	0.130	0.084	0.157	0.079	0.138
C_D	.01878	.02976	.02062	.01746	.01766	.01486	.01676	.01614	.01665	.01624	.02280	.02010	.02231	.01441	.02229
C_m	-.0053	-.0036	-.0075	-.0016	-.0010	.0009	.0023	.0006	.0011	.0013	-.0261	-.0090	-.0052	.0016	.0054
At flight Mach number:[b]															
C_L	0.174	0.239	0.118	0.090	0.092	0.075		0.101	0.102	0.099	0.130	0.084	0.157	0.079	0.138
C_D	.01881	.02962	.02071	.01746	.01748	.01486		.01669	.01665	.01624	.02280	.02036	.02243	.01441	.02229
C_m	-.0054	-.0028	-.0068	-.0016	-.0012	-.0009		.0021	.0011	.0013	-.0261	-.0075	-.0041	.0016	.0054
α, deg	4.51	6.00	3.22	2.93	3.07	2.88		3.95	4.20	4.08	2.83	2.37	4.21	3.24	5.83

[a]Results are interpolated from data at test Mach numbers of 0.75, 0.80, 0.95, 1.20, and 1.40.
[b]Corrected for compressibility effects due to differences between flight and test Mach numbers.

30

TABLE V.- ADJUSTMENTS TO WIND-TUNNEL DATA

Wind-tunnel data	P1	P2	P3	P4	P5	P6	P7	P8	P9	P10	P3L	P3H	P8L	P8H
Tip deflection:														
$\delta_{Y,L}$, deg	-1.0	23.0	23.8	60.0	64.9	60.8	63.4	63.9	61.1	24.0	23.2	23.2	64.2	64.0
$\delta_{Y,R}$, deg	-.5	24.7	25.3	63.7	67.2	63.8	61.7	62.9	63.2	24.0	24.7	24.8	62.5	62.2
ΔC_L	(a)	(a)	(a)	(a)	(a)	(a)	(a)	(a)	(a)	(a)	(a)	(a)	(a)	(a)
ΔC_D	(a)	-.00006	(a)	(a)	(a)	(a)	(a)	(a)	(a)	(a)	(a)	(a)	(a)	(a)
ΔC_m	(a)	-.0023	(a)	-.0005	(a)	-.0006	-.0005	(a)	(a)	(a)	(a)	(a)	(a)	(a)
Shaker:														
ΔC_L	0.00036	0.00036	0.00029	0.00015	0.00014	0.00003	[b]0	-0.00007	-0.00007	[b]0	0.00025	0.00025	-0.00007	-0.00007
ΔC_D	(a)	(a)	(a)	(a)	(a)	(a)	0	(a)	(a)	0	(a)	(a)	(a)	(a)
ΔC_m	(a)	(a)	-.0002	(a)	(a)	(a)	0	(a)	(a)	0	-.0002	-.0002	(a)	(a)
Afterbody:														
ΔC_L	(a)	(a)	(a)	[c]0	0	0	0	0	0	(a)	(a)	(a)	0	0
ΔC_D	0.00012	0.00012	0.00011	0	0	0	0	0	0	0.00012	0.00015	0.00015	0	0
ΔC_m	-.0008	-.0008	-.0006	0	0	0	0	0	0	(a)	-.0006	-.0006	0	0
Canopy:														
ΔC_L	(a)	(a)	(a)	(a)	(a)	(a)	(a)	[d]0	(a)	(a)	(a)	(a)	[d]0	[d]0
ΔC_D	(a)	(a)	0.00058	0.00063	0.00062	0.00049	0.00047	0	0.00031	0.00040	0.00045	0.00045	0	0
ΔC_m	(a)	-0.0010	-.0006	(a)	(a)	-.0006	-.0006	0	-.0006	-.0012	-.0006	-.0006	0	0
Spillage drag:														
$(m/m_\infty)_{wt}$	0.527	0.527	0.540	0.639	0.661	0.794	0.803	0.897	0.890	0.520	0.533	0.535	0.894	0.895
$(m/m_\infty)_{flt}$	.517	.506	.541	.642	.660	.793	.808	.898	.891	.520	.535	.538	.895	.906
ΔC_L	(a)	(a)	(a)	(a)	(a)	(e)	(e)	(e)	(e)	(a)	(a)	(a)	(e)	(e)
ΔC_D	.00020	.00035	-.00001	-.00003	(a)	(e)	(e)	(e)	(e)	(a)	-.00002	-.00003	(e)	(e)
ΔC_m	.0002	.0002	(a)	(a)	(a)	(e)	(e)	(e)	(e)	(a)	(a)	(a)	(e)	(e)
Trip:														
ΔC_D	-0.00026	-0.00033	-0.00022	-0.00015	-0.00017	-0.00028	-0.00029	-0.00037	-0.00037	-0.00033	-0.00022	-0.00022	-0.00037	-0.00037
Corrected wind-tunnel data:														
C_L	0.174	0.239	0.118	0.090	0.092	0.075	0.101	0.102	0.099	0.130	0.084	0.157	0.079	0.138
C_D	.01923	.03006	.02146	.01806	.01807	.01510	.01687	.01621	.01611	.02299	.02097	.02303	.01397	.02185
C_m	-.0060	-.0067	-.0082	-.0021	-.0012	-.0003	.0010	.0011	.0007	-.0273	-.0089	-.0055	.0016	.0054
α, deg	4.51	6.00	3.22	2.93	3.07	2.88	3.95	4.20	4.08	2.83	2.37	4.21	3.24	5.83

[a] Increment is negligible.
[b] Shaker was not installed on XB-70-1 during flights for P7 and P10.
[c] Supersonic afterbody used on basic wind-tunnel model at M = 1.6, 2.1, and 2.53 for P4 to P9.
[d] Canopy was up during P8, P8L, and P8H.
[e] Assumed to be negligible since inlet was started at M ≥ 2.0.

TABLE VI.- EXTRAPOLATION OF WIND-TUNNEL DATA TO FULL SCALE

Wind-tunnel data	P1	P2	P3	P4	P5	P6	P7	P8	P9	P10	P3L	P3H	P8L	P8H
Flight test condition:														
XB-70-1 flight	81	76	76	81	79	79	67	70	82	66	76	76	70	70
Mach number	0.76	0.93	1.18	1.60	1.67	2.10	2.15	2.53	2.50	1.06	1.15	1.17	2.51	2.56
Normal acceleration, g	1.0	1.0	1.0	1.0	1.0	1.0	1.0	1.0	1.0	1.0	0.63	1.48	0.81	1.52
c.g., percent $\bar{c}$	24.1	21.9	22.3	21.7	22.0	21.1	21.1	21.8	21.6	22.3	21.5	21.0	20.5	20.5
$R_{\bar{c}} \times 10^{-6}$	191.3	174.3	216.5	269.1	231.3	216.5	147.2	133.0	137.8	242.0	208.7	221.3	130.0	134.5
Skin friction:														
$C_{D,sf,wt}$	0.00774	0.00759	0.00732	0.00691	0.00684	0.00645	0.00639	0.00603	0.00603	0.00745	0.00735	0.00733	0.00605	0.00600
$C_{D,sf,flt}$	.00497	.00492	.00459	.00414	.00417	.00394	.00412	.00390	.00390	.00461	.00464	.00458	.00393	.00386
$\Delta C_{D,sf}$	-.00277	-.00267	-.00273	-.00277	-.00267	-.00251	-.00227	-.00213	-.00213	-.00284	-.00271	-.00275	-.00212	-.00214
Bleed dump:														
ΔC_L	(a)	(a)	(a)	(a)	(a)	(a)	(a)	(a)	(a)	(a)	(a)	(a)	(a)	(a)
ΔC_D	0.00004	0.00004	0.00041	0.00036	0.00035	0.00029	0.00028	0.00021	0.00022	0.00042	0.00041	0.00041	0.00023	0.00027
ΔC_m	(a)	-.0018	-.0011	-.0005	-.0004	(a)	(a)	.0007	.0006	-.0017	-.0012	-.0011	.0006	.0007
Closure:														
ΔC_D	(a)	(a)	0.00006	0.00005	0.00005	0.00004	0.00004	0.00004	0.00004	0.00007	0.00006	0.00006	0.00004	0.00004
Bypass doors:														
δ_{bp}, deg	0	0	3.23	3.27	2.80	7.40	6.78	1.80	3.80	1.51	3.37	3.17	2.09	2.08
ΔC_D	0	0	.00004	.00002	.00001	.00007	.00006	(a)	.00002	.00002	.00004	.00004	(a)	(a)
ΔC_m	0	0	.0010	(a)	(a)	(a)	(a)	(a)	(a)	.0010	.0010	.0010	(a)	(a)
Flexibility:														
ΔC_L	-0.008	-0.009	-0.011	-0.006	-0.005	0.001	(a)	(a)	(a)	bNC	-0.014	-0.009	0.000	0.000
ΔC_D	-.00084	-.00126	-.00057	-.00038	-.00034	.00005	0.00001	-0.00004	-0.00004	bNC	-.00017	-.00055	-.00004	-.00003
ΔC_m	.0026	.0034	.0059	.0029	.0025	-.0005	-.0001	.0002	.0002	bNC	.0073	.0046	.0002	.0001
Roughness, protuberance, and leakage:														
$\Delta C_{D,rough}$	0.00015	0.00016	0.00017	0.00020	0.00019	0.00016	0.00014	0.00012	0.00012	0.00018	0.00017	0.00017	0.00012	0.00012
$\Delta C_{D,prot}$	.00017	.00041	.00086	.00059	.00056	.00039	.00038	.00035	.00035	.00086	.00086	.00086	.00035	.00035
$\Delta C_{D,leak}$	.00001	.00001	.00001	.00002	.00002	.00002	.00004	.00004	.00003	.00002	.00001	.00001	.00004	.00004
Air interference drag:														
$\Delta C_{D,bli}$	0.00003	0.00005	0.00005	0.00007	0.00008	0.00005	0.00006	0.00007	0.00005	0.00009	0.00005	0.00005	0.00007	0.00007
$\Delta C_{D,div}$	.00031	.00030	.00026	.00021	.00017	.00023	.00013	.00014	.00016	.00023	.00026	.00026	.00014	.00014
$\Delta C_{D,bpi}$	0	0	.00017	.00006	.00005	.00050	.00037	.00014	.00002	.00008	.00017	.00017	.00014	.00014
Base drag:														
$\Delta C_{D,base}$	0.00097	-0.00036	0.00275	0.00162	0.00132	0.00049	0.00036	0.00000	0.00000	0.00231	0.00269	0.00270	-0.00010	-0.00020
Extrapolated results:														
C_L	0.166	0.230	0.107	0.084	0.087	0.076	0.101	0.102	0.099	0.130	0.070	0.148	0.079	0.138
C_D	.01730	.02674	.02294	.01811	.01786	.01488	.01647	.01515	.01495	.02443	.02281	.02446	.01284	.02059
C_m	-.0034	-.0051	-.0024	.0003	.0009	-.0008	.0009	.0020	.0015	-.0280	-.0018	-.0010	.0024	.0062
α, deg	4.51	6.00	3.22	2.93	3.07	2.88	3.95	4.20	4.08	2.83	2.37	4.21	3.24	5.83

aIndicates increment is negligible.
bIndicates increment was not calculated.

TABLE VII.- XB-70-1 WETTED AREAS, LENGTHS, AND SHAPE FACTORS

Component	Wetted area		Average length		Shape factors									
	m²	ft²	m	ft	Due to taper	Due to dynamic pressure				Total of taper and dynamic pressure			
						M ≤ 1.2	M = 1.6	M = 2.1	M = 2.53	M ≤ 1.2	M = 1.6	M = 2.1	M = 2.53
Fuselage and boundary-layer gutter	264.8	2850.0	54.9	180.0	1.000	1.015	1.000	1.000	1.000	1.015	1.000	1.000	1.000
Wing top	520.7	5605.2	17.6	57.6	.974	1.027	1.000	1.000	1.000	1.000	.974	.974	.974
Wing bottom	344.0	3702.5	15.0	49.2	.974	1.027	1.037	1.166	1.258	1.000	1.010	1.136	1.224
Duct sides	91.2	981.2	27.1	88.9	1.000	1.075	1.010	1.090	1.150	1.075	1.010	1.090	1.150
Duct bottom	227.6	2449.4	27.1	88.9	1.000	1.075	1.000	1.000	1.000	1.075	1.000	1.000	1.000
Canard	49.5	532.5	3.8	12.6	.996	1.030	1.000	1.000	1.000	1.026	.996	.996	.996
Vertical tails	87.1	937.7	4.5	14.8	.992	1.038	1.000	1.000	1.000	1.030	.992	.992	.992
Shaker vane	.8	8.5	.3	1.0	.997	1.114	1.000	1.000	1.000	1.111	.997	.997	.997

TABLE VIII.- COMPARISON OF FLIGHT ANGLE OF ATTACK AND PREDICTED ANGLE OF ATTACK AT THE FLIGHT LIFT COEFFICIENT

Test parameters	Point													
	P1	P2	P3	P4	P5	P6	P7	P8	P9	P10	P3L	P3H	P8L	P8H
$C_{L,flt}$	0.166	0.230	0.107	0.082	0.085	0.077	0.106	0.098	0.098	0.122	0.073	0.153	0.080	0.141
α_{flt}	4.4	5.7	3.2	3.1	2.9	2.9	4.3	4.7	4.6	3.9	2.2	4.4	3.7	6.7
α_{pred}	4.5	6.0	3.2	2.9	3.0	2.9	4.1	4.1	4.0	2.6	2.4	4.3	3.3	6.0
$\Delta\alpha$	-.1	-.3	.0	.2	-.1	.0	.2	.6	.6	1.3	-.2	.1	.4	.7
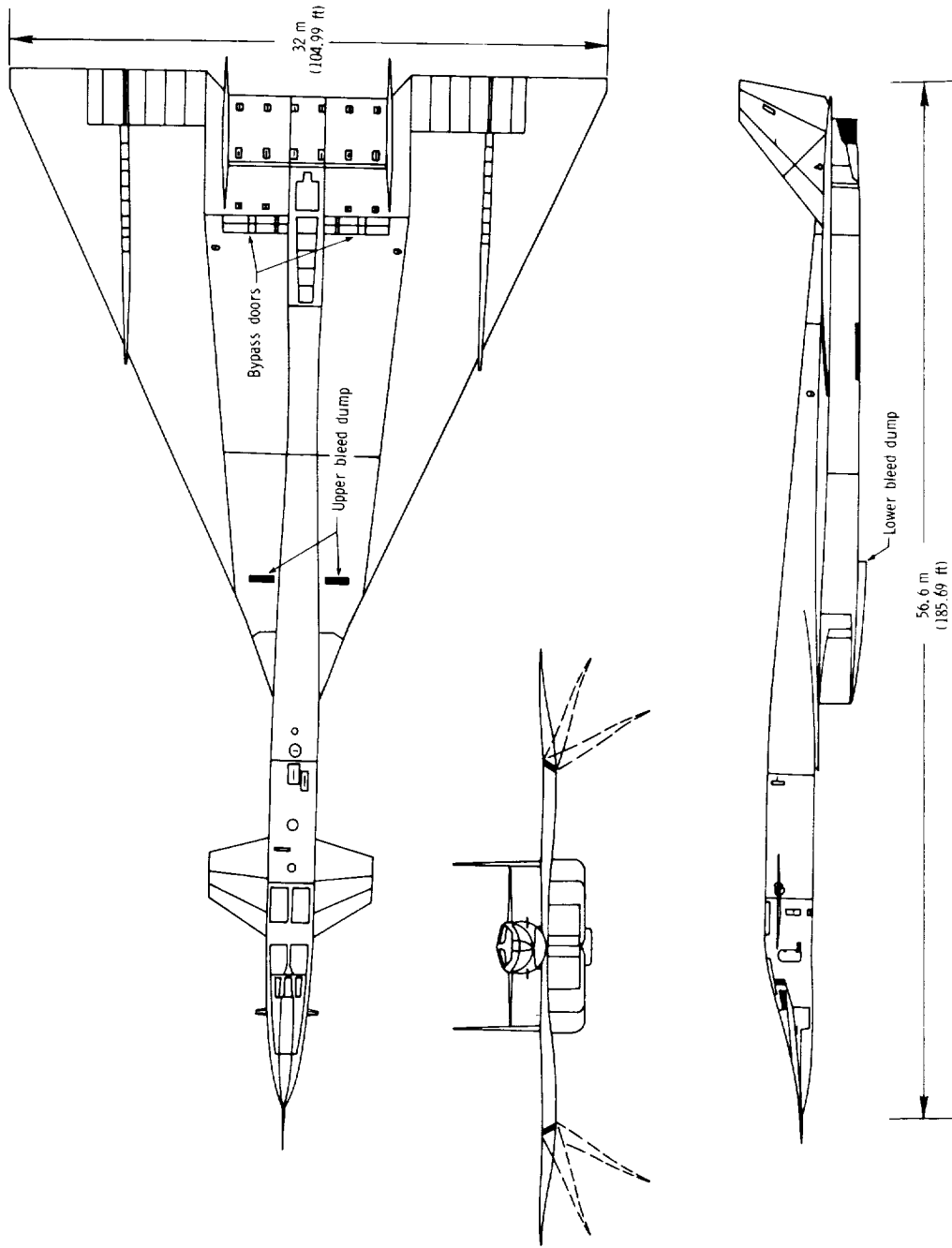
Figure 1.- Three-view drawing of XB-70-1 airplane.

32 m
(104.99 ft)

Bypass doors

Upper bleed dump

Lower bleed dump

56.6 m
(185.69 ft)

34
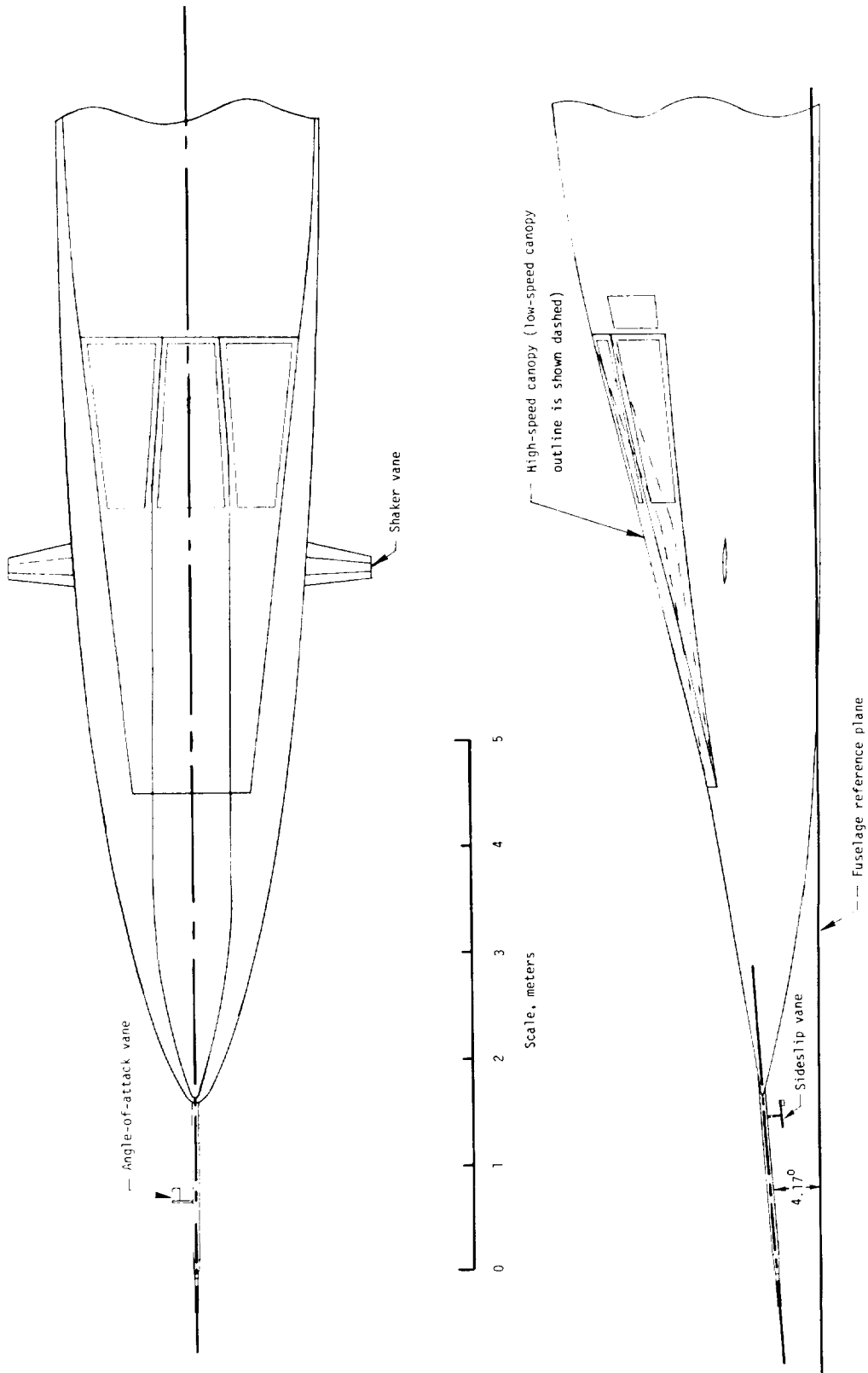
Figure 2.- Drawing of XB-70-1 nose section showing high- and low-speed canopies, shaker vane, and nose boom.

Angle-of-attack vane

Shaker vane

Scale, meters

High-speed canopy (low-speed canopy outline is shown dashed)

Fuselage reference plane

Sideslip vane

4.17^0

35
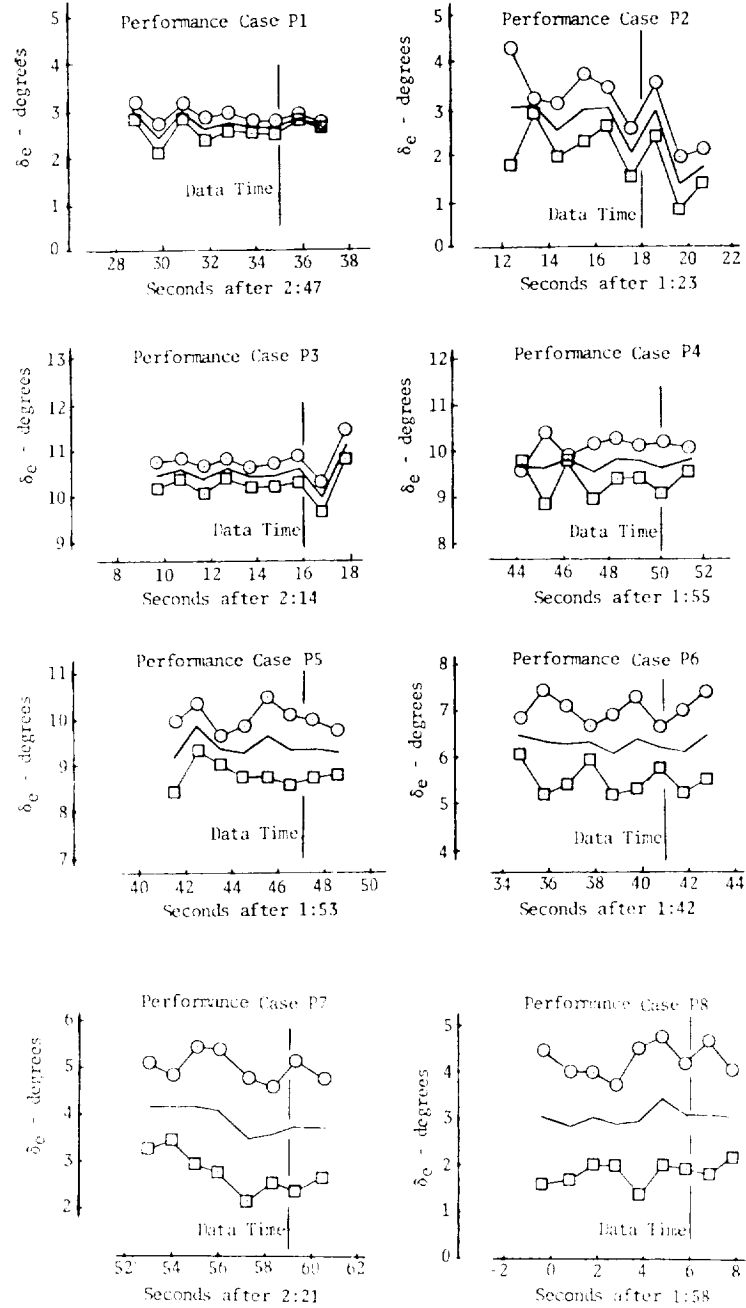
Figure 3.- Time histories of elevon deflections.

36
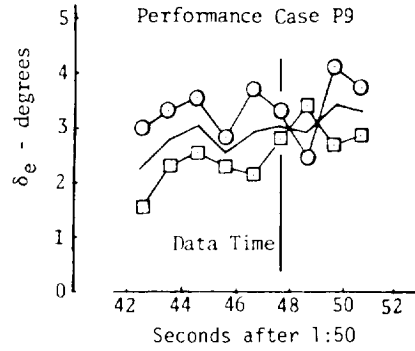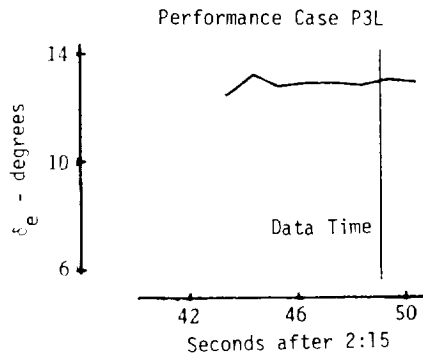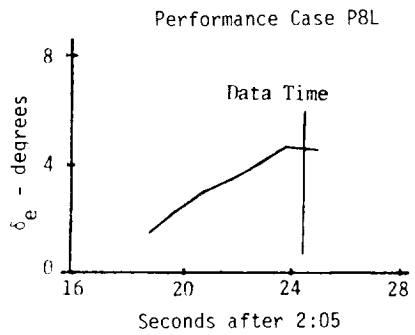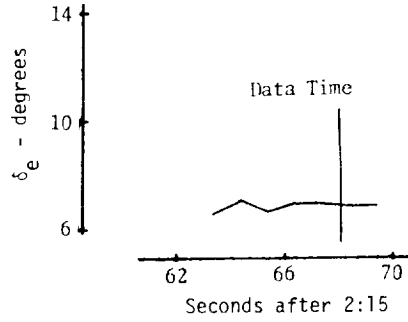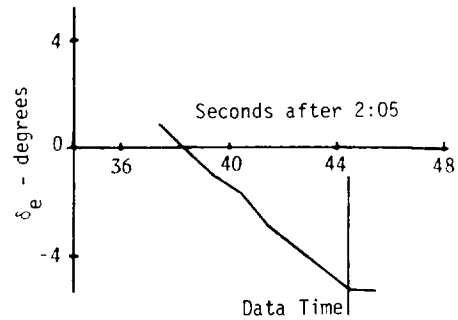
Figure 3.- Concluded.
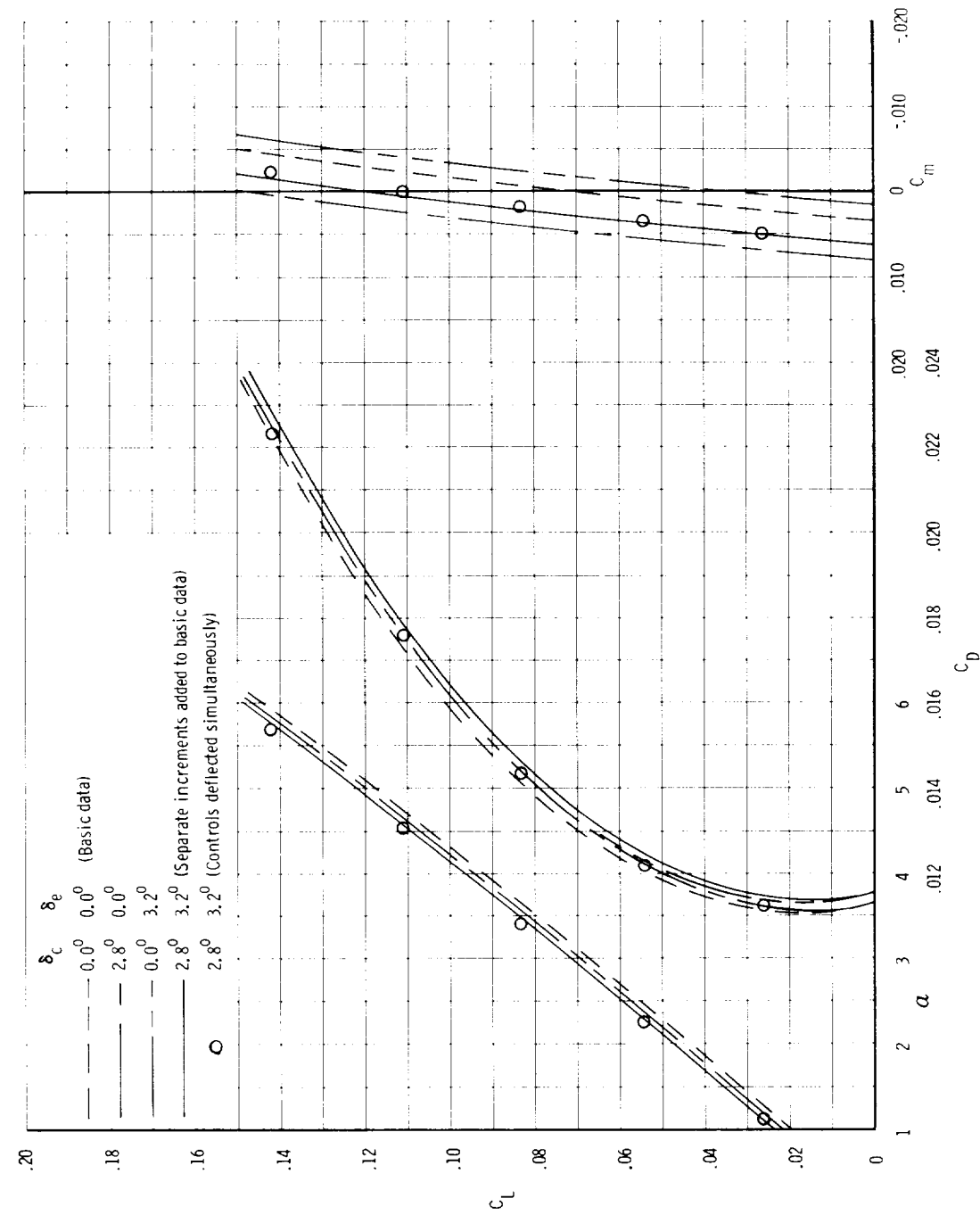
Figure 4.- Comparison of results obtained from addition of increments due to canard and elevon being deflected separately with results obtained from deflection of canard and elevon simultaneously at M = 2.53.
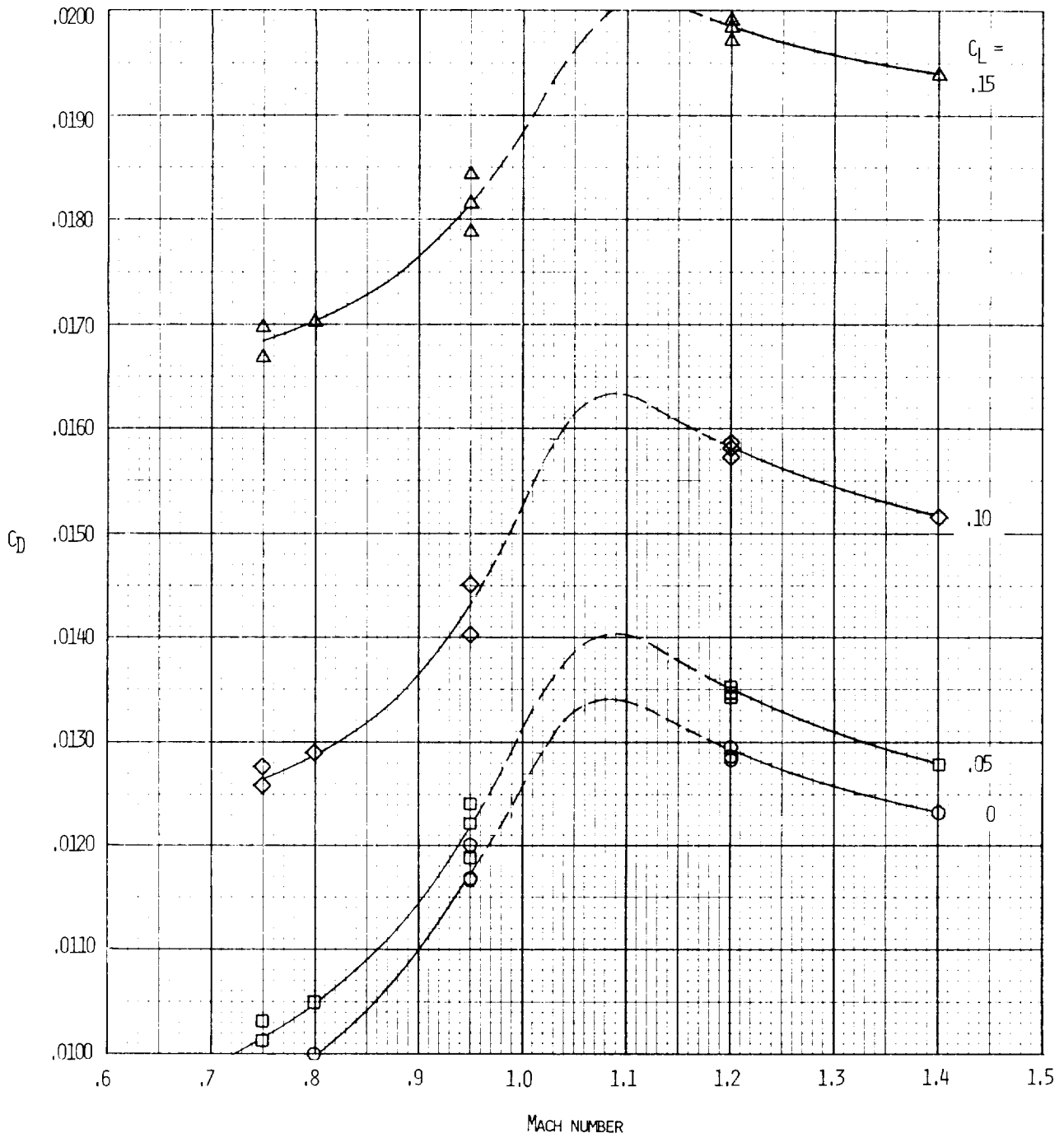
Figure 5.- Effect of Mach number on C_D at various values of C_L for $\delta_y = 25^O$ and $\delta_c = \delta_e = 0^O$.
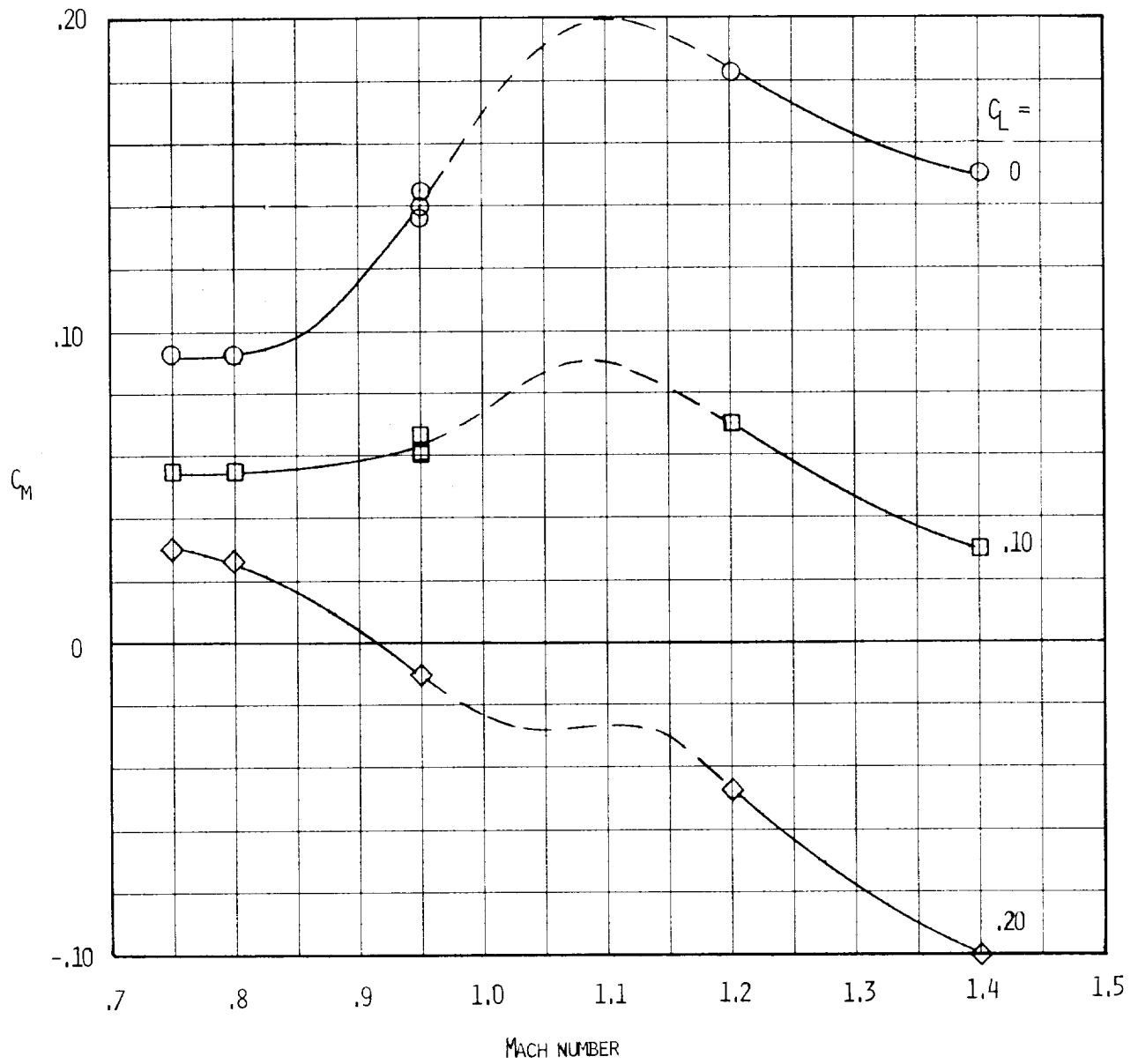
Figure 6.- Effect of Mach number on C_m for $\delta_y = 25^o$ and $\delta_c = \delta_e = 0^o$.
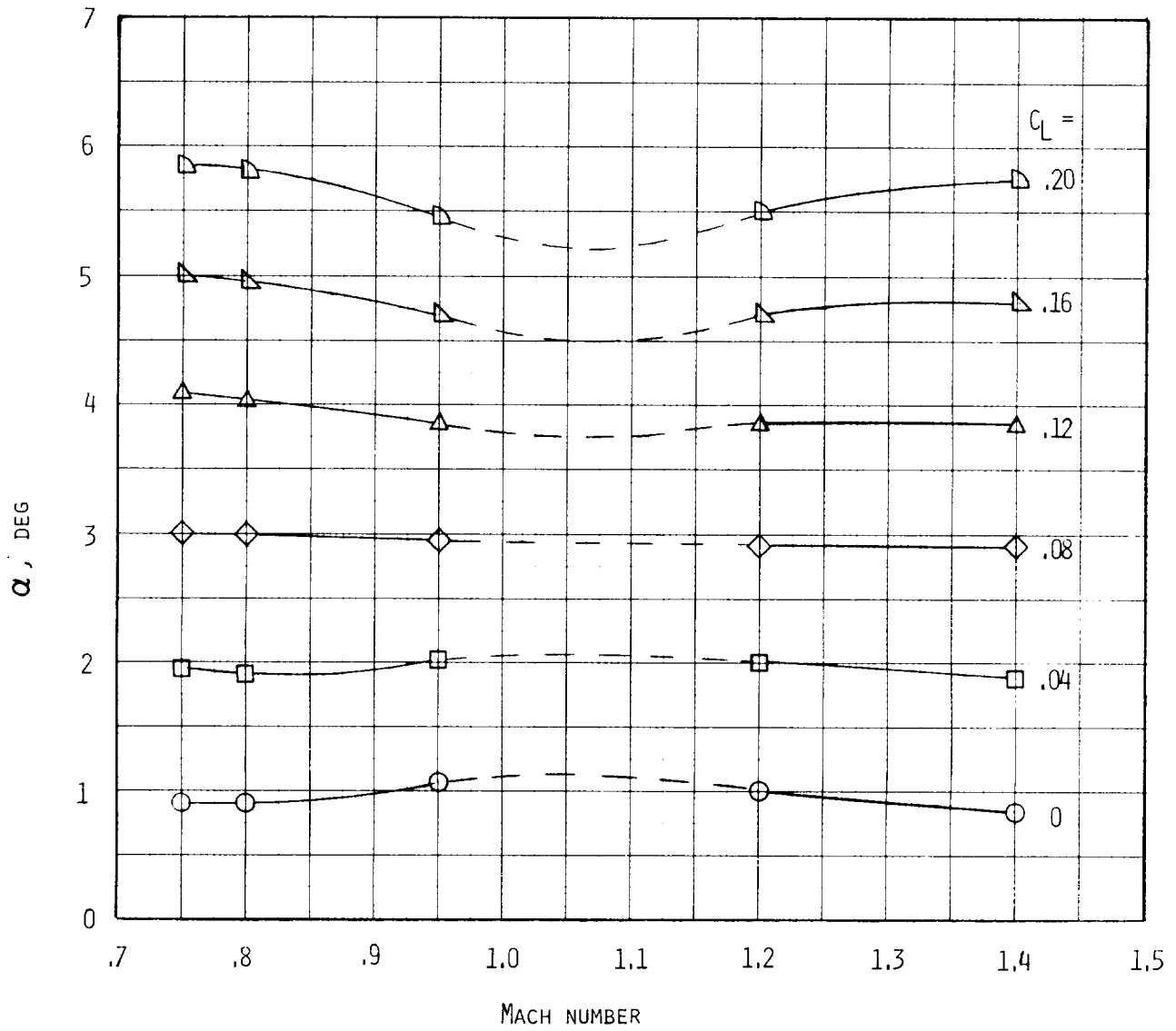
Figure 7.- Effect of Mach number on α for $\delta_y = 25^o$ and $\delta_c = \delta_e = 0^o$.
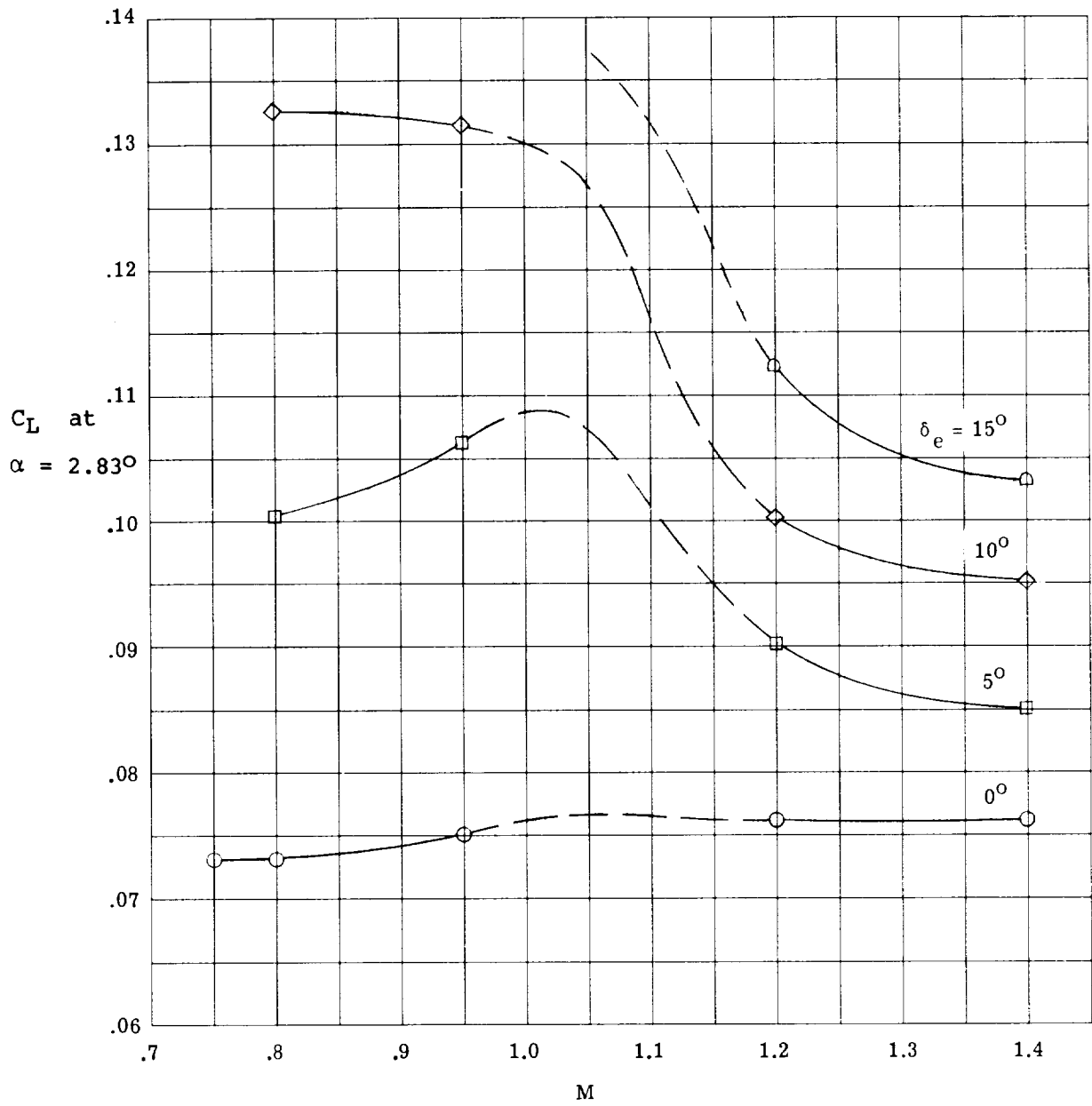
Figure 8.– Effect of δ_e on C_L at $\alpha = 2.83^O$ and $\delta_y = 25^O$.
(Effect of δ_c is negligible.)

42
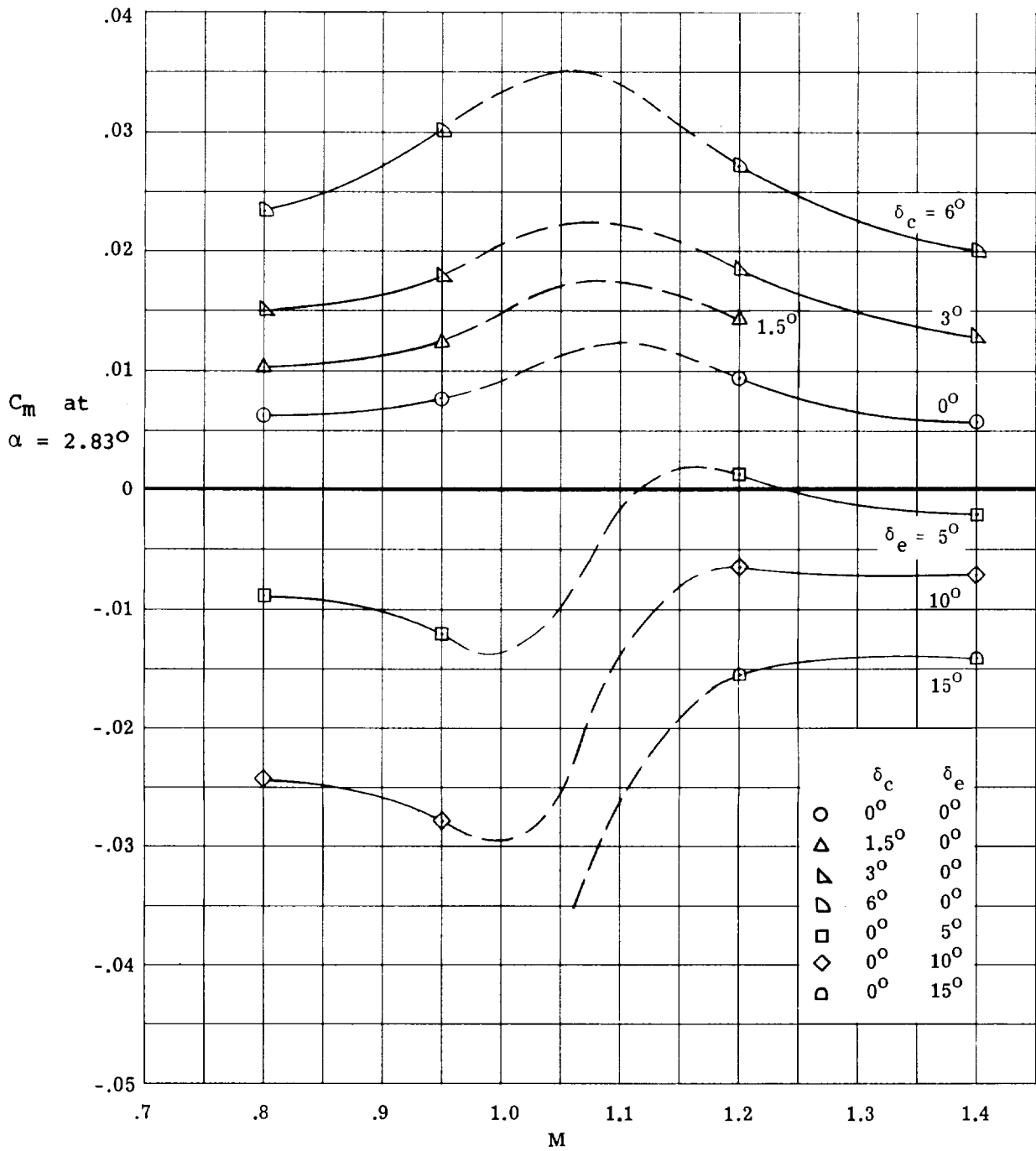
Figure 9.- Effect of δ_c and δ_e on C_m at $\alpha = 2.83°$ and $\delta_y = 25°$.
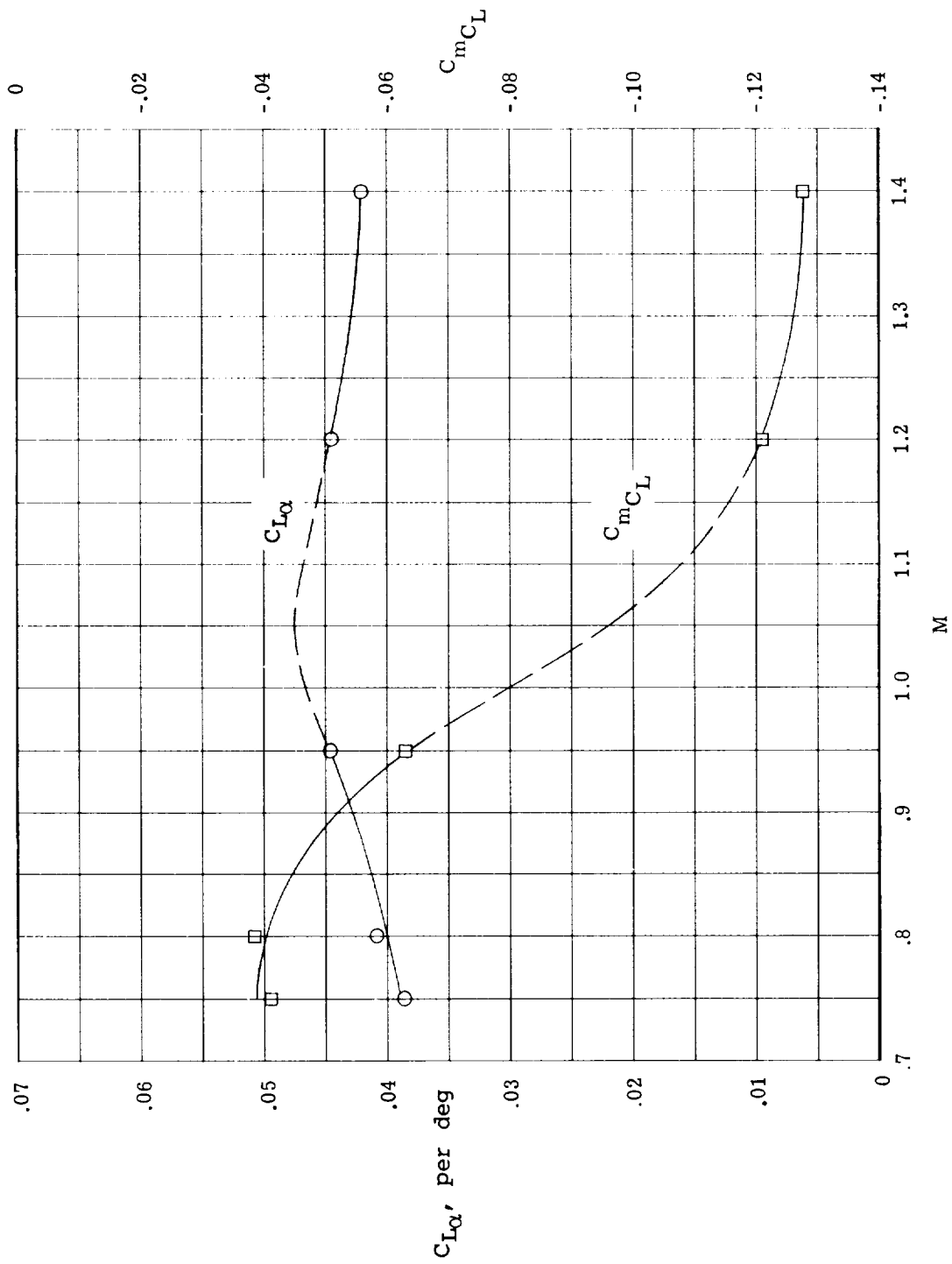
Figure 10.- $C_{L\alpha}$ and $C_{m_{C_L}}$ at transonic speeds for $\delta_y = 25^\circ$.
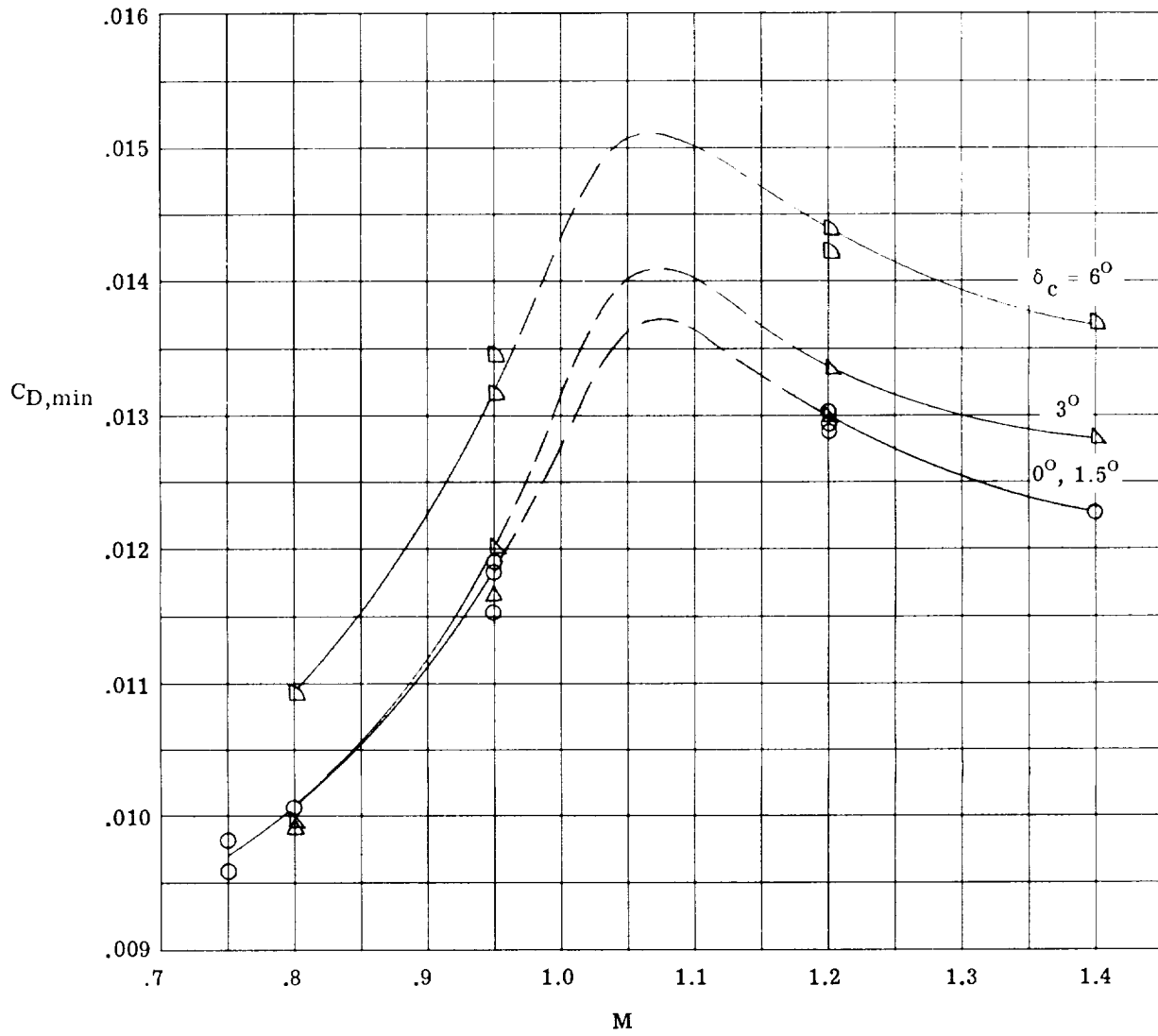
Figure 11.- Effect of canard deflection on $C_{D,min}$ for $\delta_y = 25^O$.
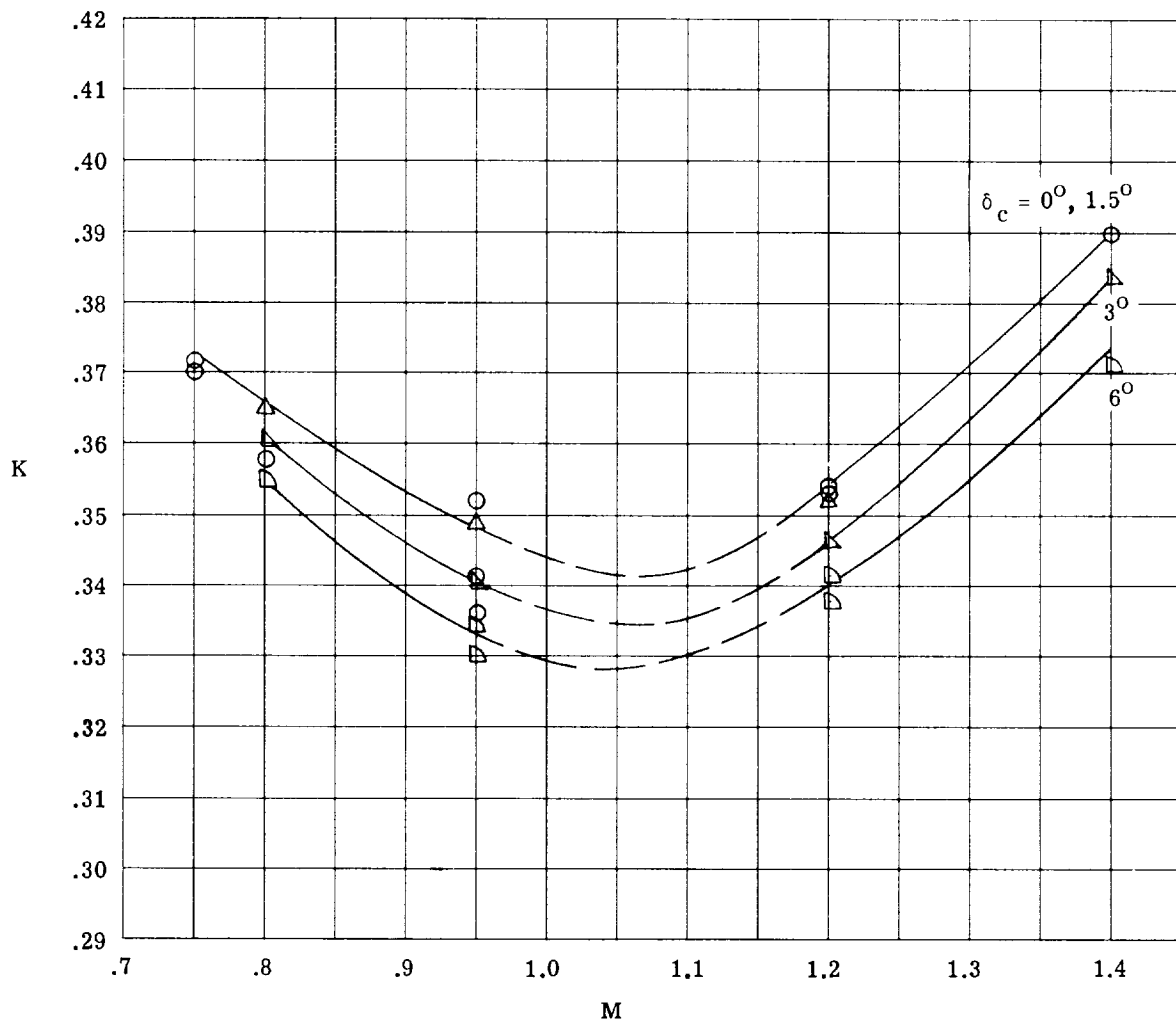
Figure 12.- Effect of canard deflection on drag-due-to-lift
parameter K for $\delta_y = 25°$.
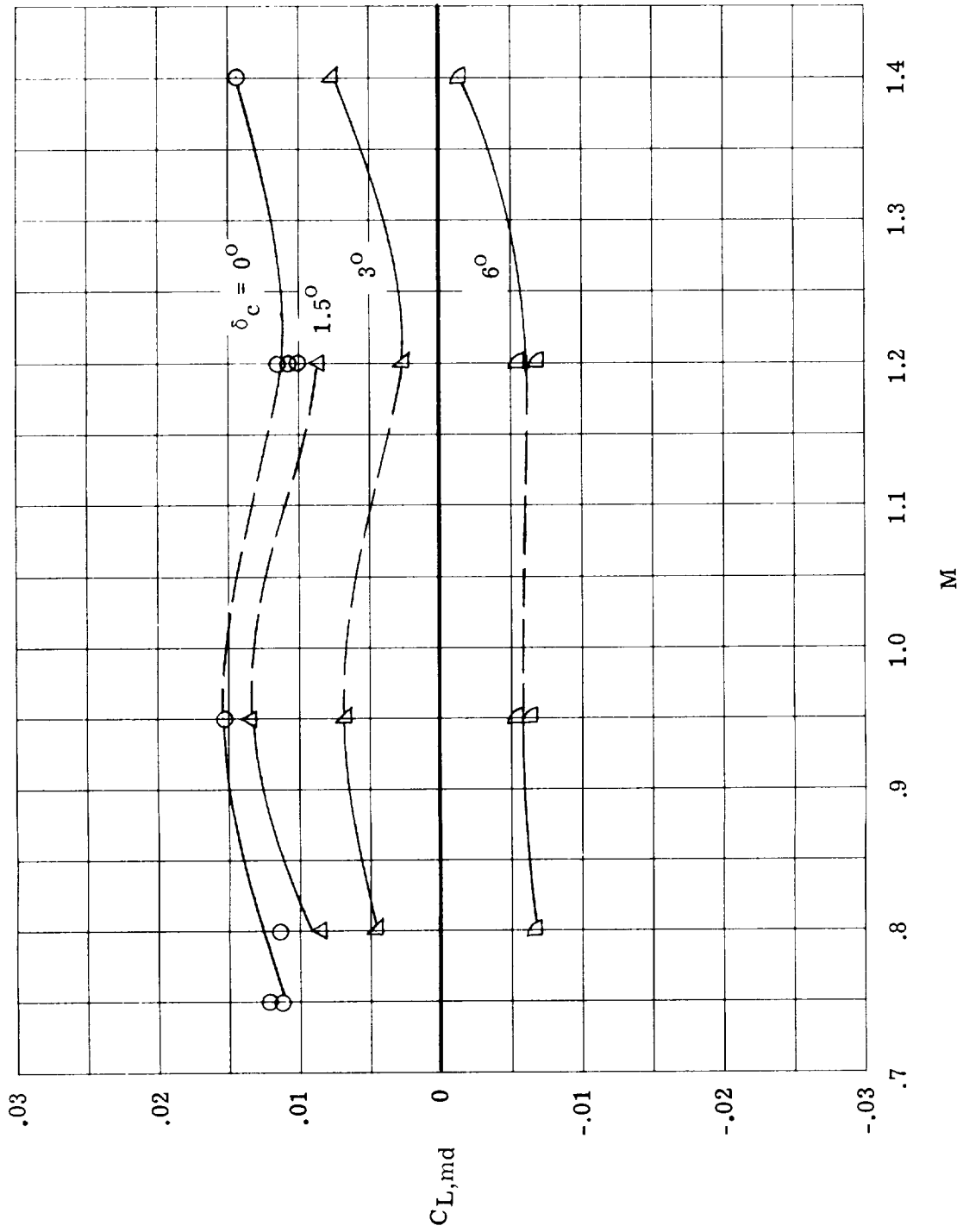
Figure 13.- Effect of canard deflection on $C_{L,md}$ for $\delta_y = 25^o$.
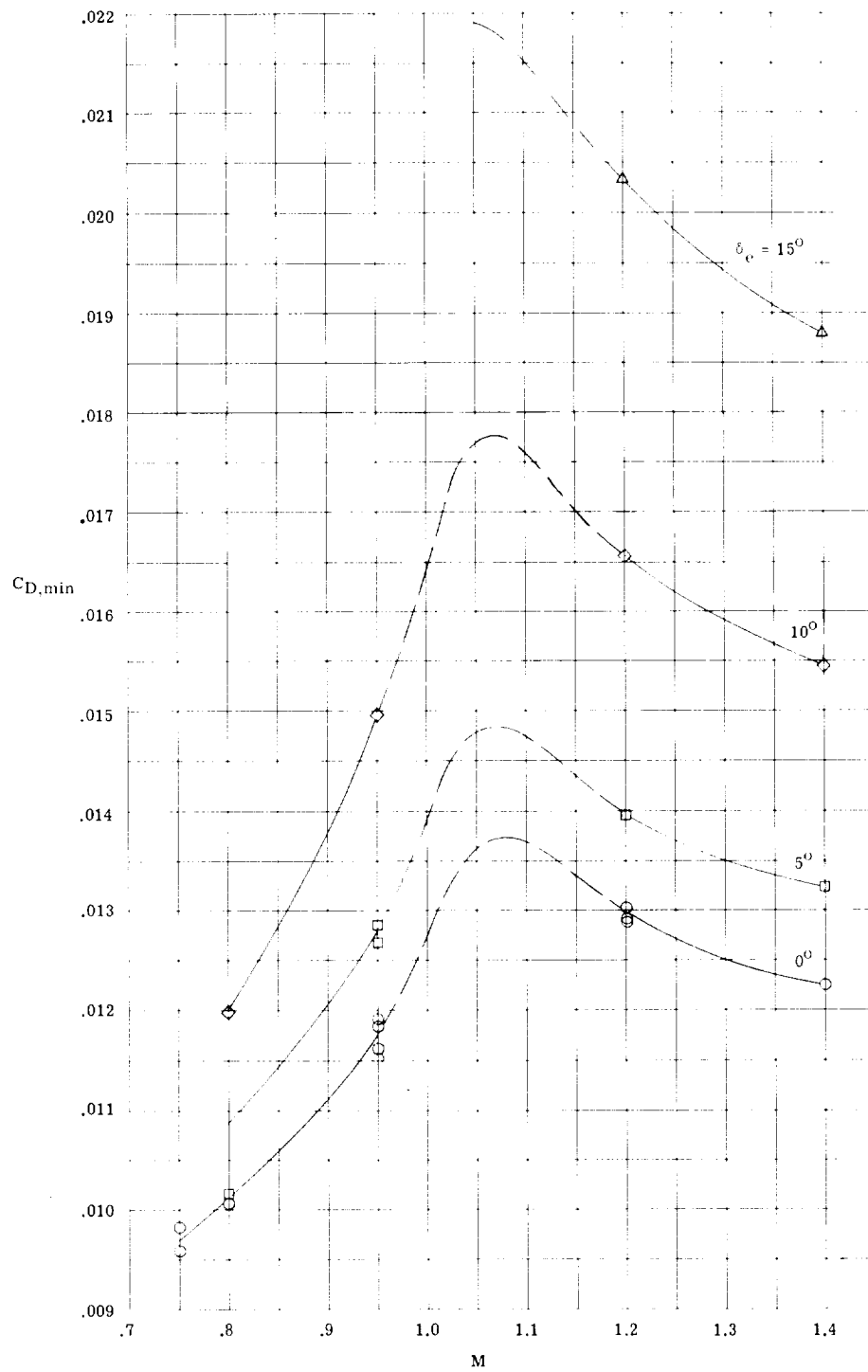
Figure 14.- Effect of elevon deflection on $C_{D,min}$ for $\delta_y = 25^o$.
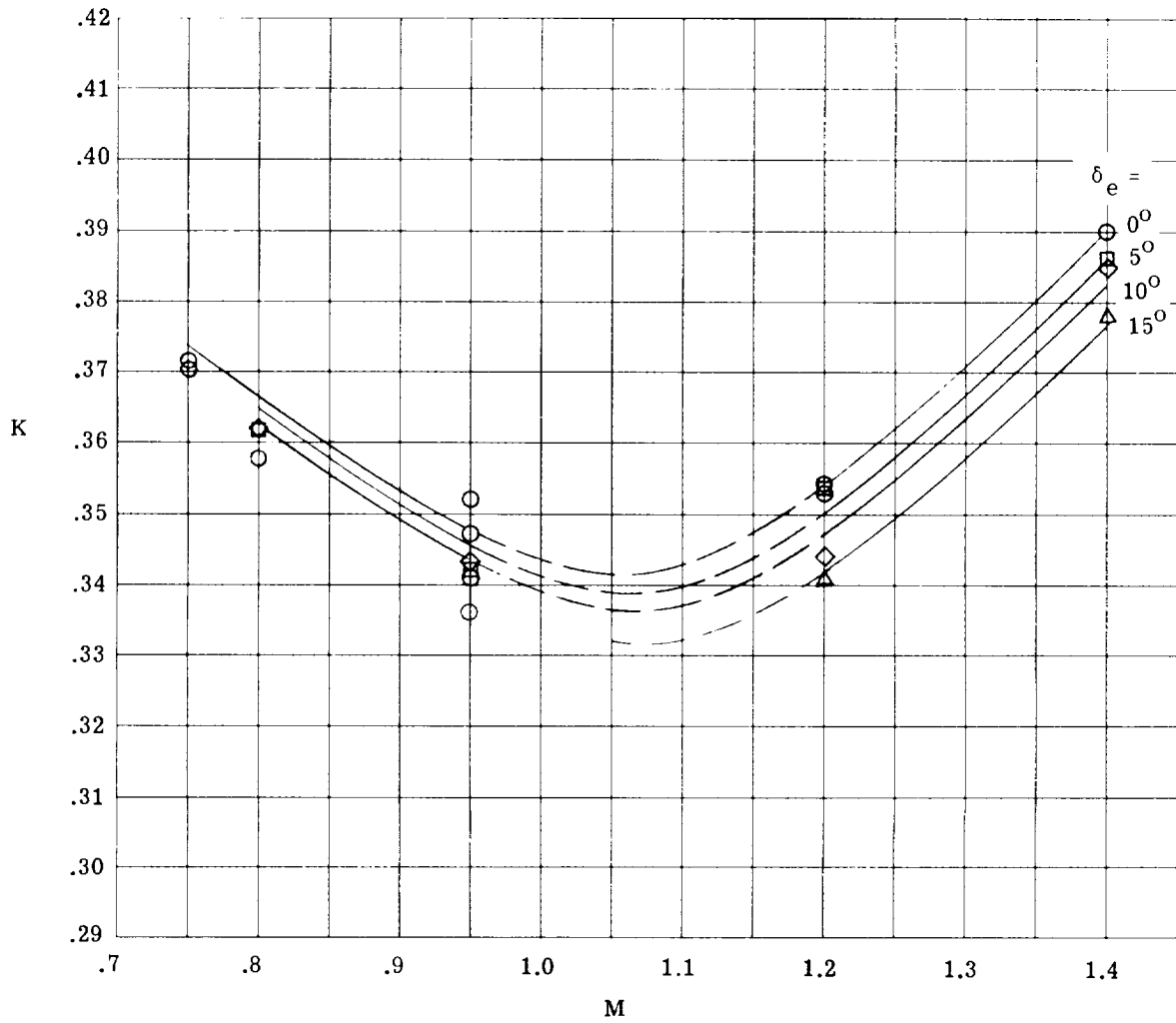
Figure 15.- Effect of elevon deflection on drag-due-to-lift
parameter K for $\delta_y = 25^O$.
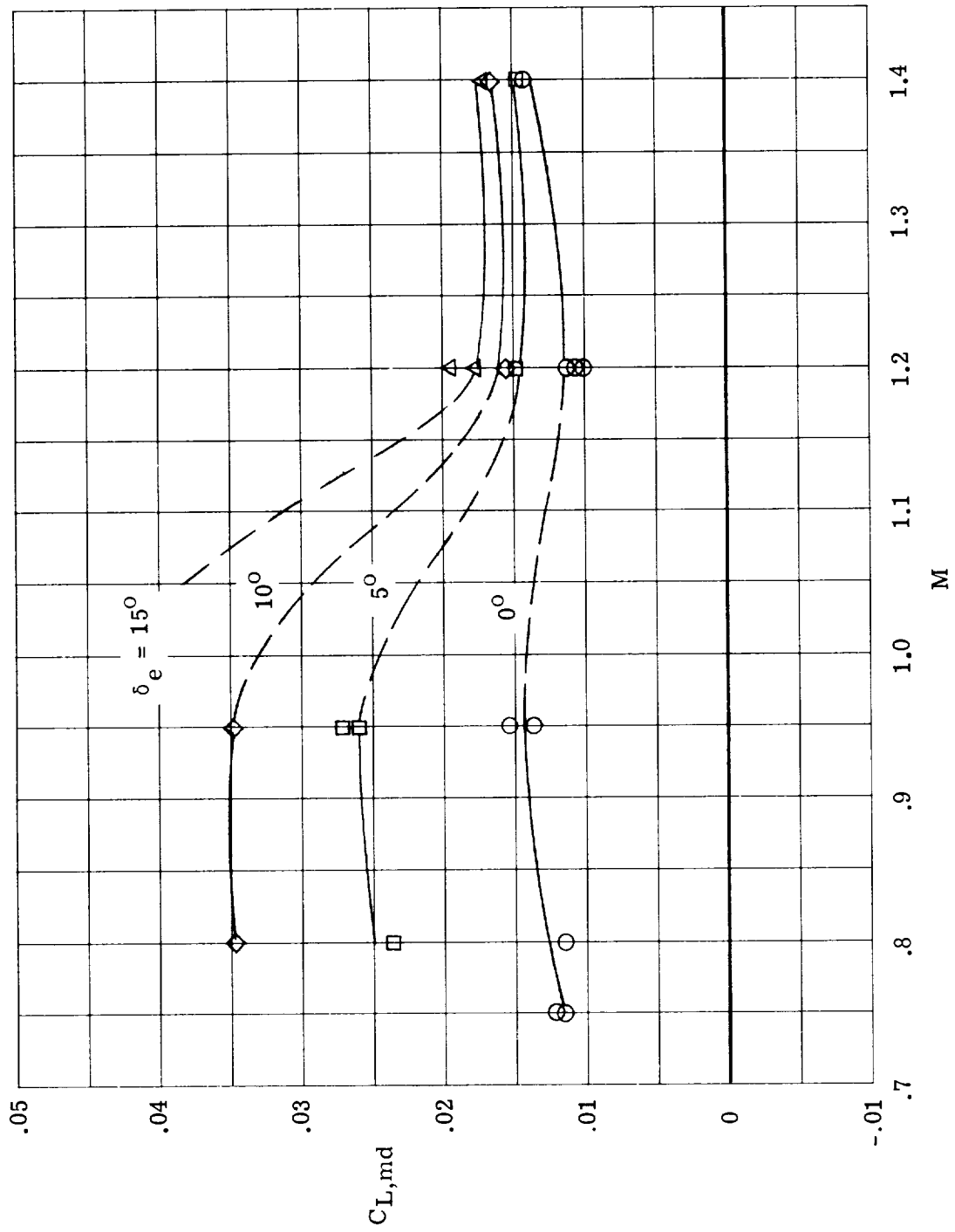
Figure 16.- Effect of elevon deflection on $C_{L,md}$ for $\delta_y = 25^{\circ}$.
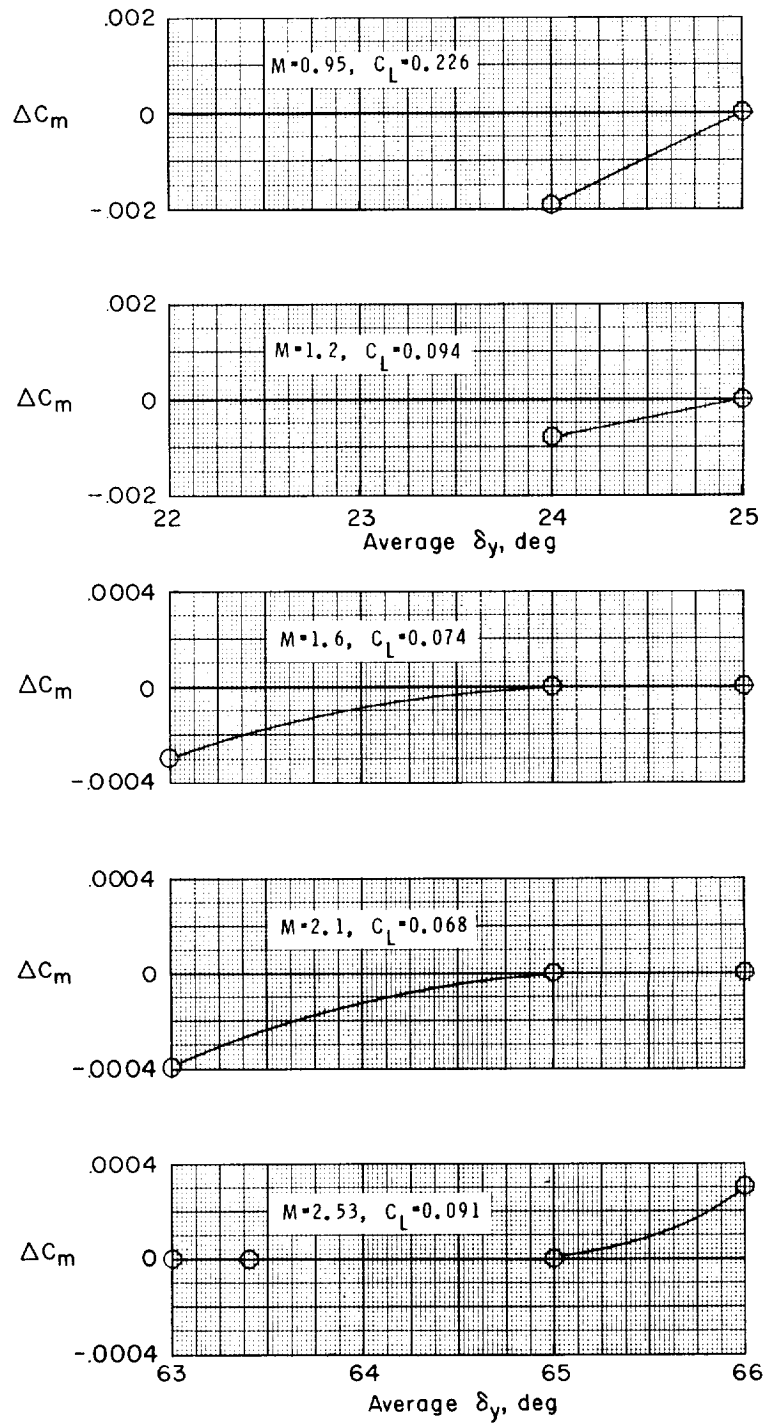
Figure 17.- Effect of average tip deflection angle on C_m.
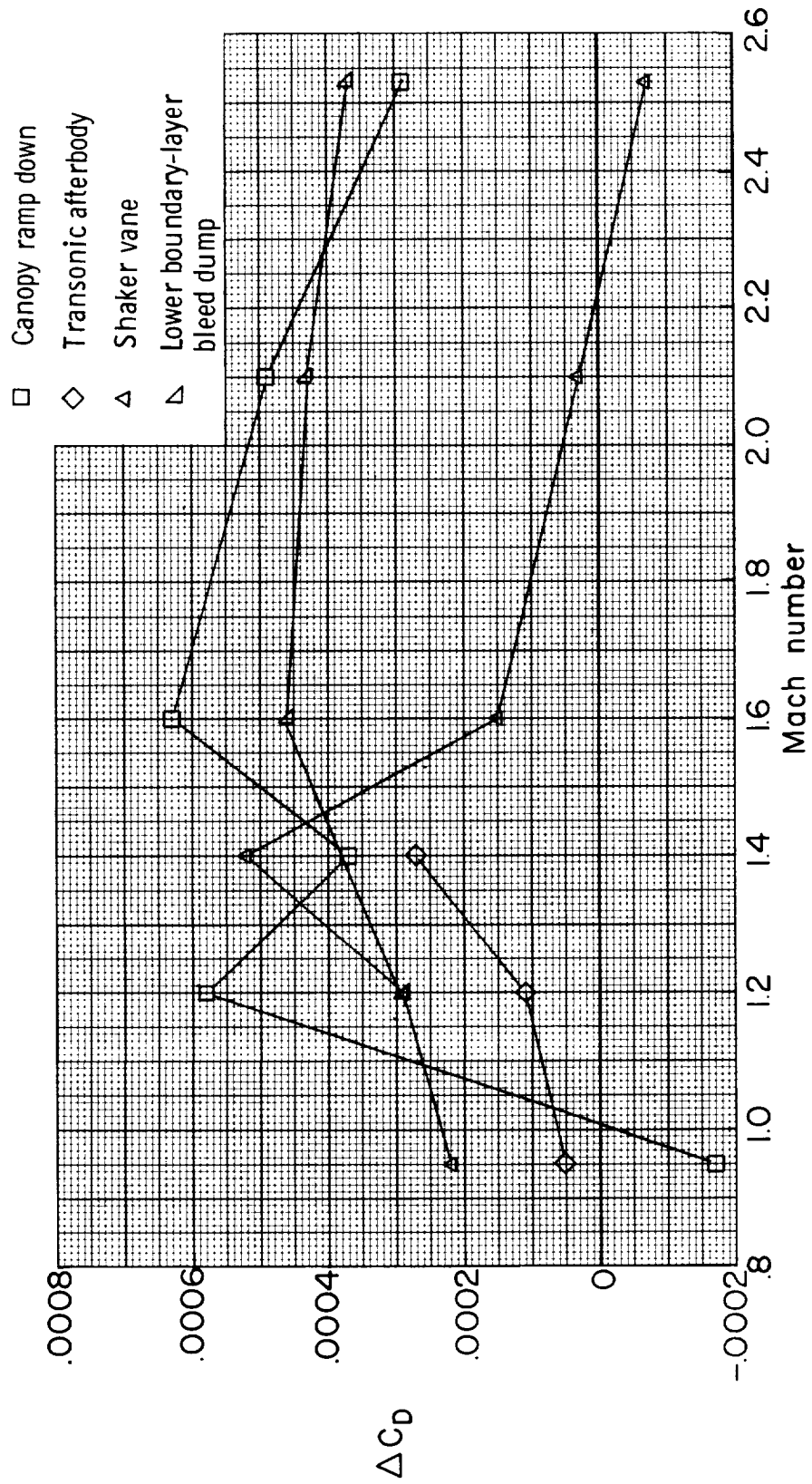
Figure 18.- Drag increment ΔC_D due to various components for $C_L = 0.1$.
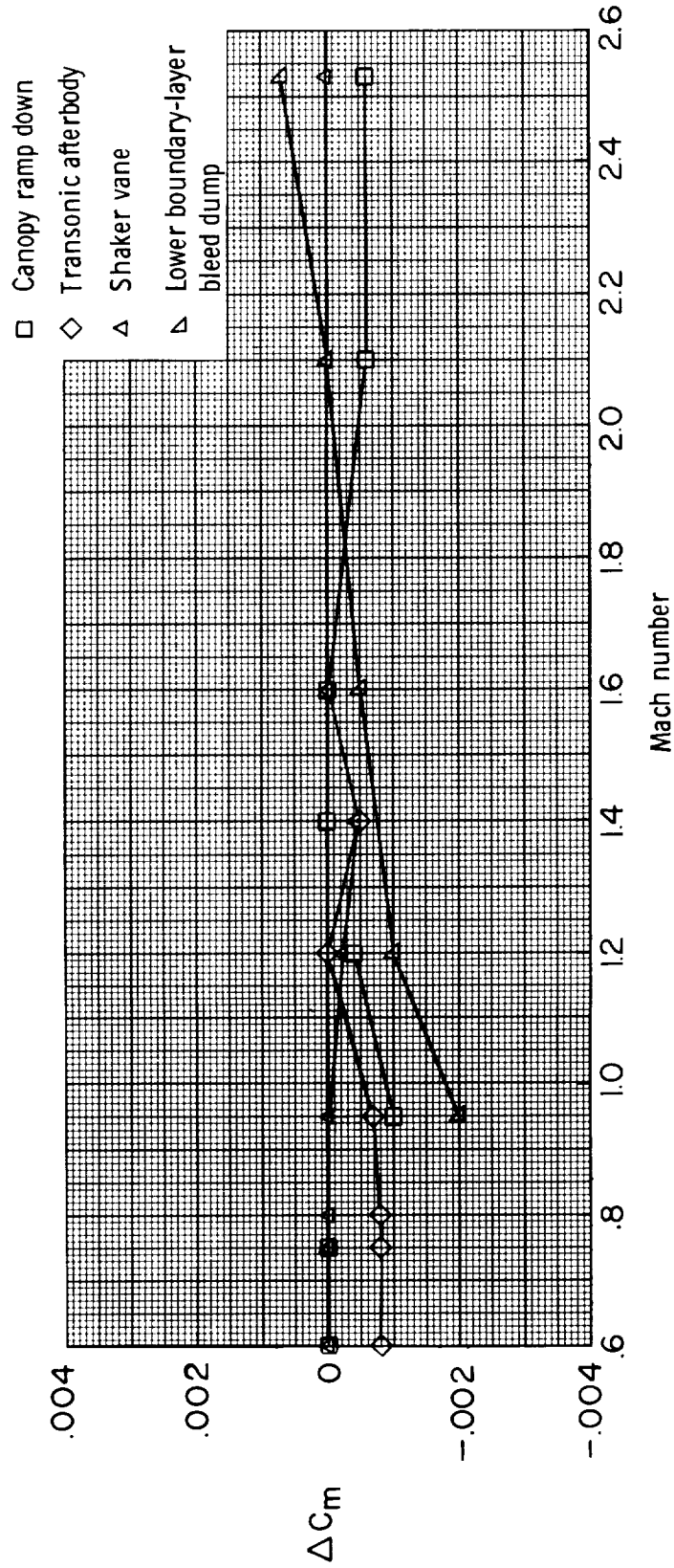
Figure 19.- Moment increment ΔC_m due to various components for $C_L = 0.1$.

53
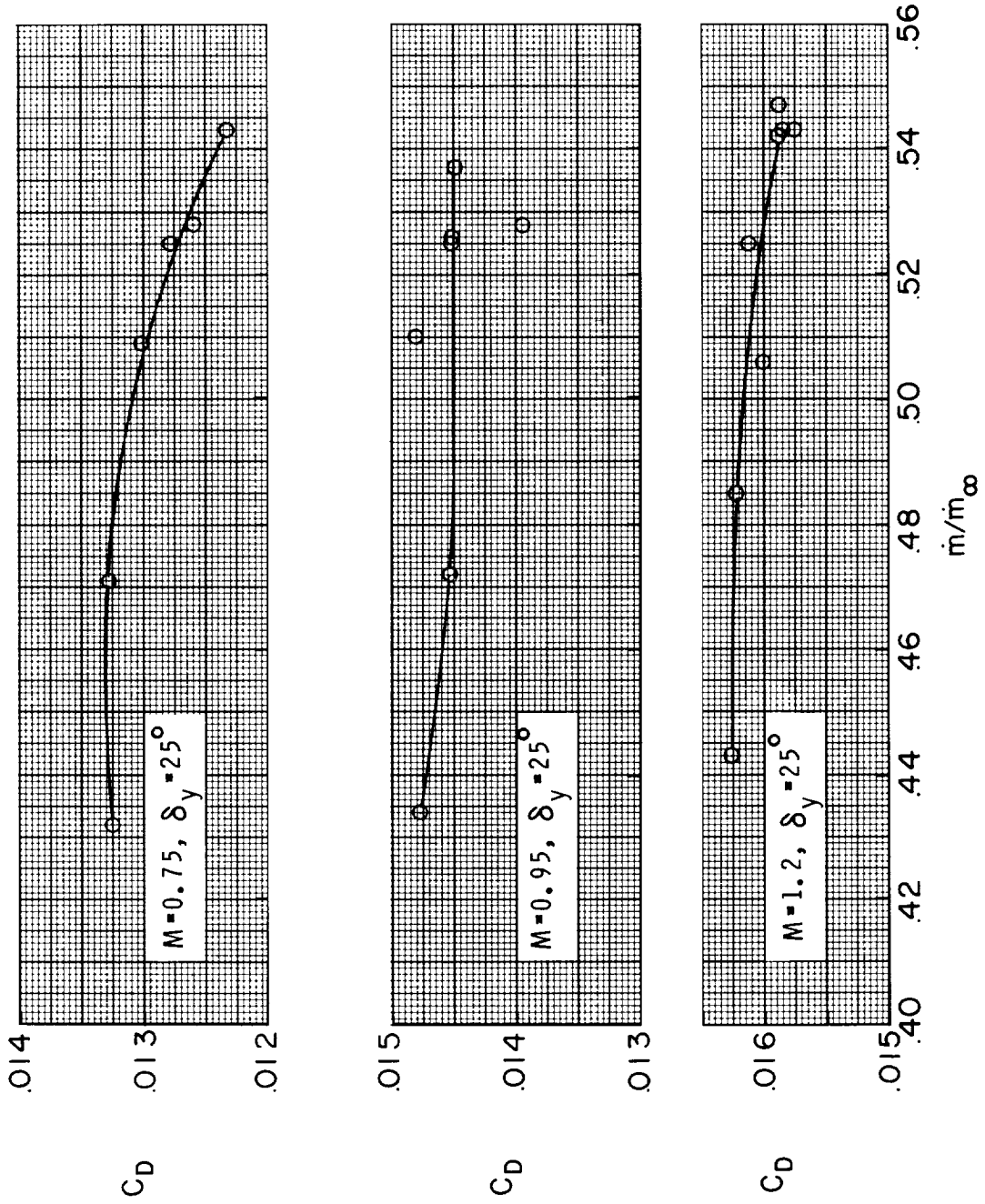
Figure 20.- Effect of mass flow ratios on C_D for $C_L = 0.1$.

54
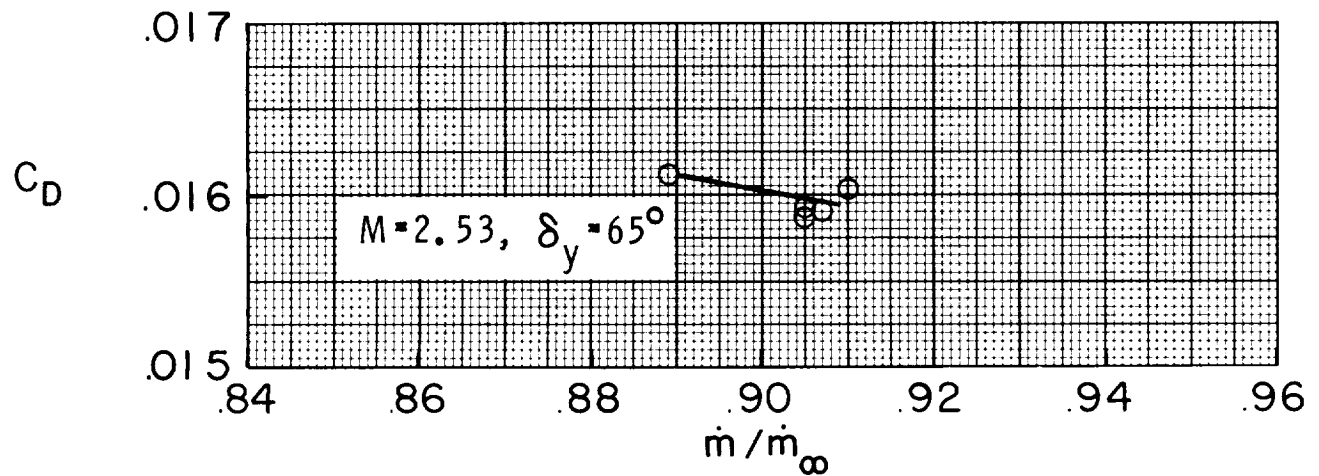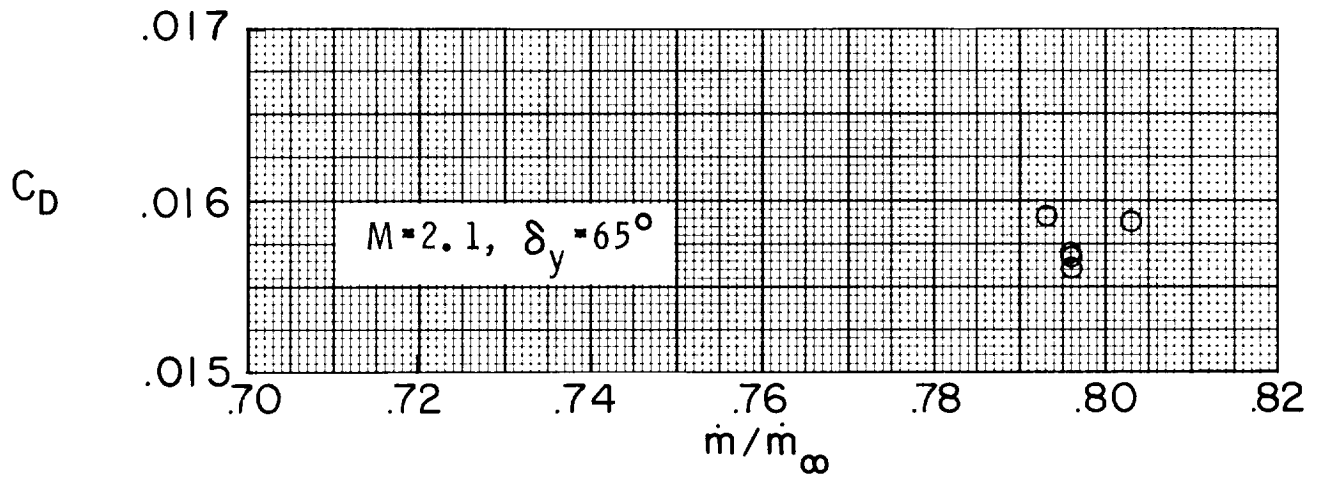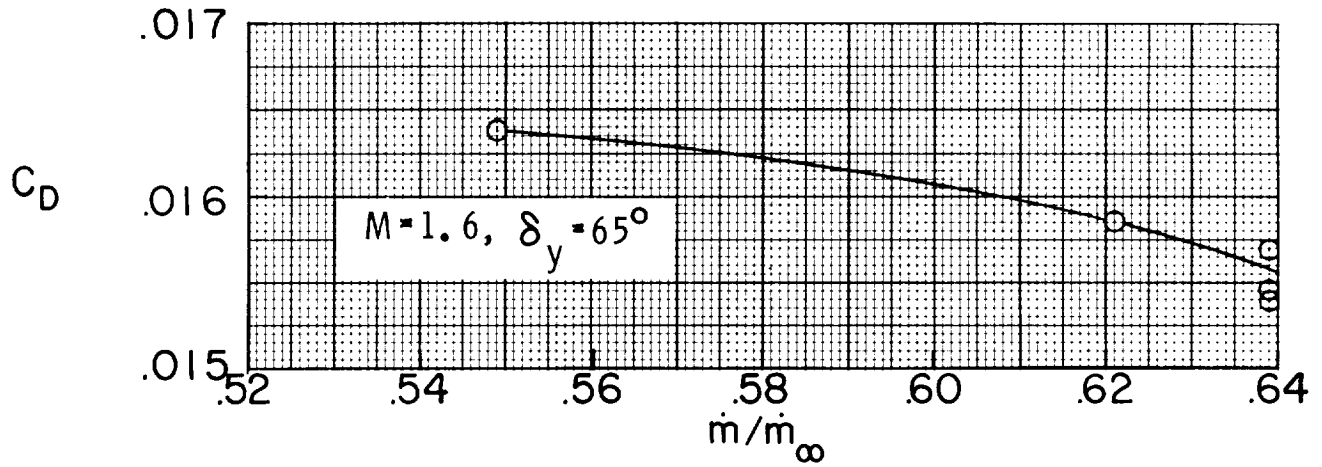
Figure 20.- Concluded.
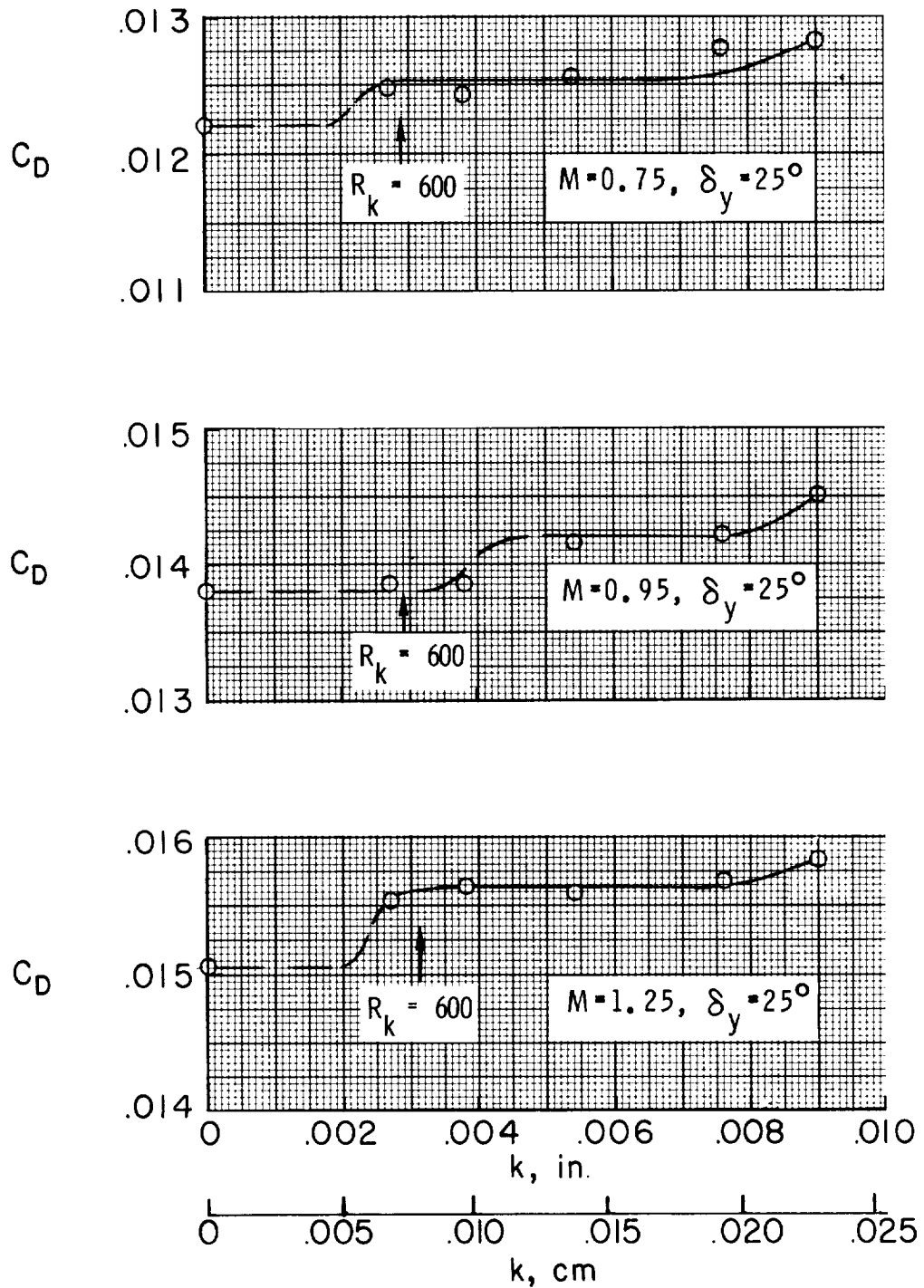
Figure 21.- Effect of boundary-layer trip size, k, on drag at $C_L = 0.1$.
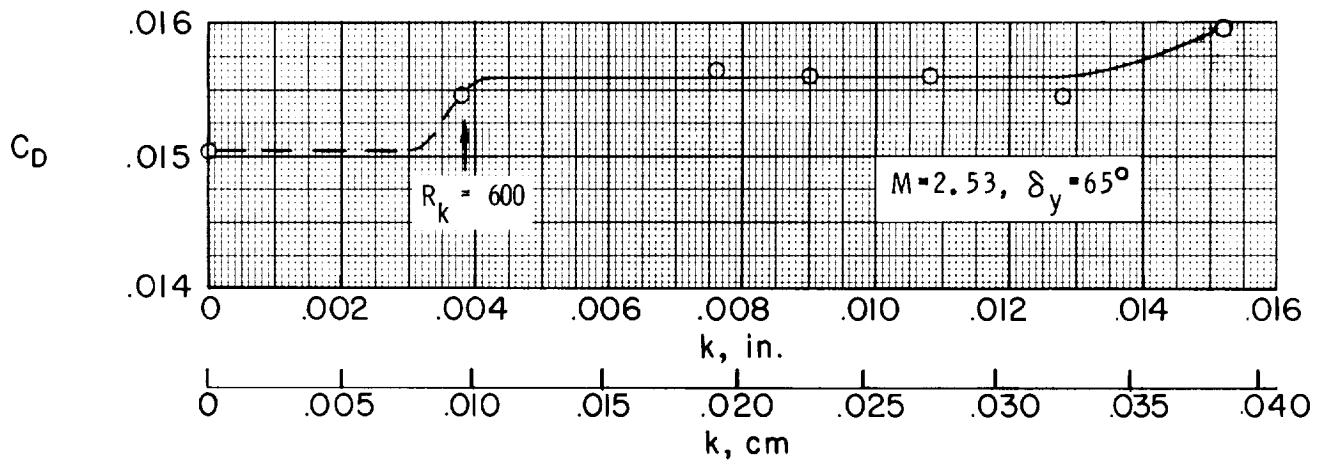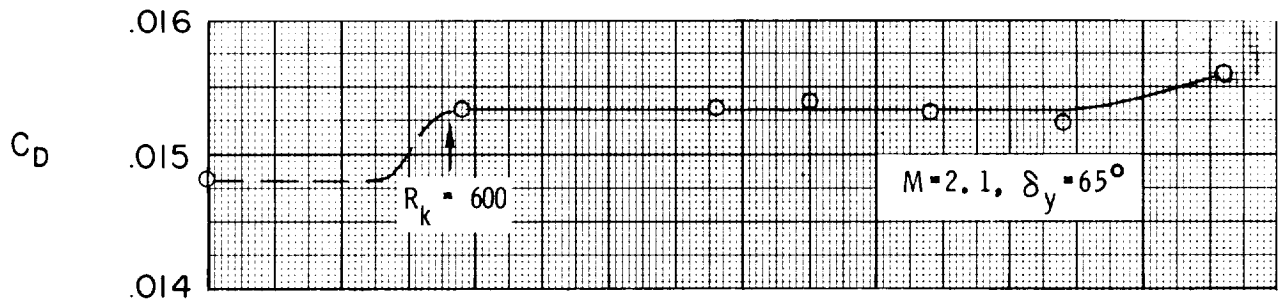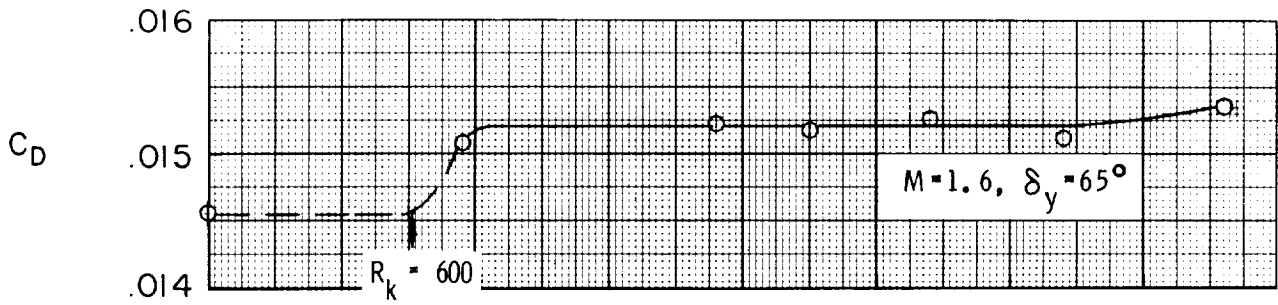
Figure 21.- Concluded.
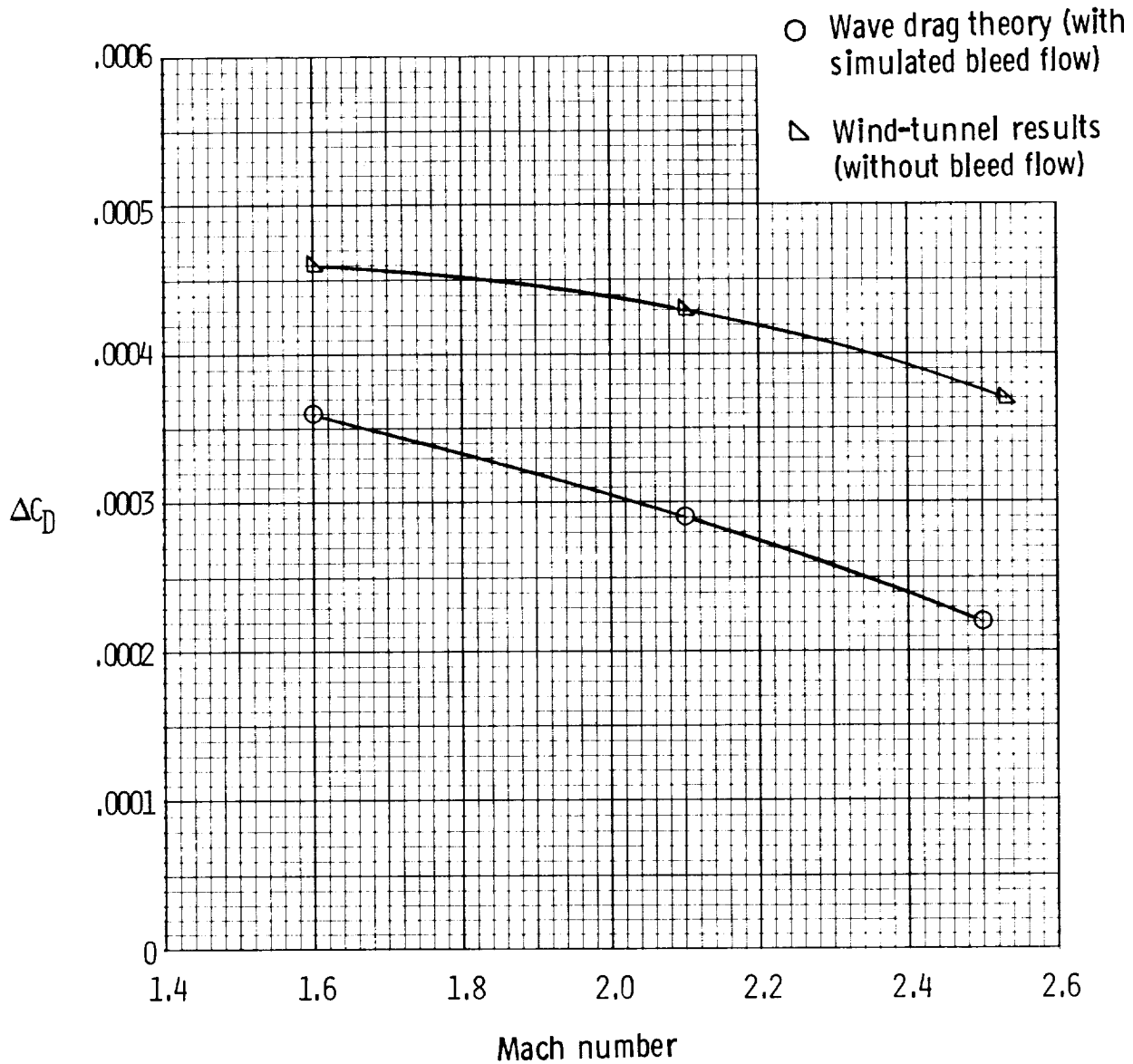
Figure 22.- Drag increment due to lower boundary-layer bleed dump.
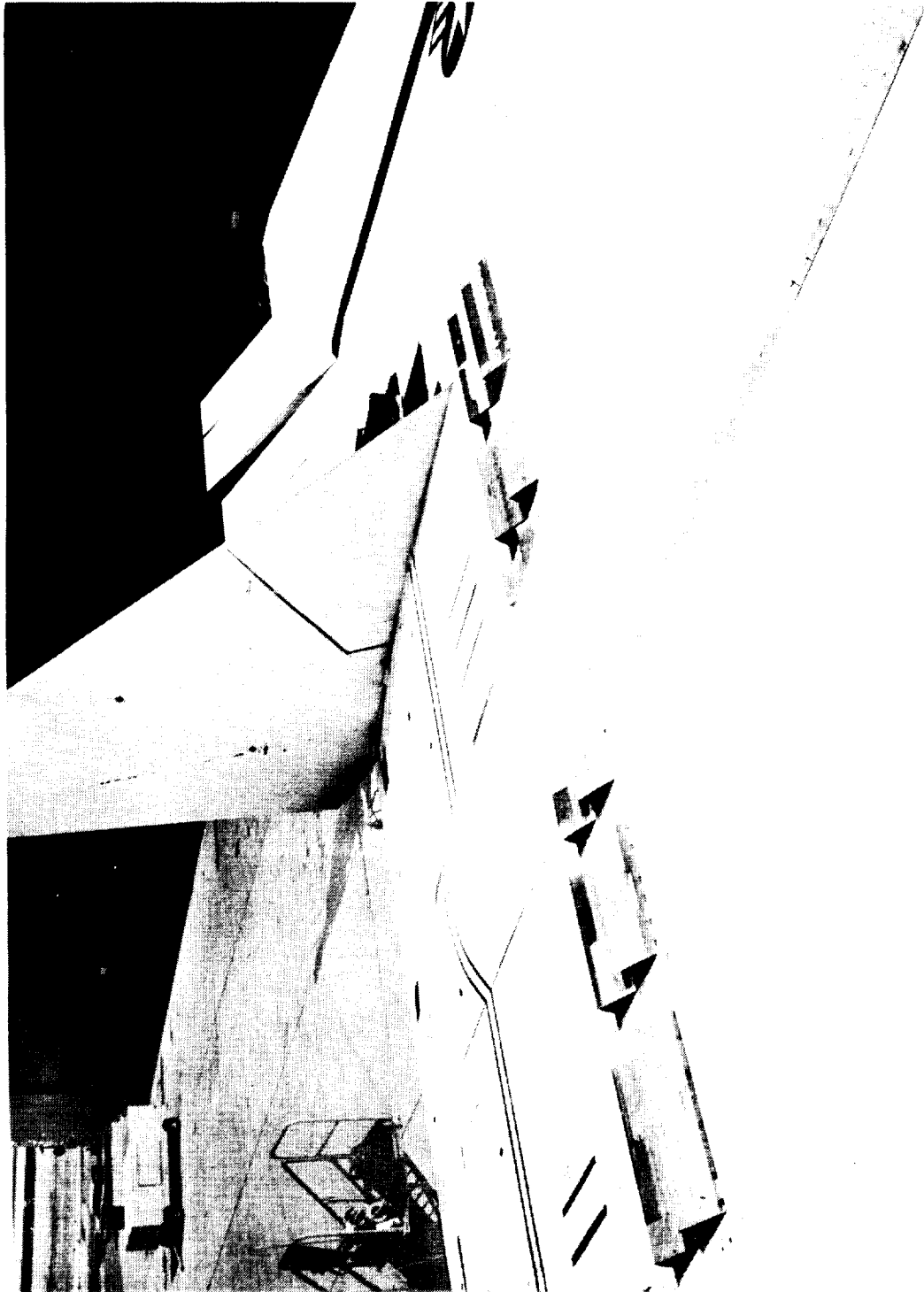
Figure 23.- Bypass doors of XB-70-1.
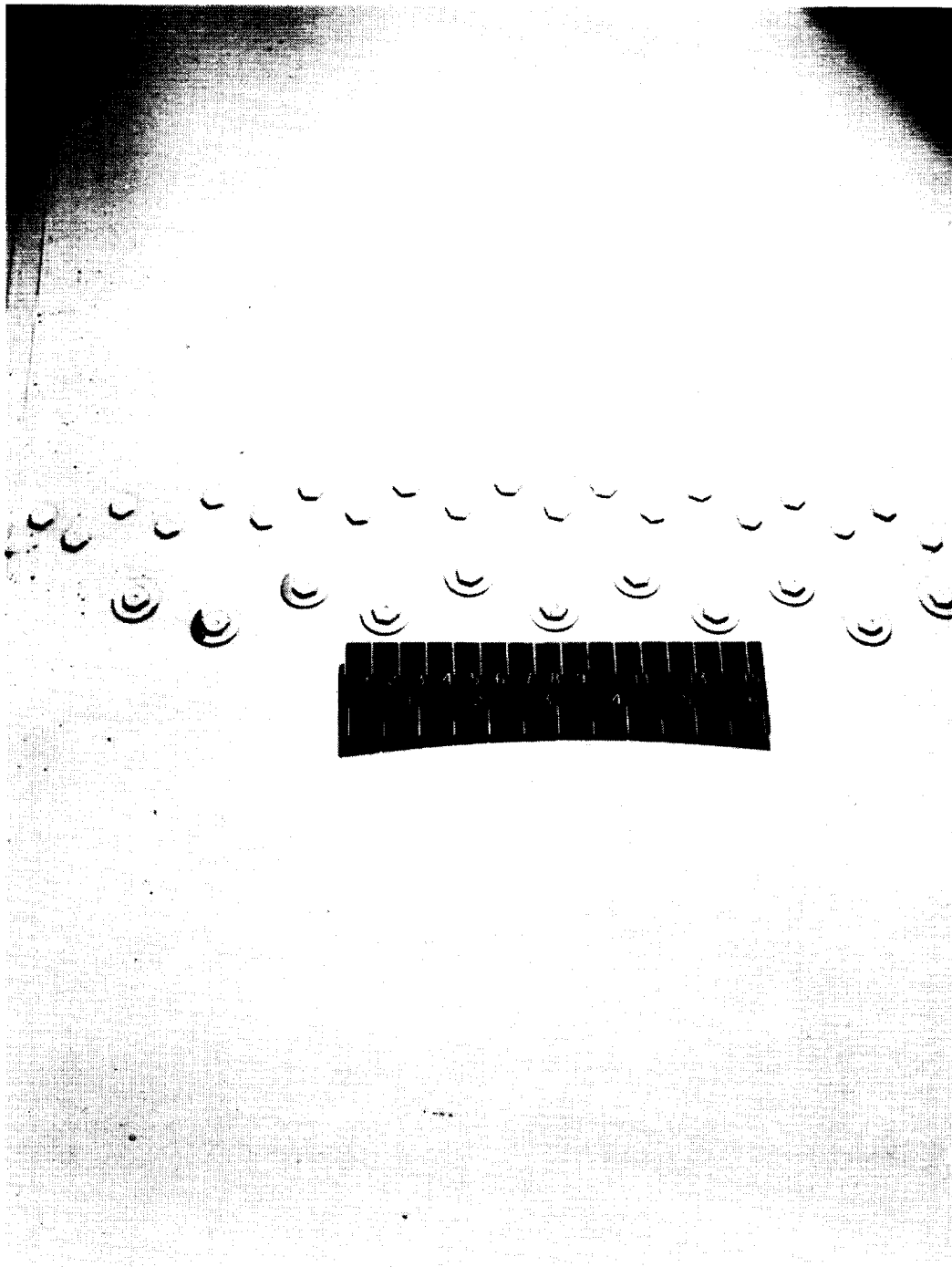
L-79-289

(a) Screw-head roughnesses on fuselage.

Figure 24.- Typical roughnesses on XB-70-1.

60

FUEL TANK NO.3 ACCESS
FUEL PROBE'COOLING LOOP PUMPS
LEVEL CONTROL VALVES
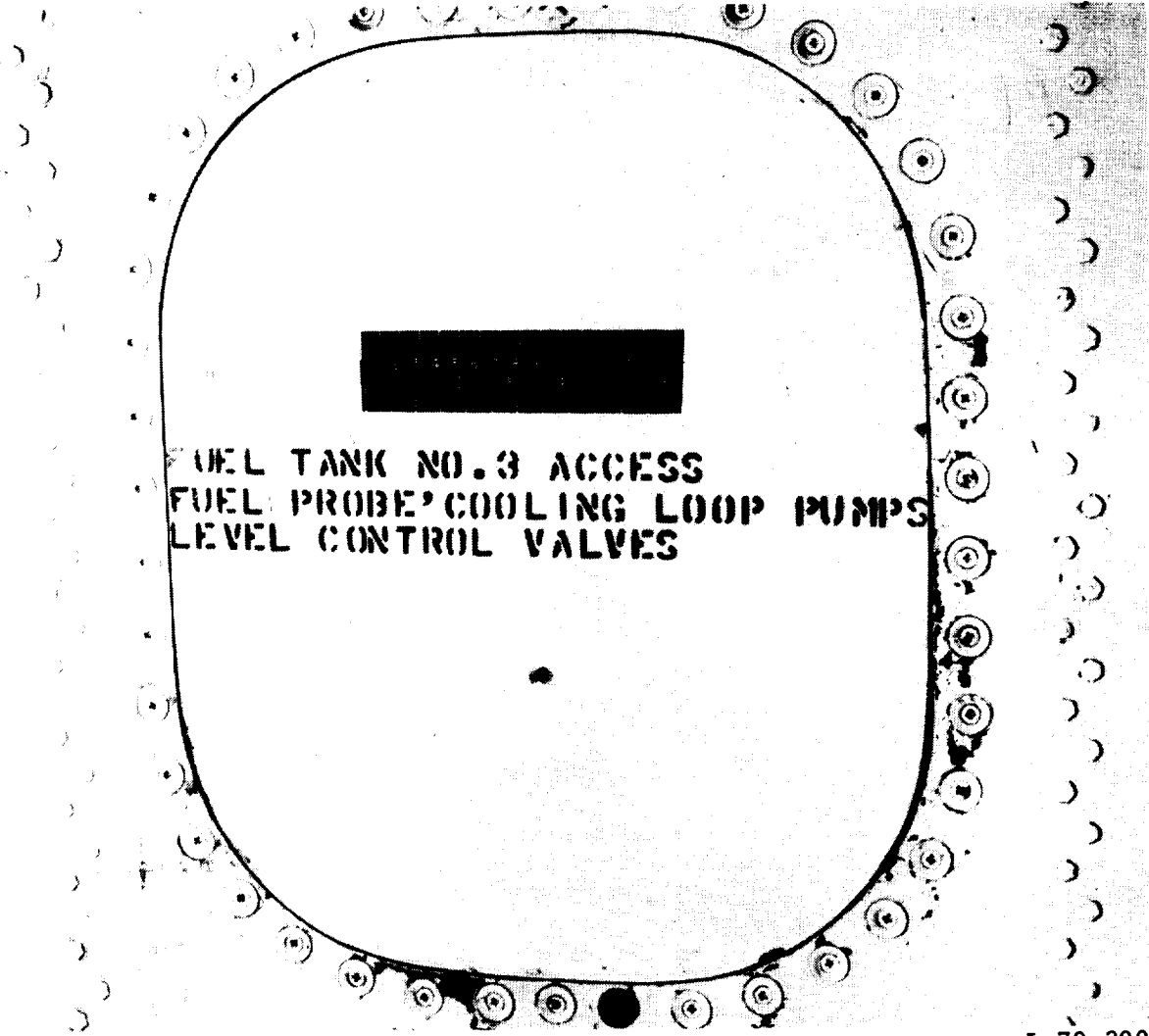
L-79-290

(b) Access door on fuselage.

Figure 24.- Continued.
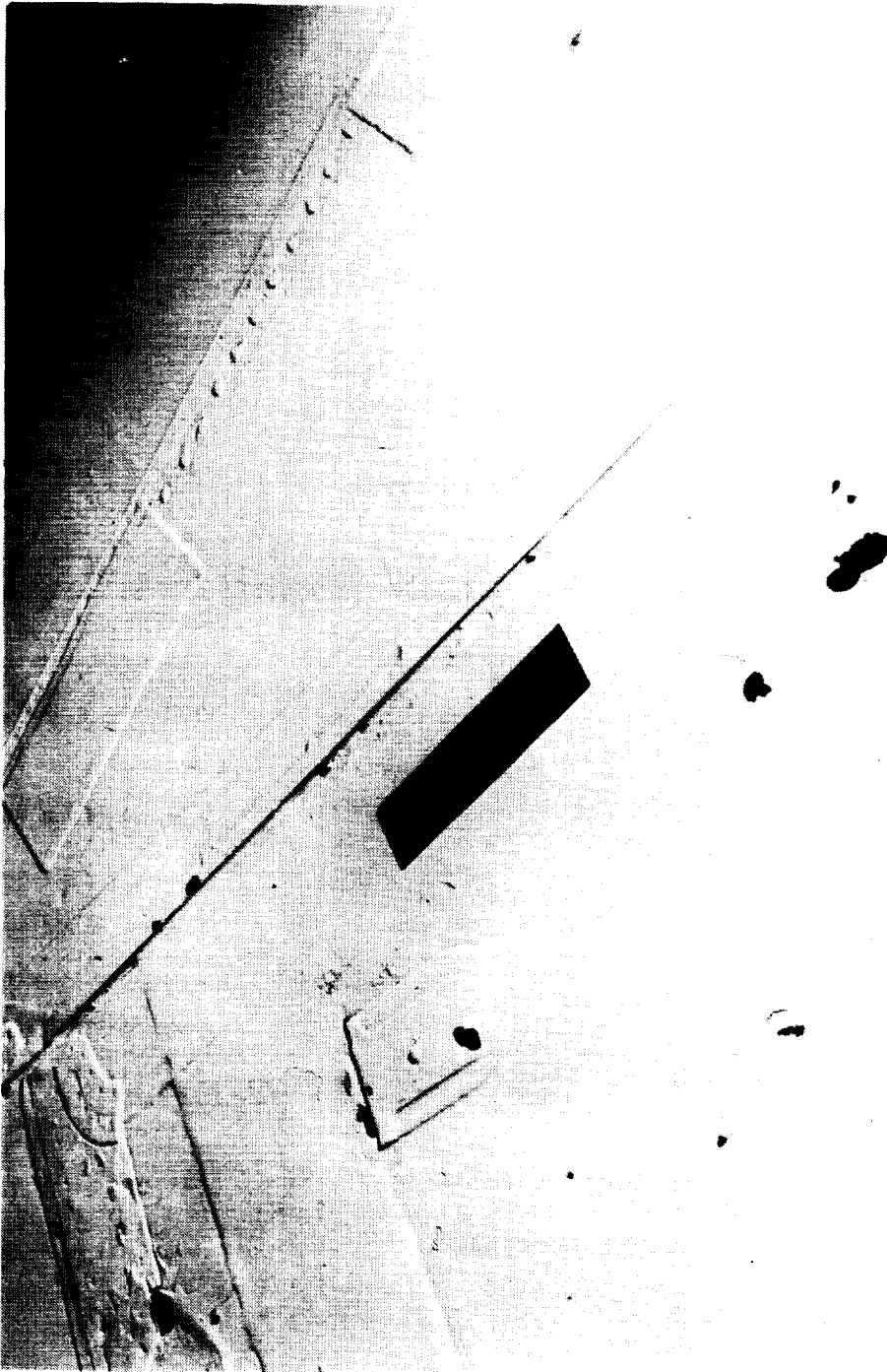
(c) Patches on wing.

Figure 24.- Continued.
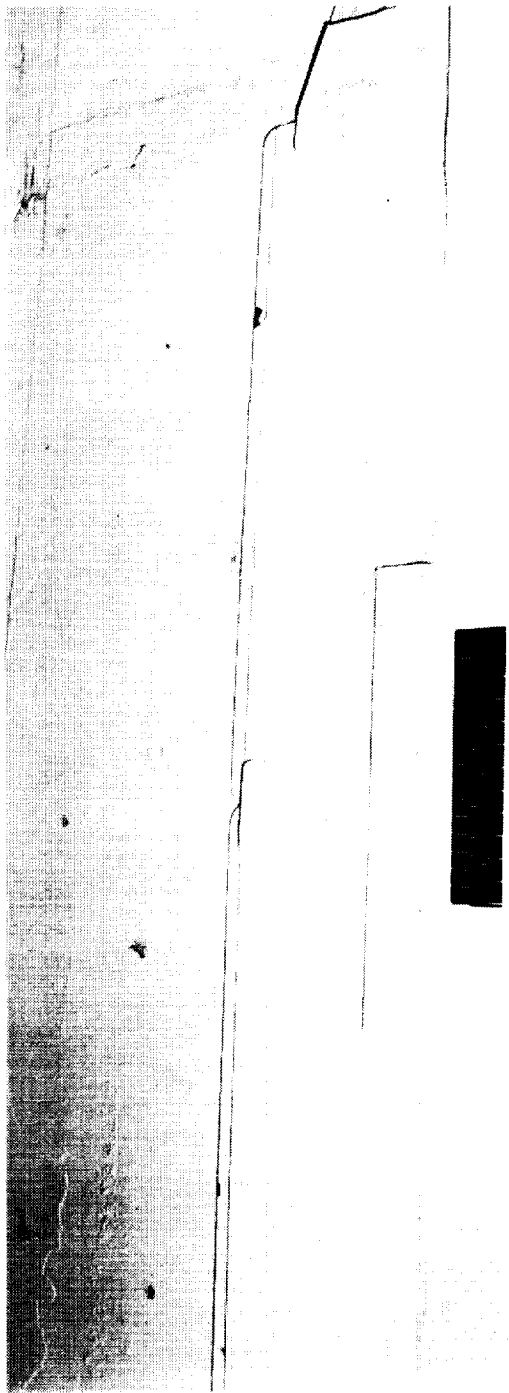
(d) Lap joints on wing.

Figure 24.- Concluded.
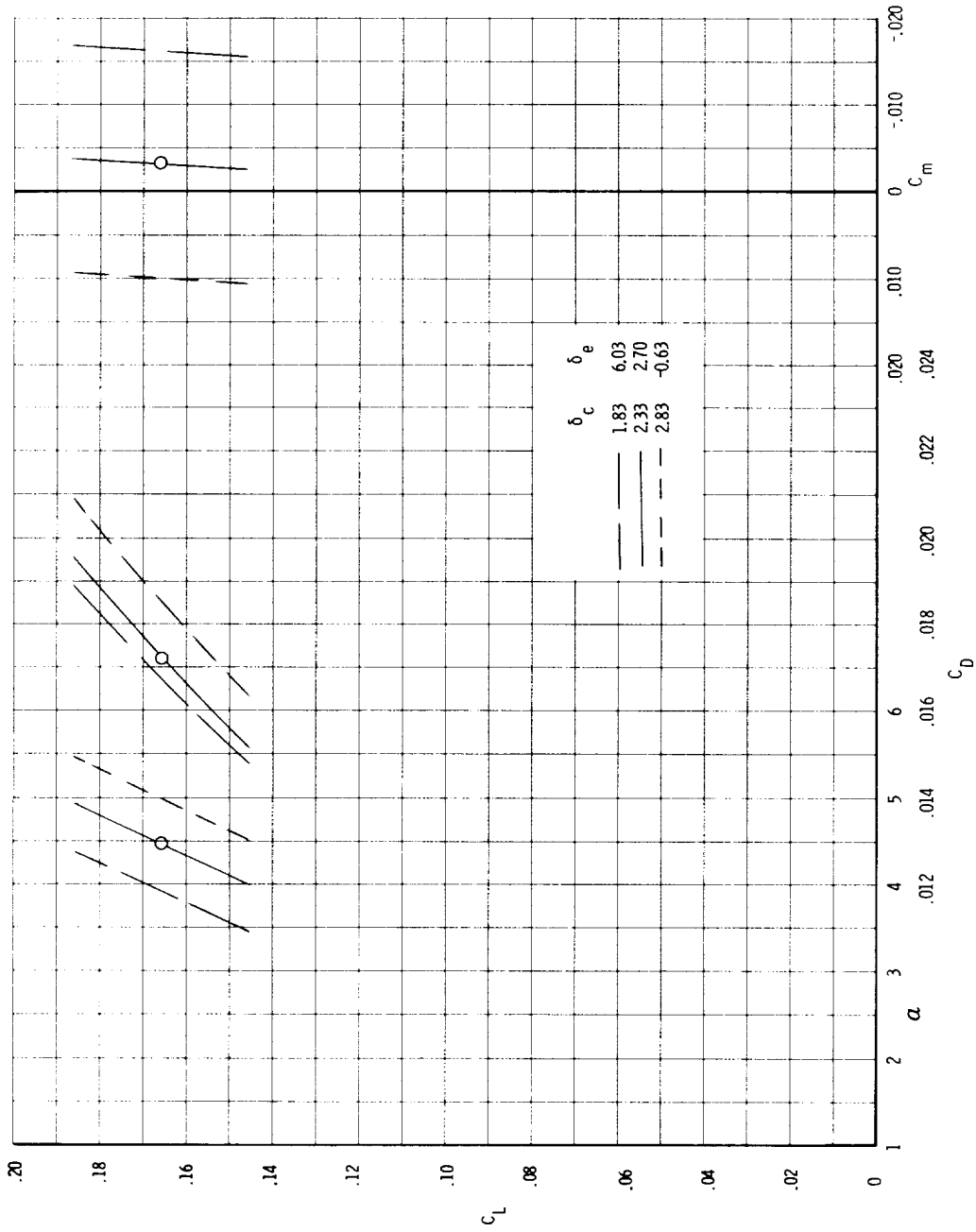
(a) P1 at M = 0.76.

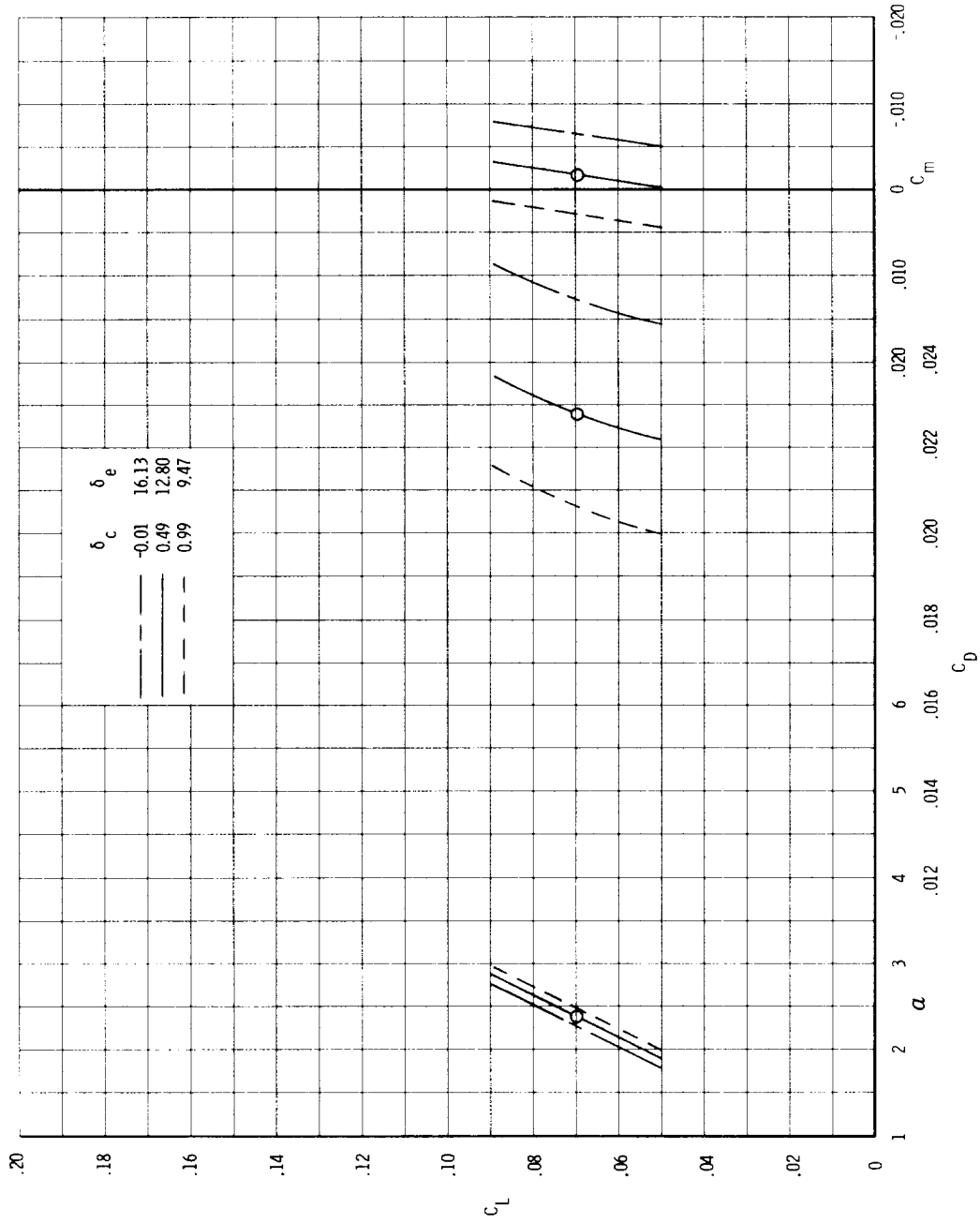Figure 25.- Predicted XB-70-1 full-scale aerodynamic characteristics.
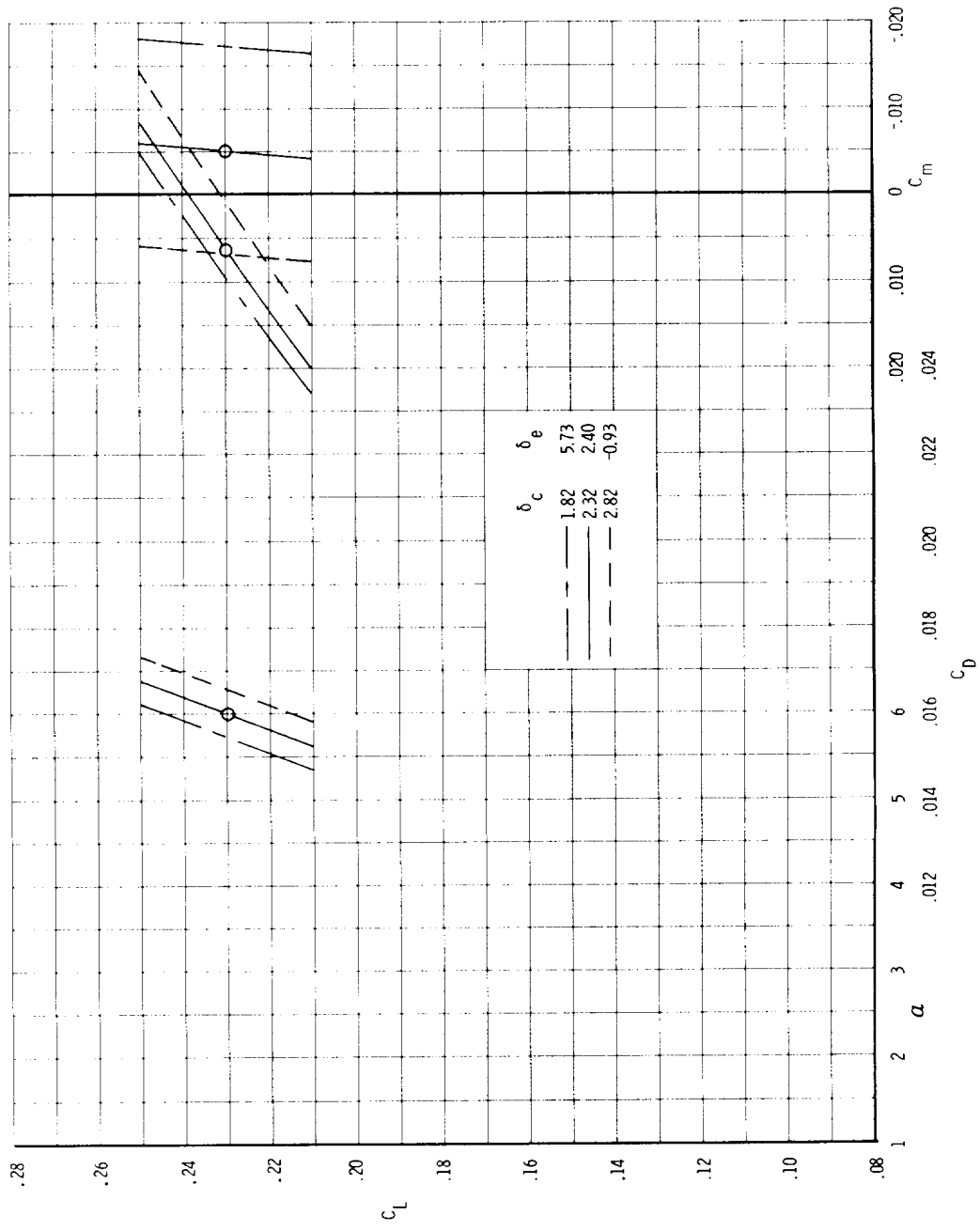
(b) P2 at M = 0.93.

Figure 25.- Continued.
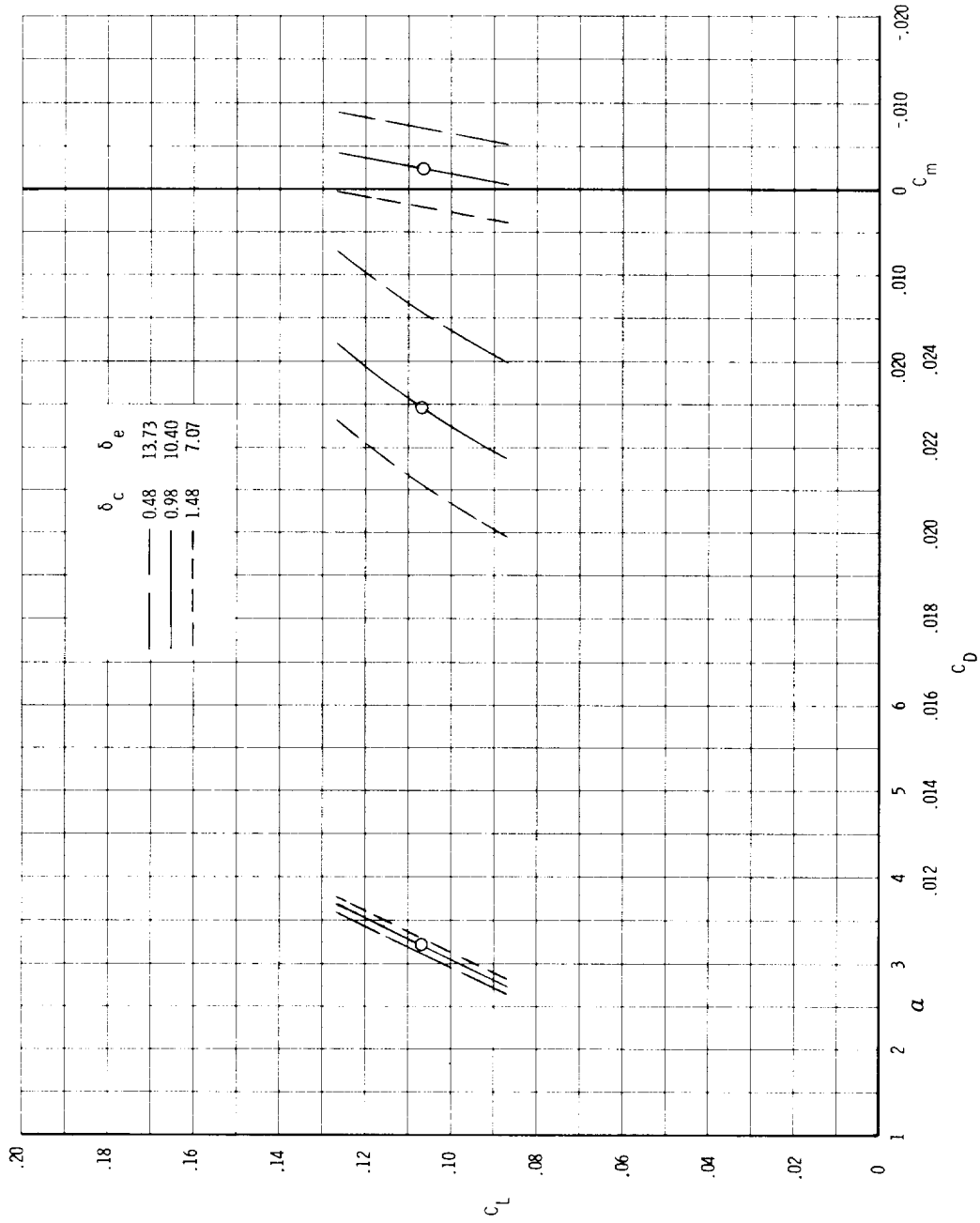
(c) P3 at M = 1.18.

Figure 25.- Continued.
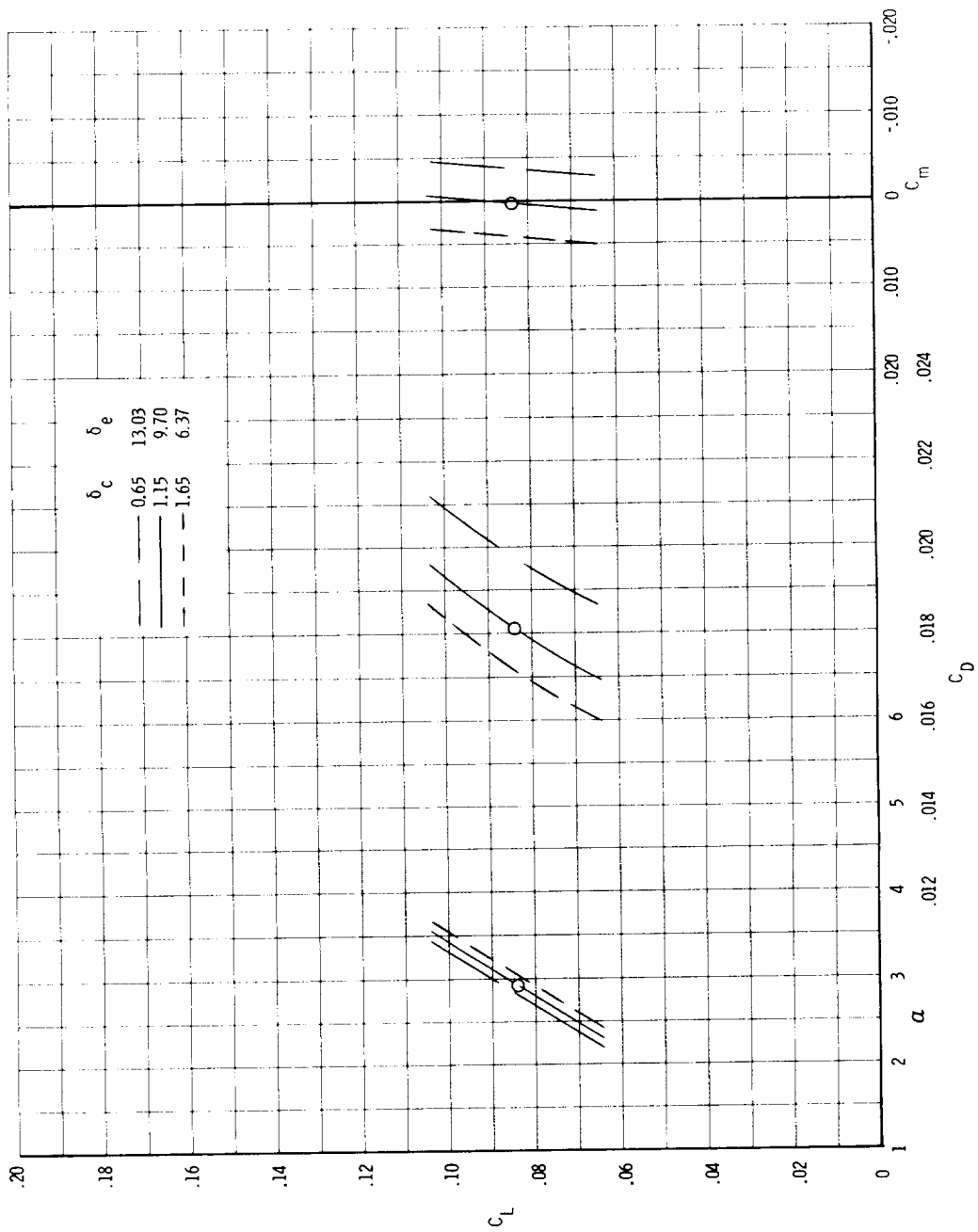
(d) P4 at M = 1.60.

Figure 25.- Continued.
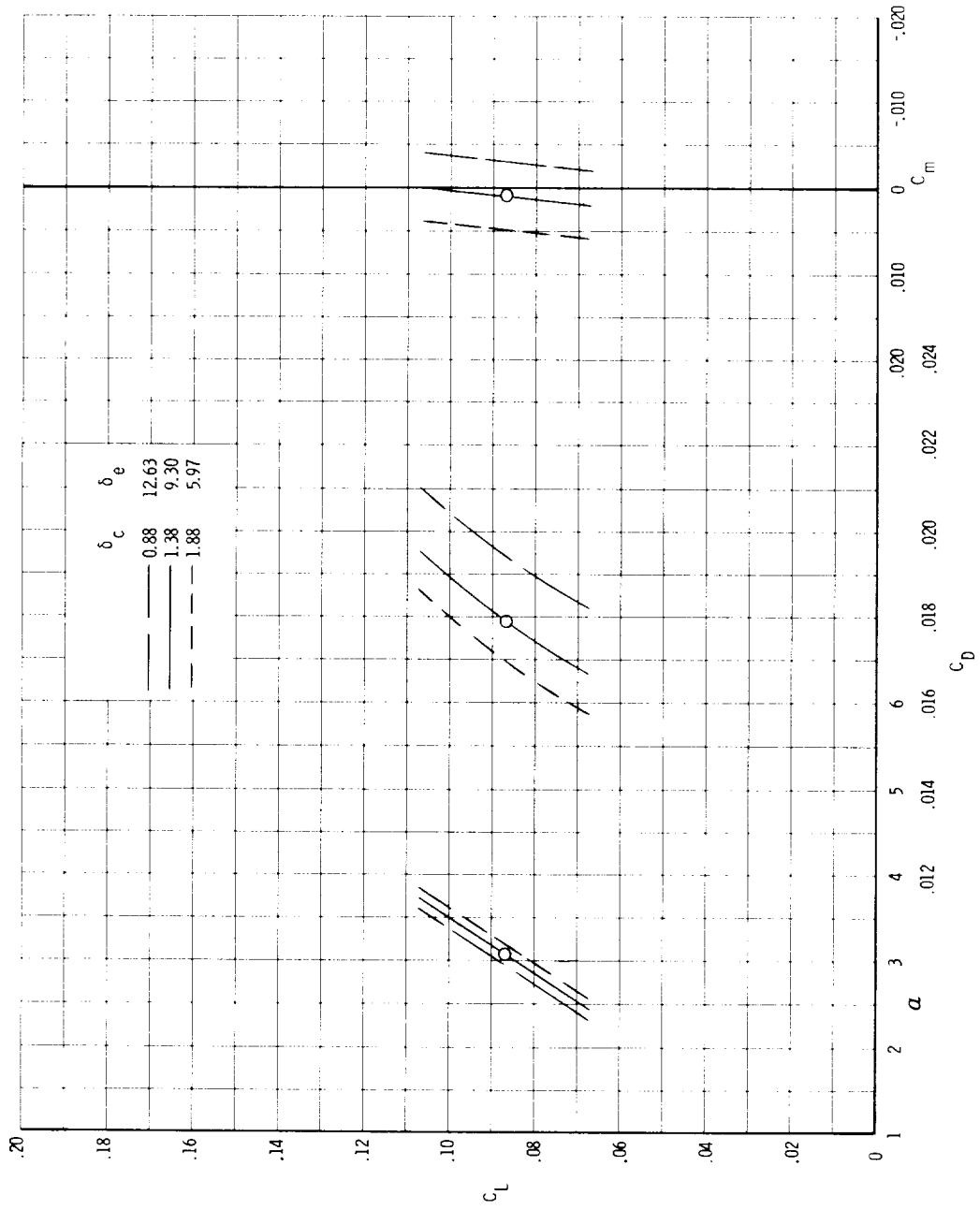
(e) P5 at M = 1.67.

Figure 25.- Continued.
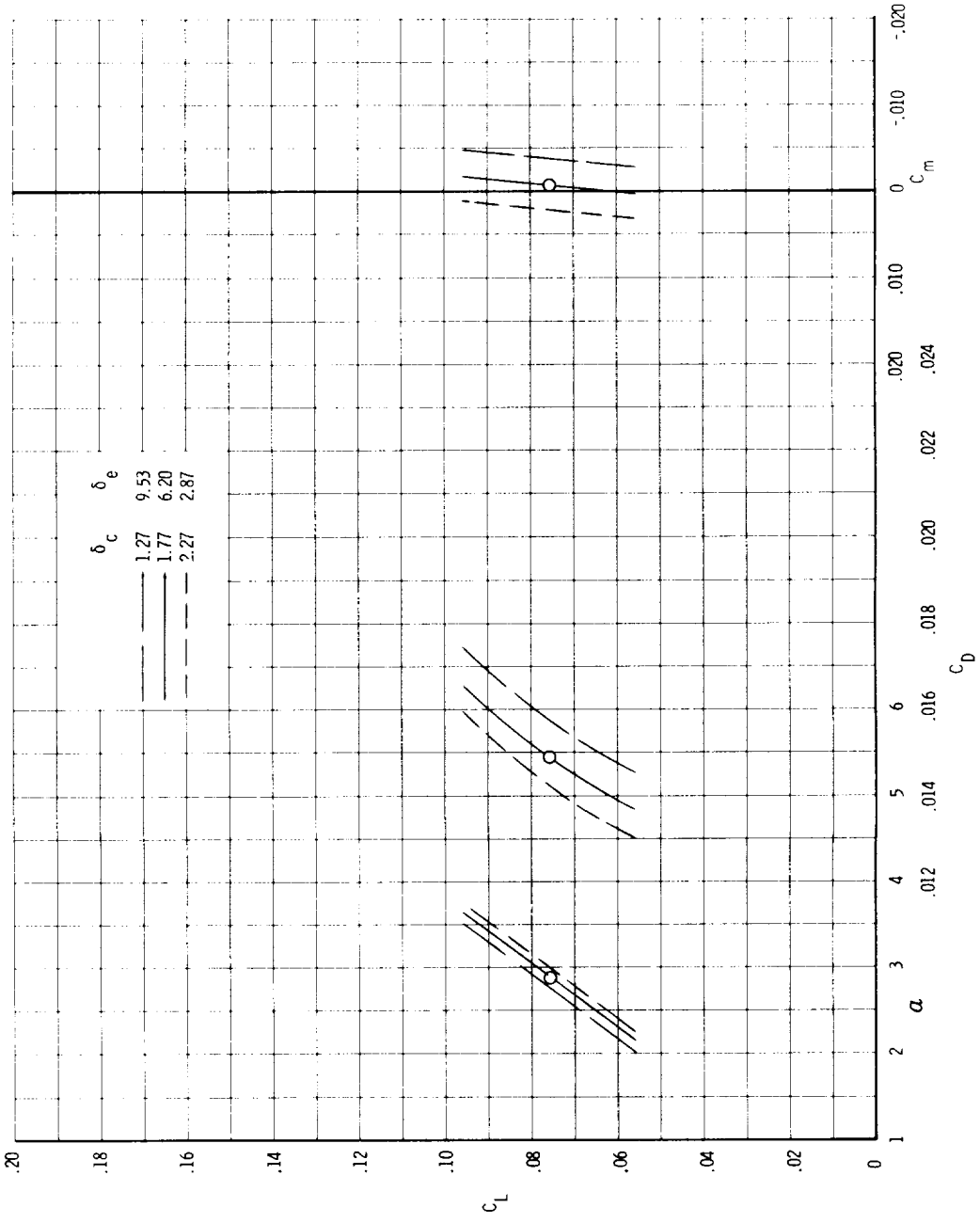
(f) P6 at M = 2.10.

Figure 25.- Continued.
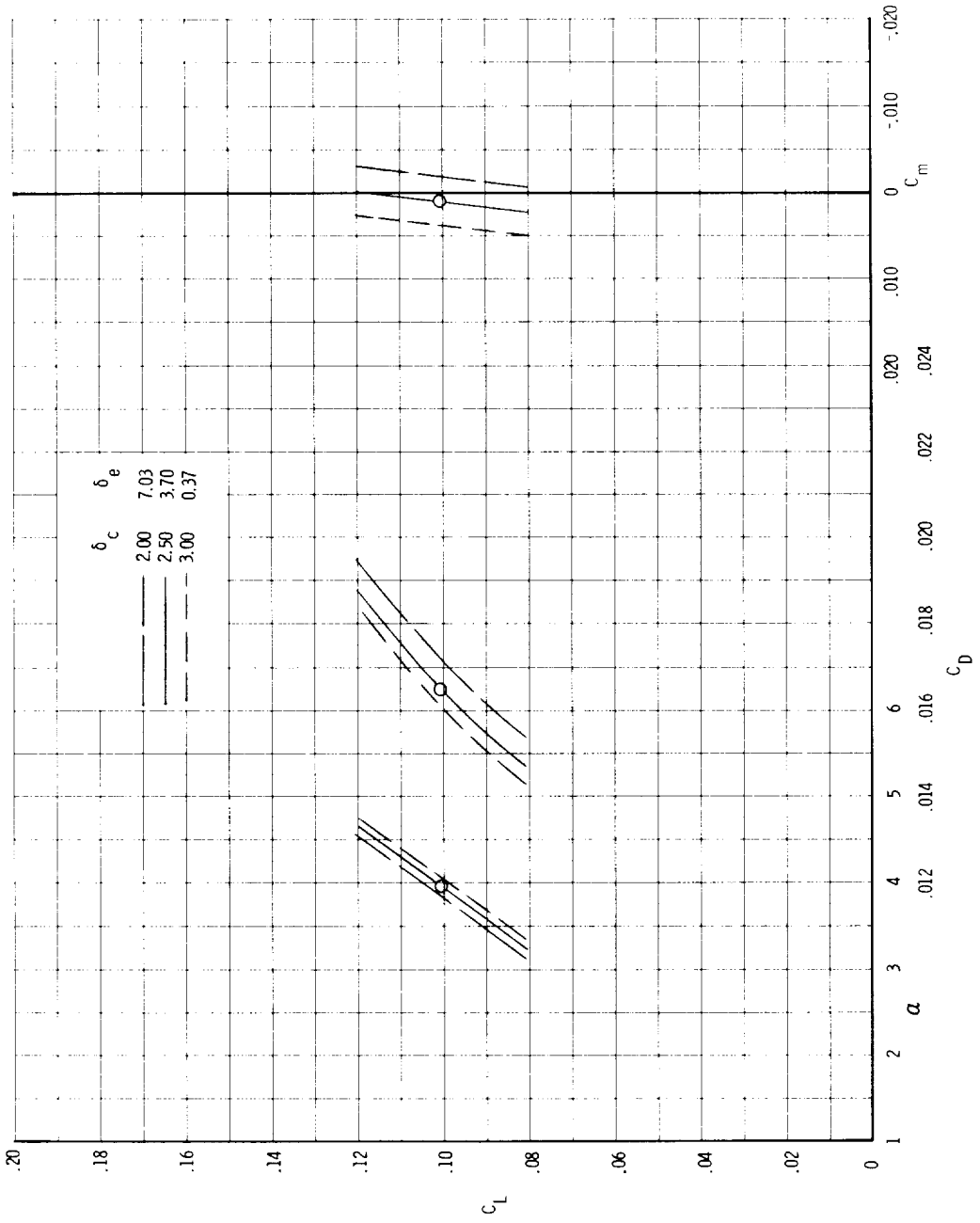
(g) P7 at M = 2.15.

Figure 25.- Continued.
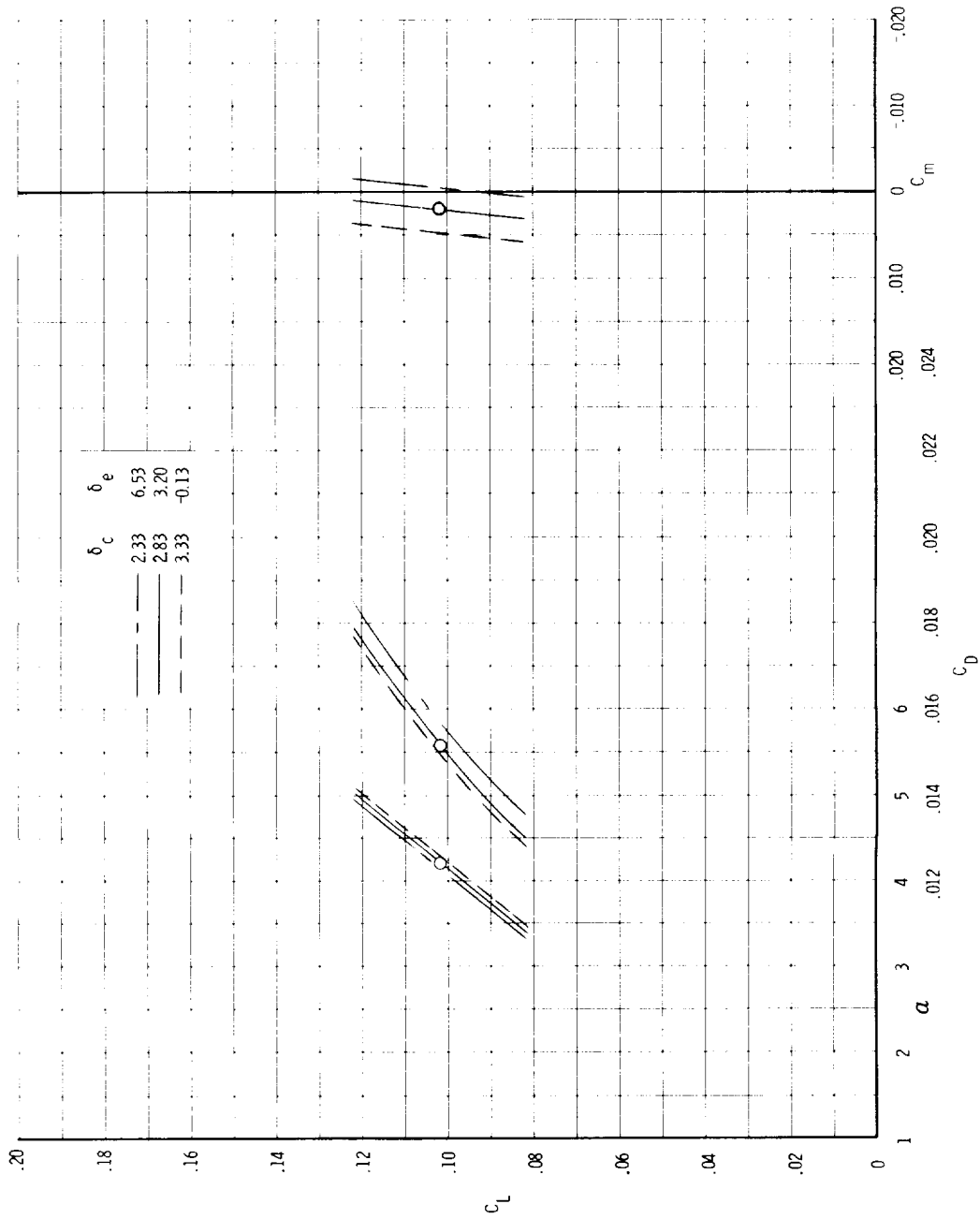
(h) P8 at M = 2.53.

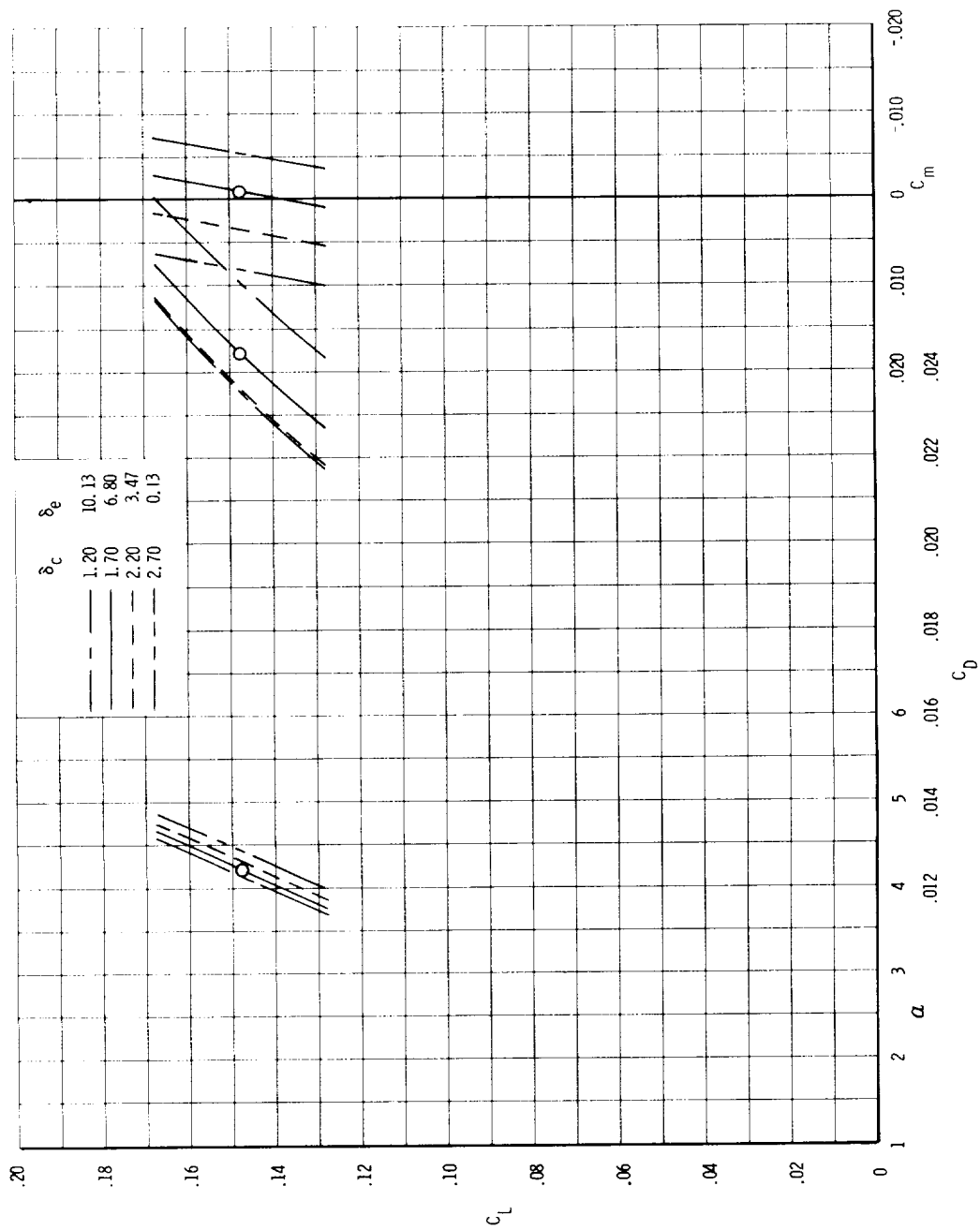Figure 25.- Continued.
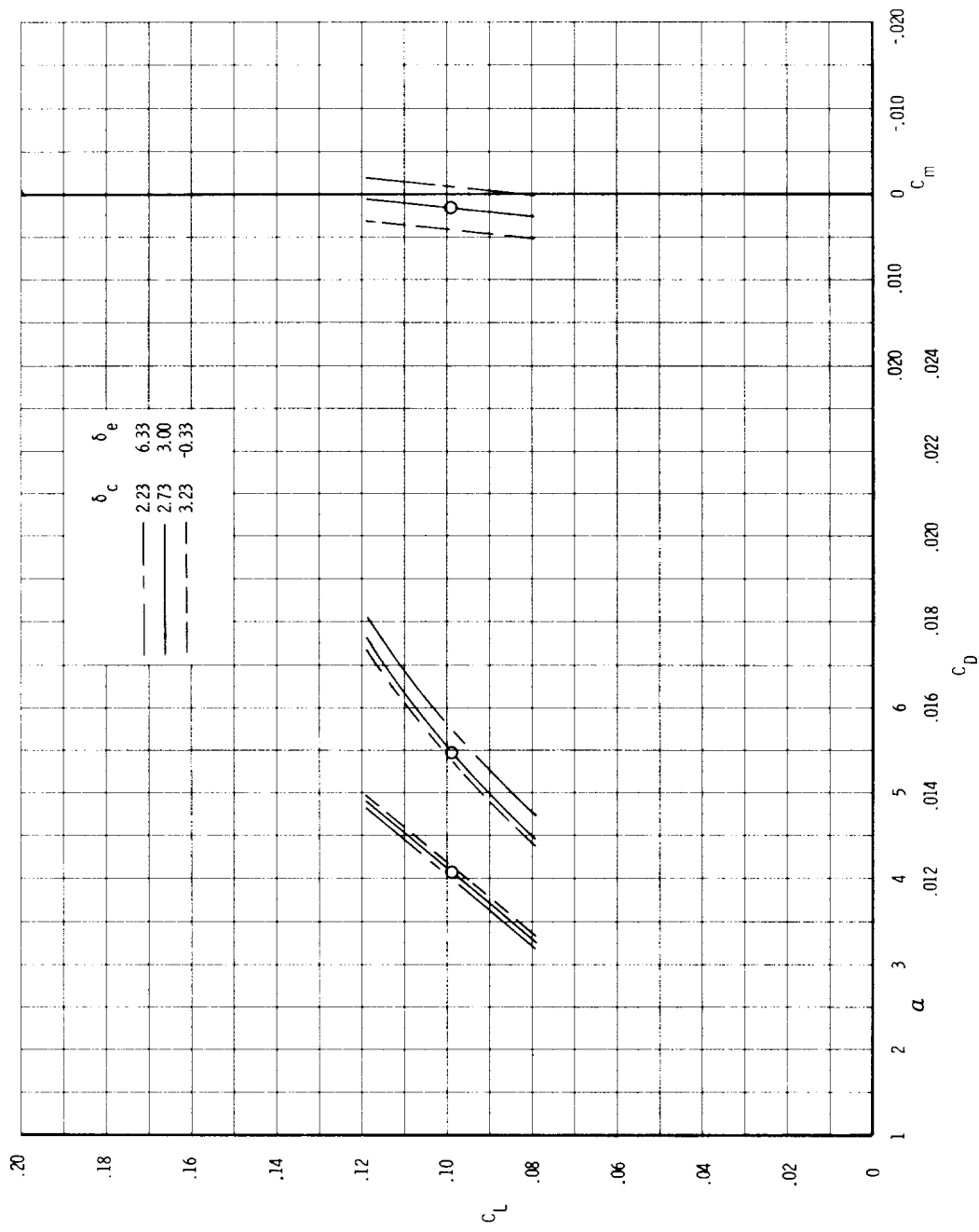
(i) P9 at M = 2.50.

Figure 25.- Continued.
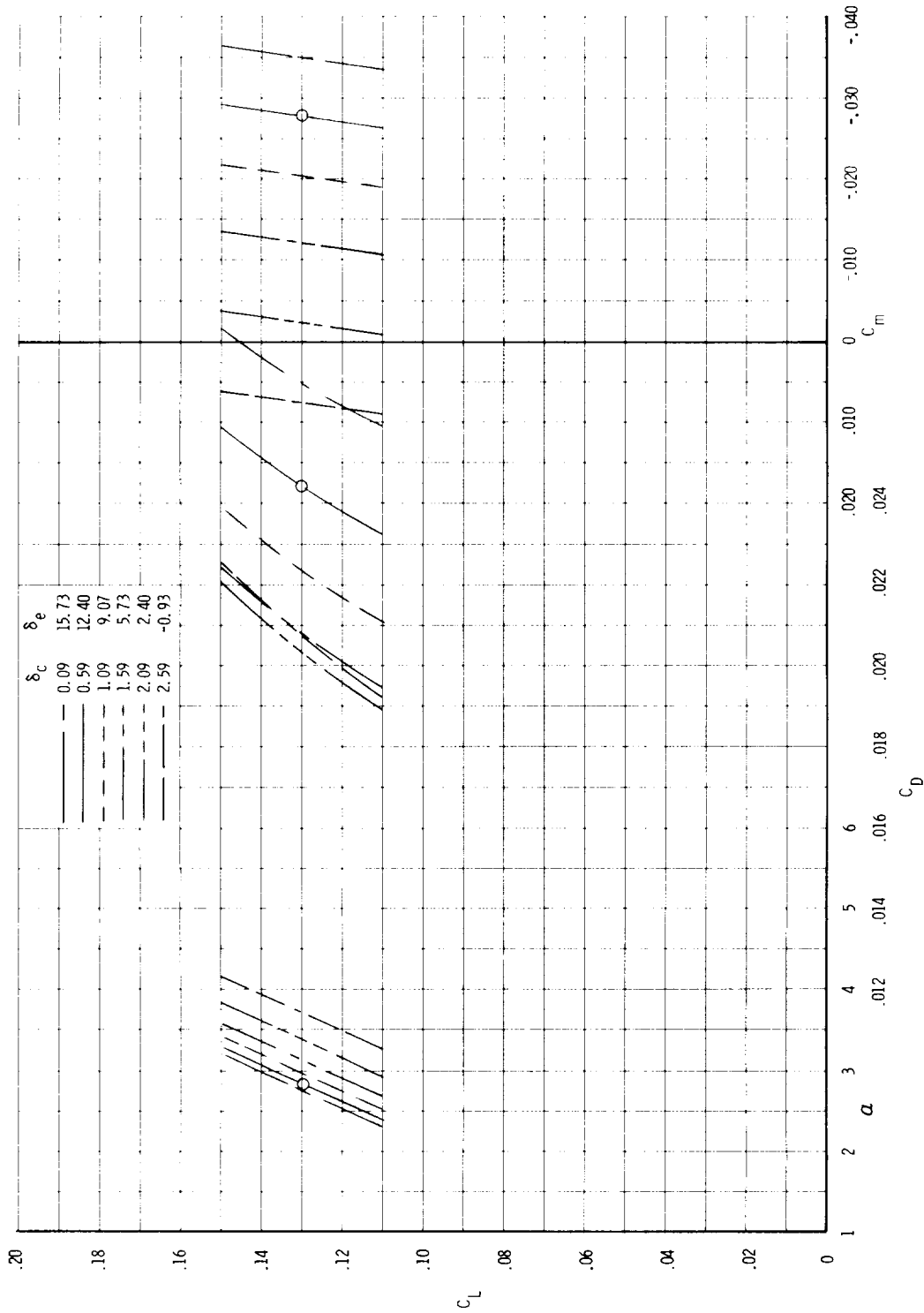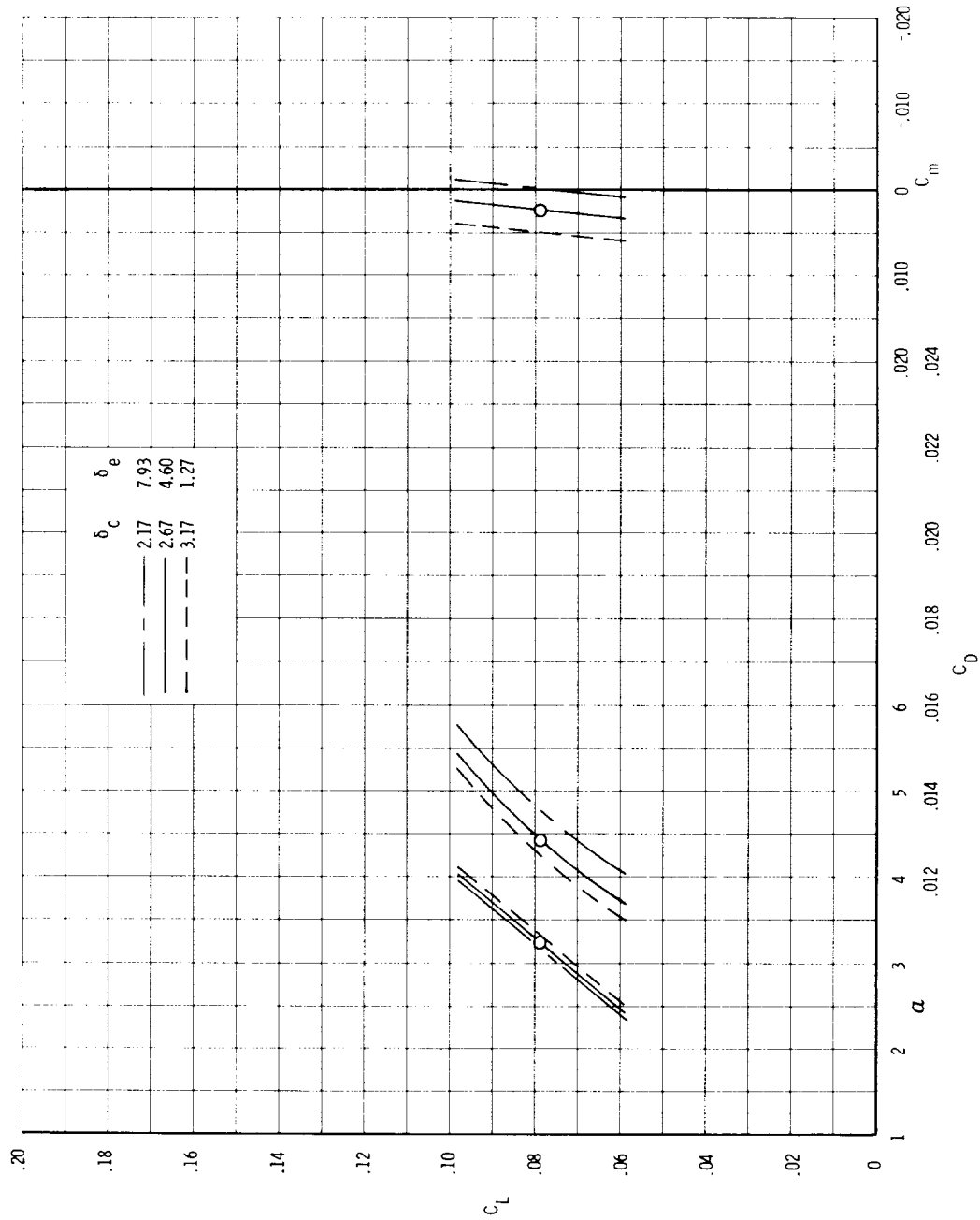
(j) P10 at M = 1.06.

Figure 25.- Continued.

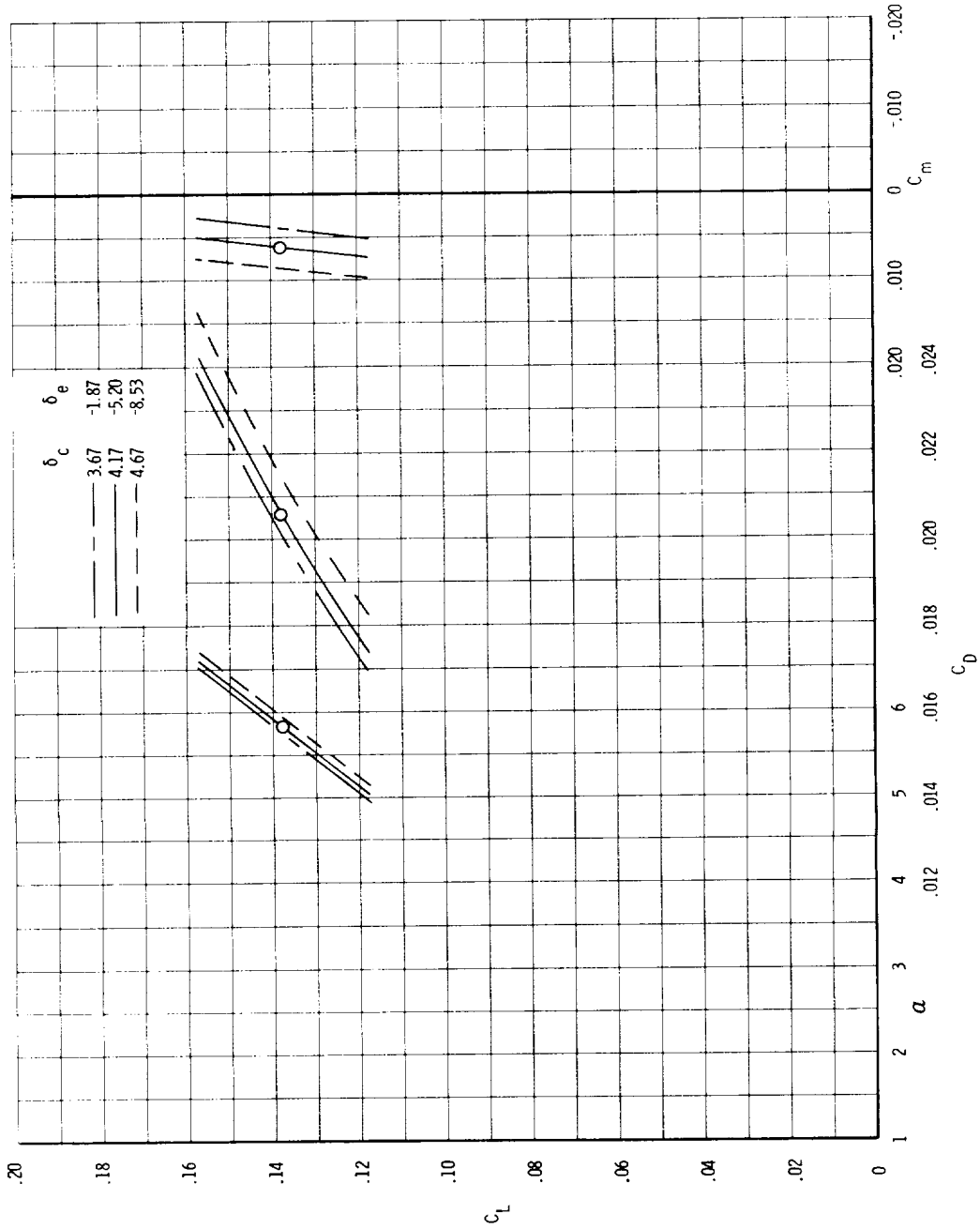(k) P3L at M = 1.15.

Figure 25.- Continued.

(1) P3H at M = 1.17.

Figure 25.- Continued.

(m) P8L at M = 2.51.

Figure 25.- Continued.

76

(n) P8H at M = 2.56.

Figure 25.- Concluded.

1. Report No. NASA TP-1515	2. Government Accession No.	3. Recipient's Catalog No.
4. Title and Subtitle WIND-TUNNEL/FLIGHT CORRELATION STUDY OF AERODYNAMIC CHARACTERISTICS OF A LARGE FLEXIBLE SUPERSONIC CRUISE AIRPLANE (XB-70-1). II - EXTRAPOLATION OF WIND-TUNNEL DATA TO FULL-SCALE CONDITIONS		5. Report Date February 1980
		6. Performing Organization Code
7. Author(s) John B. Peterson, Jr., Michael J. Mann, Russell B. Sorrells III, Wallace C. Sawyer, and Dennis E. Fuller		8. Performing Organization Report No. L-12688
9. Performing Organization Name and Address NASA Langley Research Center Hampton, VA 23665		10. Work Unit No. 505-11-13-03
		11. Contract or Grant No.
12. Sponsoring Agency Name and Address National Aeronautics and Space Administration Washington, DC 20546		13. Type of Report and Period Covered Technical Paper
		14. Sponsoring Agency Code

15. Supplementary Notes

Part I - NASA TP-1514.
Part III - NASA TP-1516.

16. Abstract

This report contains the results of calculations necessary to extrapolate performance data on an XB-70-1 wind-tunnel model to full scale at Mach numbers from 0.76 to 2.53. The extrapolation was part of a joint program between the NASA Ames, Langley, and Dryden Flight Research Centers to evaluate present-day performance prediction techniques for large flexible supersonic airplanes similar to a supersonic transport. The extrapolation procedure included: interpolation of the wind-tunnel data at the specific conditions of the flight test points; determination of the drag increments to be applied to the wind-tunnel data, such as spillage drag, boundary-layer trip drag, and skin-friction increments; and estimates of the drag items not represented on the wind-tunnel model, such as bypass doors, roughness, protuberances, and leakage drag. In addition, estimates of the effects of flexibility of the airplane were determined.

17. Key Words (Suggested by Author(s))		18. Distribution Statement
Performance prediction Supersonic aircraft Wind-tunnel tests Aerodynamic drag Airplane performance	Flight tests Comparison B-70 airplane Correlation	Unclassified - Unlimited Subject Category 02

19. Security Classif. (of this report) Unclassified	20. Security Classif. (of this page) Unclassified	21. No. of Pages 77	22. Price* $6.00